

Proteome analysis of chicken lymphocytes after infection and transformation
by the oncogenic Marek's disease virus

Inauguraldissertation

zur

Erlangung des akademischen Grades eines
Doktors der Naturwissenschaften (Dr. rer. nat.)

der

Mathematisch-Naturwissenschaftlichen Fakultät

der

Ernst-Moritz-Arndt-Universität Greifswald

vorgelegt von

Viktoria Isabella Pauker

geboren am 10.12.1990

in Schneizdreuth

Greifswald, 26.04.2018

Dekan: Prof. Dr. Werner Weitschies

1. Gutachter: Prof. Dr. Dr. h.c. Thomas C. Mettenleiter

2. Gutachter: Priv.-Doz. Dr. med. vet. Sonja Härtle

Tag der Promotion: 24.07.2018

A goal without a plan is just a wish

-Antoine de Saint-Exupéry

To my family

Content

| | |
|--|----|
| Content..... | 4 |
| 1. Introduction..... | 8 |
| 1.1. Marek's disease..... | 8 |
| 1.1.1. First description of Marek's disease..... | 8 |
| 1.2. The Marek's disease virus | 9 |
| 1.3. Pathogenesis of MDV | 12 |
| 1.4. Importance of Marek's disease and vaccination..... | 13 |
| 1.4.1. Vaccination | 14 |
| 1.4.2. MD as a model for tumorigenesis | 15 |
| 1.4.3. Genetic manipulation of MDV in bacterial artificial chromosomes | 15 |
| 1.4.4. <i>In vitro</i> infection system for MDV | 16 |
| 1.4.5. The role of lymphocytes in MD | 17 |
| 1.5. Proteome analysis | 19 |
| 1.5.1. Principles of mass spectrometry | 21 |
| 1.5.2. Protein and peptide fractionation techniques | 24 |
| 1.5.3. Quantitative mass spectrometry..... | 25 |
| 1.5.4. Quality of database | 27 |
| 1.6. Difficulties with proteomic analysis of MD tumors..... | 28 |
| 1.6.1. Laser-capture microdissection | 29 |
| 2. Objectives and analytic strategy | 31 |
| 3. Materials..... | 33 |
| 3.1. Animals..... | 33 |
| 3.2. Chemicals..... | 33 |
| 3.3. Viruses | 35 |
| 3.4. Enzymes, antibodies and size markers..... | 35 |
| 3.5. Buffers | 35 |
| 3.5.1. Buffers for SDS-PAGE..... | 35 |
| 3.5.2. Buffers for cell lysis and digestion | 36 |
| 3.5.3. Buffers for OFFGEL IEF..... | 37 |
| 3.5.4. Buffers for agarose gels..... | 37 |
| 3.5.5. Buffers for Immunohistochemistry | 38 |
| 3.6. Kits | 38 |
| 3.7. PCR Primers | 39 |
| 3.8. Apparatus and equipment..... | 40 |
| 3.9. Consumables | 41 |
| 3.10. Softwares..... | 42 |
| 4. Methods | 44 |

| | | |
|-----------|--|----|
| 4.1. | Proteome analysis of naïve primary chicken lymphocytes | 44 |
| 4.1.1. | In-solution digestion..... | 44 |
| 4.1.2. | Desalting of the labeled peptides with Pierce™ C18 Tips..... | 44 |
| 4.1.3. | Lysis of cells and protein extraction | 45 |
| 4.1.4. | Filter aided sample preparation (FASP) digest | 45 |
| 4.1.5. | Dimethyl labeling..... | 46 |
| 4.1.6. | Modified FASP digest and dimethyl labeling as one-pot reaction | 46 |
| 4.1.7. | Desalting of the labeled peptides with Empore™ Cartridges | 47 |
| 4.1.8. | OFFGEL Isoelectric focusing of labeled peptides..... | 47 |
| 4.1.9. | Comparison of OG IEF fractionation efficiency of labeled and unlabeled peptides | 47 |
| 4.1.10. | Liquid chromatography and mass spectrometry | 48 |
| 4.1.11. | Statistical evaluation | 49 |
| 4.1.11.1. | Label-free quantitation..... | 49 |
| 4.1.11.2. | Quantification based on isotope ratio..... | 49 |
| 4.1.12. | Gene Ontology analysis | 50 |
| 4.2. | Proteomic analysis of primary B lymphocytes infected with MDV | 50 |
| 4.2.1. | Lysis of cells and extraction of proteins | 51 |
| 4.2.2. | Determination of protein content of primary chicken B cells..... | 52 |
| 4.2.3. | Filter aided sample preparation (FASP) digest | 52 |
| 4.2.4. | Dimethyl labeling..... | 52 |
| 4.2.5. | LC-MALDI TOF/TOF mass spectrometry | 52 |
| 4.2.6. | Confirmation of infection markers by RNA sequencing..... | 53 |
| 4.2.6.1. | RNA isolation | 53 |
| 4.2.6.2. | Quality assessment of isolated RNA..... | 54 |
| 4.2.6.3. | Isolation of mRNA from purified total RNA..... | 54 |
| 4.2.6.4. | Fragmentation of whole transcriptome RNA from total RNA samples and construction of whole transcriptome libraries..... | 54 |
| 4.2.6.5. | Quality assessment of transcriptome library | 56 |
| 4.2.6.6. | Second purification and amplification..... | 56 |
| 4.2.6.7. | KAPA PCR..... | 57 |
| 4.2.6.8. | Pooling of libraries..... | 58 |
| 4.2.6.9. | OneTouch reaction and Sequencing of Libraries..... | 59 |
| 4.3. | Proteome analysis of MD tumors..... | 61 |
| 4.3.1. | Cryosectioning of snap frozen liver samples..... | 61 |
| 4.3.2. | Hematoxylin and eosin staining and immunohistochemistry | 62 |
| 4.3.3. | Immunohistochemistry | 62 |
| 4.3.4. | Quantitation of cell types with HALO™ imaging software..... | 63 |
| 4.3.5. | Laser capture microdissection..... | 63 |

| | | |
|---------|---|-----|
| 4.3.6. | Lysis of samples and protein extraction | 64 |
| 4.3.7. | Densitometric determination of protein content | 64 |
| 4.3.8. | FASP digest, dimethyl labeling and desalting of peptides | 64 |
| 4.3.9. | OFFGEL Isoelectric focusing (OG IEF) of peptides | 64 |
| 4.3.10. | LC-MALDI TOF/TOF MS of IEF fractions | 65 |
| 4.3.11. | RNA isolation for qPCR | 65 |
| 4.3.12. | Confirmation of potential transformation markers by qRT-PCR | 65 |
| 4.3.13. | Quantification by one-step RT-qPCR | 66 |
| 5. | Results | 67 |
| 5.1. | Proteomic characterization of naive chicken B- and T lymphocytes | 67 |
| 5.1.1. | Proteomic analysis of unlabeled chicken B and T cells | 67 |
| 5.1.2. | Proteomic analysis of dimethyl labeled and OG IEF fractionated B and T cell peptides | 68 |
| 5.2. | Proteomic analysis of infected chicken B cells in the cytolytic phase | 79 |
| 5.2.1. | <i>In vitro</i> infection of primary B cells | 79 |
| 5.2.2. | Determination of protein content of primary B cells | 79 |
| 5.2.3. | Identification of changes in protein expression profiles of MDV infected B cells | 80 |
| 5.2.4. | Sequence analysis of mRNA isolated from MDV-infected B lymphocytes | 86 |
| 5.3. | Proteomic analyses of Marek's Disease lymphomas | 101 |
| 5.3.1. | Evaluation of MD tumor morphology | 101 |
| 6. | Discussion | 108 |
| 6.1. | Characterization of naïve chicken lymphocytes | 108 |
| 6.2. | MDV Infection of primary B cells | 110 |
| 6.2.1. | MDV induced changes in expression levels of host proteins | 110 |
| 6.2.2. | Alterations in expression levels of immune system associated proteins after MDV infection | 112 |
| 6.2.3. | MDV infection downregulates avBD2 | 113 |
| 6.2.4. | Correlation of changes in transcriptome and proteome of MDV infected B cells | 114 |
| 6.2.5. | MDV induced changes in expression levels of host mRNA | 115 |
| 6.2.6. | Alterations in expression levels of immune system associated transcripts | 116 |
| 6.2.7. | Alterations in expression levels of stress response transcripts | 117 |
| 6.2.8. | Alterations in expression levels of transcripts associated with signaling cascades | 117 |
| 6.2.9. | Alterations in expression levels of transcripts associated with autophagy | 118 |
| 6.2.10. | Transcripts downregulated after MDV infection | 119 |
| 6.2.11. | Conclusion and Outlook | 119 |
| 6.3. | Proteome analysis of MD tumors | 120 |
| 6.3.1. | Evaluation of MD tumor morphology | 120 |
| 6.3.2. | MDV induced changes in expression levels of host proteins during transformation . | 122 |

| | | |
|--------|---|-----|
| 6.3.3. | Proteins upregulated in MD lymphomas | 122 |
| 6.3.4. | Proteins downregulated in MD lymphomas | 124 |
| 6.3.5. | Conclusion and Outlook | 124 |
| 7. | List of Abbreviations | 126 |
| 8. | List of Figures | 131 |
| 9. | List of Tables | 132 |
| 10. | Summary | 133 |
| 11. | Zusammenfassung | 136 |
| 12. | References | 140 |
| 13. | Attachments | 150 |
| 13.1. | Publications and contributions at Conferences | 150 |
| 13.2. | Acknowledgment | 153 |

1. Introduction

1.1. Marek's disease

Marek's disease (MD) is a neoplastic and lymphoproliferative disease of chickens caused by the oncogenic *Gallid herpesvirus 2* also known as *Marek's disease virus* (MDV) [1]. In general, symptoms of MD can vary widely between chicken lines. Four different forms of MD have been described: the neurological, visceral, cutaneous and ocular form [2]. Neurological symptoms are caused by dysfunction of peripheral nerves commonly leading to unilateral paralysis of the legs. Ocular symptoms include graying of eyes and misshaping of the iris, which can lead to blindness. Lesions and ulcers around feather follicles define the cutaneous form of MD. While neurological, cutaneous and ocular symptoms can be diagnosed early, visceral symptoms are mostly detected post mortem. Chickens with MD lymphomas in various visceral organs do not show obvious clinical symptoms, but depression or comatose state can occur occasionally and are frequently observed in experimentally infected animals [2]. The early phase of infection is characterized mainly by immunosuppression. Blindness, lesions in visceral organs and neurological disorders are observed later in the course of the disease.

1.1.1. First description of Marek's disease

In 1907, the Hungarian veterinarian József Marek examined the bodies of four young roosters, which had suffered from severe paralysis of the legs and wings. After pathologic examination he observed thickened plexus and sciatic nerves and described for the first time a disease in chickens that he called polyneuritis [1]. Several years later two groups, Kaupp in the USA [3] and Van der Walle and Winkler-Junius [4] from the Netherlands independently observed pathologic changes in the nervous system of chickens that had died following severe paralysis of the extremities. Investigations by Van der Walle and Winkler-Junius revealed infiltrations of leukocytes in the swollen nerves [4] and Kaupp observed blindness in chickens affected by polyneuritis [3]. In 1929, Pappenheimer *et al.* described for the first time several lymphomas in visceral organs of paralyzed chickens, which showed similarities with lesions found in peripheral nerves and renamed the disease to neurolymphomatosis gallinarium [5, 6].

This was the first evidence that the disease not only affects the nervous system but is also characterized by enhanced lymphoproliferation resulting in lymphoma formation [6]. More than thirty years later the disease was finally named 'Marek's disease'. In 1961, Biggs suggested to rename fowl paralysis to Marek's disease to reduce the chance of misdiagnosis as avian leukosis [7]. The term Marek's disease was discussed and agreed upon during the first Conference of the World Veterinary Poultry Association [6].

The high number of cases of MD suggested it has an infectious origin. Pappenheimer *et al.* started a study of disease epidemiology and uncovered frequent reoccurrences of fowl paralysis outbreaks in the same farms, which indicated an endemic character of the disease [5]. He published the results of an experimental trial to prove the transmission of MD, which was based on the first experiments of Van der Walle and Winkler-Junius in 1924 [8]. However, the results were difficult to interpret due to differences symptoms of inoculated chickens and the fact that control chickens developed similar symptoms [8]. Even though Van der Walle and Winkler-Junius, as well as Pappenheimer *et al.*, suggested an infectious agent as cause for MD, the evidence for a viral infection was only presented in the 1960s [6]. In 1962, Sevoian and Chamberlain finally were able to prove the transmissibility of MD between chickens by inoculating healthy chickens with tumor cell suspensions, blood and tissue from infected birds [9]. In 1967, Churchill and Biggs were able to identify a herpesvirus as causative agent of MD [10].

1.2. The Marek's disease virus

The causative agent of Marek's disease is the highly cell associated and oncogenic Marek's disease virus (MDV). One fundamental characteristic of MDV is the ability to transform T cells, which leads to formation of lymphoma in visceral organs. MDV, an enveloped DNA virus, belongs to the genus *Mardivirus* within the subfamily of *Alphaherpesvirinae*. Due to its tropism for lymphocytes and its transforming potential resulting in the formation of lymphoma, MDV was assumed to be related to Epstein-Barr-virus (EBV) [11] and classified as member of the *Gammaherpesvirinae* subfamily.

However, studies of the genome organization of MDV resulted in the reclassification as an alphaherpesvirus [11]. The genome of MDV strains ranges between 170 and 180 kbp in length and is divided into a unique long (U_L) and unique short (U_S) region, each flanked by an internal repeat (IR) and terminal repeat (TR) region [12] (**Figure 1**). Between the IR_L and IR_S short α -like sequences are found that contain two telomeric repeat regions: the multiple telomeric repeats (mTMR) and short telomeric repeats (sTMR) [13]. The short TR_S and IR_S , as well as the long TR_L and IR_L , respectively, have identical sequences but inverted orientation [14]. This also suggested that MDV is more closely related to Herpes simplex virus-1 (HSV-1) than to EBV [15].

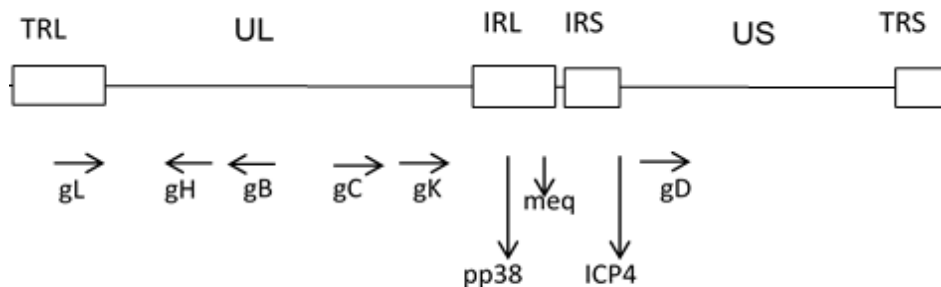


Figure 1 Genome organization of Marek's disease virus, adapted from Venugopal and Payne [12]

Hence, MDV was assigned to the *Alphaherpesvirinae* on basis of the typical genome organization and sequence similarity [11, 16]. There are three MDV serotypes. Serotype 1 contains highly infectious and lymphoma-inducing oncogenic strains. The natural occurring but non-pathogenic strains belong to serotype 2. Serotype 3 includes the closely related herpesvirus of turkeys (HVT), which is non-pathogenic in chickens [17].

All three serotypes of MDV share significant sequence homology throughout the genome except within the long repeat regions [18]. Genes associated with transformation are found within the TR_L and IR_L regions of the genome [19]. The complete genomes of several representative MDV serotype 1 strains, including the virulent GA strain [20] and the very virulent Md5 strain [21] have been sequenced, which gave detailed insights into the genome organization. Hence, several genes could be identified that are involved in tumor development.

Two copies of the gene MDV *EcoRI*-Q (*meq*) are located in TR_L and IR_L [19] and share sequence homologies with cellular transcription factors such as the N-terminal basic leucine zipper (bZIP) domain [18]. *Meq* transformation of cells relies on activation of the *v-Jun* transcriptional cascade by upregulation of JTAP-1, JAC and HB-EGF transcription. Stable dimers of *meq* with cellular Jun could be observed that activate AP-1 promoters [18]. The similarity of *meq* with *v-Jun*, a known oncogene of Avian sarcoma virus 17 [22], makes *meq* a highly interesting factor and therefore the best studied MDV protein. It was shown that *meq* is consistently expressed in MD induced tumor cells [23]. However, many studies have shown that *meq* is required, but not sufficient for transformation [16]. This was supported by experiments conducted by Lupiani *et al.*, showing that deletion of *meq* resulted in reduced virus reactivation while replication rates were similar to wild type (WT) virus, which suggests that *meq* is not essential for cytolytic infection but plays a role in latency and reactivation [24]. In addition, the authors showed that overexpression of *meq* leads to enhanced transformation, morphological changes and shortened G1 phase in Rat-2 and DF-1 cells, clearly indicating a role of *meq* as an oncogene [24].

Among the MDV genes involved in transformation only *meq* has direct transforming abilities, while other genes support the transformation process, such as the viral telomerase RNA (*vTR*). Others have indirect roles in tumor formation, e.g. the viral interleukin-8 homologue (*vIL-8*), the viral lipase homologue (*vLIP*), *RLORF4* and the phosphoprotein 38 (*pp38*) [19]. The activity of telomerase is often enhanced in transformed cells, which allows an increased cell proliferation by avoiding induction of senescence and apoptosis [25, 26]. Several oncogenic viruses including the herpesviruses Epstein-Barr-virus (EBV) and Kaposi sarcoma-associated herpesvirus (KSHV) target cellular telomerase during infection mainly by increasing the activity of the enzyme [27, 28]. Similarly, the MDV *vTR* promotes lymphomagenesis in chicken. MDV is the only virus that encodes its own telomerase RNA under control of a promoter with higher transcriptional activity than the chicken promoter for *chTR* [29]. Deletion of or mutations in the template sequence of *vTR* led to reduction in tumor progression, lymphoma size and dissemination, while the lytic replication was not affected [30, 31].

1.3. Pathogenesis of MDV

The Cornell-model [32] of the MDV infection cycle (**Figure 2**) has three distinct phases: the early cytolytic phase, characterized by immunosuppression, the late cytolytic phase and the latent phase with transformation [33]. A natural infection starts with inhalation of cell-free infectious virus [34], which is taken up in the lung by macrophages, dendritic cells, and B cells. Infected cells then transport the virus to the lymphoid organs where it is also transferred to T cells. The lytic replication takes place primarily in B cells (83-92 % [35]), but also in macrophages and dendritic cells. This cytolytic infection leads to depletion of lymphoid cells and to severe immunosuppression. The infection and the resulting depletion of B cells lead to attraction and activation of T cells. The close interaction between B cells and T cells enables the transfer of MDV between the lymphocytes [16]. T cells carrying the Ia antigen can be preferentially infected with MDV, as activation of the T cells increases susceptibility of the cells [12, 35]. During infection of T cells, the virus enters a latent state. Infection of T cells can lead to transformation and formation of lymphomas, which manifest in various visceral organs. However, infectious virus is only produced in the feather follicle epithelial cells, where the virus replicates and is shed to the environment. The replication cycle is completed after 18-20 h, which leads to semi-productive infection and, thus, production of cell-associated progeny viruses [32].

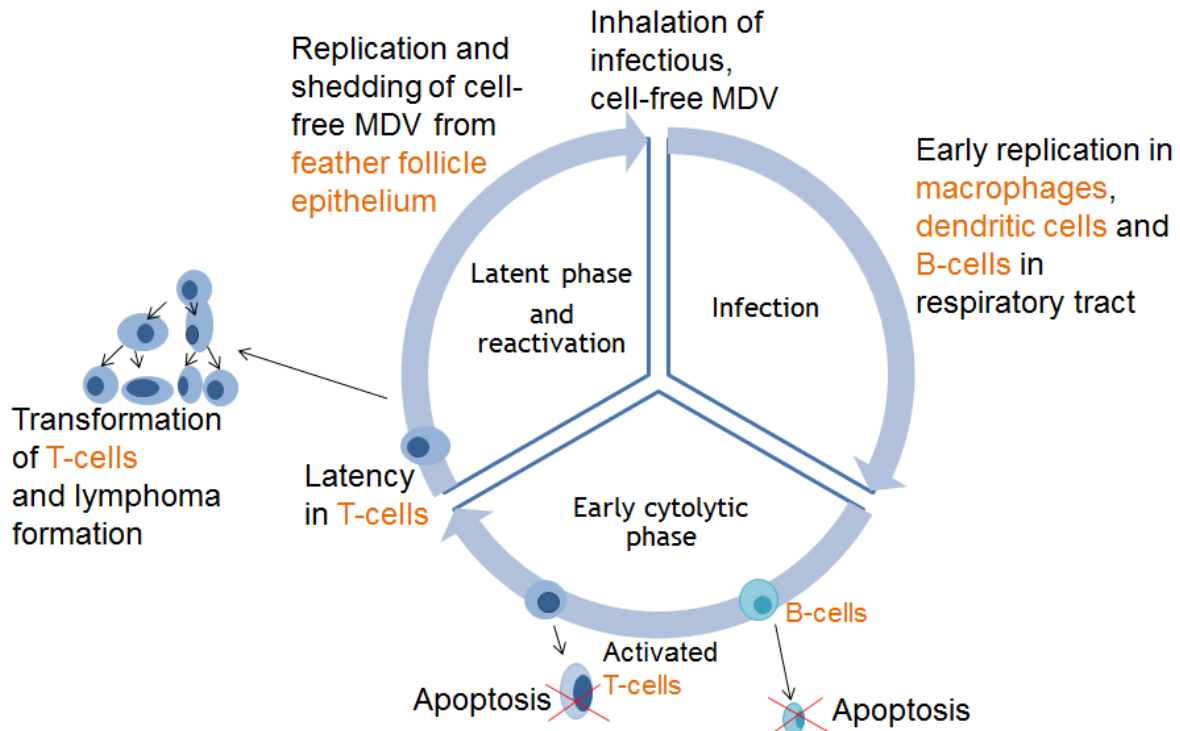


Figure 2 Pathogenesis of Marek's disease virus infection adapted from [2]. The infection cycle consists of three major phases: cytolitic phase, latent phase and transformation. After inhalation of cell-free virus, the virus is taken up mostly by macrophages and dendritic cells, which transport it to lymphoid organs and transfer it to B cells. The virus lytically replicates in B cells leading to apoptosis of B cells and immunosuppression. Infection of B cells attracts and activates T cells, to which the virus is finally transferred. MDV first cytolitically infects also T cells, but also a latent infection can be established, leading to transformation of T cells and finally to formation of T cell-lymphomas. Infectious virus is only produced in the feather follicle epithelial cells, where the virus replicates fully and is shed to the environment.

1.4. Importance of Marek's disease and vaccination

Due to mortality rates of up to 100 %, depending on chicken line and virus strain, MD leads to great economic losses in the poultry industry worldwide [11, 36]. Introduction of efficient vaccines against MDV significantly reduced the mortality rates, but economic losses still add up to 1-2 billion US\$ worldwide [37]. The economic loss can be explained by costs of vaccination, reduced egg production and high mortality rate of MD itself [2]. These costs may still be underestimated as MD is not notifiable in all countries and, thus, the occurrence of the disease is difficult to follow. In Germany, MD is not

notifiable but has to be reported in order to gain knowledge about disease incidence, occurrence and course [38].

1.4.1. Vaccination

Although chickens of every age can be infected, susceptibility decreases with increasing age and the development of the immune system [39]. The mortality rate of MD depends mainly on the susceptibility of the chicken line and the virulence of the MDV strain [40]. Despite the availability of efficient vaccines many cases of MD are still encountered throughout the world. The possible emergence of more virulent MDV strains due to vaccine failure and evolution driven by suboptimal vaccination still makes MDV a high risk for the poultry industry [2, 41]. Vaccine failure is mainly caused by incorrect handling of the vaccine as MDV vaccines are prone to inactivation [42]. In addition, virulent MDV strains can evolve when the vaccine only reduces the disease symptoms but does not prevent infection and virus replication. Hence, transmission and spread of more virulent strains is possible as the host survives the infection [41]. Based on the ability to infect and cause disease even in vaccinated chickens, MDV strains are divided into three different pathotypes differentiating virulent, very virulent and virulent plus strains [19]. Present MDV vaccines are usually based on live viruses. The first MDV vaccine, licensed in 1970 in the United Kingdom, was composed of the attenuated HPRS-16 strain [39, 43]. This vaccine provided not only the first protection against MD, but also was the first vaccine protective against virus-induced tumor formation [44]. One major obstacle of MDV vaccines is the fact that they need to be produced in cultured chick embryo cells due to the highly cell associated nature of the virus. The related apathogenic turkey herpesvirus (HVT) can be produced as cell-free suspension and hence, HPRS-16 was soon replaced by a HVT-based vaccine [39]. However, after introduction of the cell free HVT vaccine high numbers of vaccine failures were observed from which more virulent MDV strains could be isolated. Soon it was clear, that the HVT vaccine was less potent, as cell-free HVT could easily be neutralized by maternal antibodies [39]. As result a bivalent vaccine consisting of a non-oncogenic MDV strain SB-1 and HVT was developed, which provided synergistic protection [44]. Nevertheless, after several years new and even more virulent strains of MDV were isolated from

vaccinated flocks. Already in 1971, another very efficient vaccine based on the CVI988 serotype I MDV strain was introduced in the Netherlands [39, 43]. The vaccine originated from a low pathogenic MDV field strain that was attenuated by serial passage in duck embryo fibroblasts [43]. During the passaging it retained its 'A' antigen and could still spread from animal to animal [43]. Only in the 1990s, other countries also started to use the CVI988 vaccine in their chicken flocks [44], which proved to be very effective in the protection also against very virulent strains. The CVI988 vaccine is still the gold standard for vaccination against Marek's disease [45]. Vaccination of 1 day old chickens usually provides protection even against highly pathogenic MDV strains [45]. Vaccine viruses establish persistent productive infections in the host, where the virus still lytically infects, replicates and is also shed in to the environment. In general, the vaccine protects from most symptoms, including gross lesions and tumor formation, and thus lowers mortality [39, 44]. However, the vaccine strains can still be pathogenic in animals highly susceptible to MD [43].

1.4.2. MD as a model for tumorigenesis

MDV is not only studied as a major animal pathogen with economic importance but also as a model for virus-induced tumorigenesis. The study of MDV infection and lymphomagenesis in this natural small-animal virus-host model is of great value [11, 33]. Especially the observed overexpression of CD30 molecules in MD tumors has made MD a suitable model for Hodgkin's disease [46]. Drawbacks of MDV in cancer studies were the difficult manipulation of the MDV genome [11], the incomplete annotation of the chicken genome and proteome as well as a lack in the functional characterization of many chicken genes. While the knowledge gap concerning the functional characterization of chicken genes persists, manipulation of the viral genome has been optimized by the introduction of bacterial artificial chromosome (BAC)-based genetic systems [11] for the generation of recombinant viruses.

1.4.3. Genetic manipulation of MDV in bacterial artificial chromosomes

Different strains of MDV, including representatives of all serotypes, have been constructed as infectious BAC systems to facilitate the functional characterization of individual virus genes by

mutagenesis [47]. Investigations of MD pathogenicity require infection with virulent and very virulent MDV strains to fully induce symptoms. The RB-1B strain, isolated in the 1980s from a flock of chickens, which had been vaccinated with the HVT-based vaccine, caused MD with 100 % tumor incidence in various chicken lines and was characterized as highly oncogenic strain [48]. A BAC clone of this strain was constructed [49] which allowed easy manipulation of the genome and was used to determine oncogenic determinants [50]. Tagging of viral proteins with fluorescent proteins using the BAC system allowed the tracking of viral infection *in vitro* and allowed fluorescence activated sorting of infected cells [51]. Jarosinski *et al.* constructed a BAC clone of RB-1B by two-step Red-mediated mutagenesis, where the green fluorescent protein (GFP) was fused to C-terminus of the tegument protein pUL47 [51]. However, although the replication rate was similar to the parental virus, the fluorescent fusion protein was expressed only weakly [51].

As part of his doctoral thesis, my collaboration partner Luca Bertzbach at the Freie Universität Berlin in the laboratory of Prof. Dr. Benedikt Kaufer constructed several fluorescently tagged viruses based on RB-1B, allowing the fluorescence-based detection and isolation of infected primary lymphocytes, which were then used to analyze the proteome of infected cells. In order to identify lytically infected cells, they constructed an RB-1B BAC clone that expresses GFP under the control of the early HSV-1 TK promoter in the BAC backbone (mini-F) [52]. Recombinant virus was generated using the infectious RB-1B BAC clone previously published by Petherbridge and colleagues [50]. Similarly, a CVI988/Rispens vaccine strain expressing GFP under the HSV-1 TK promoter was constructed [53]. In order to elucidate the role of viral telomerase RNA (vTR) during the transformation process, a recombinant MDV deletion mutant was generated that lacks vTR [54].

1.4.4. *In vitro* infection system for MDV

Analysis of the cytolytic infection of B cells and T cells, the first major target cells of a natural MDV infection, has been difficult due to the short survival time of primary lymphocytes in cell culture. So far, most investigations on host gene or protein expression during lytic infection of MDV have been

conducted using stable cell lines, chicken embryo fibroblasts or organ cells isolated from *in vivo* infected animals [55-60]. However, the studies of MDV infection in permanent cell lines and fibroblasts hardly reflect a natural infection. Another major obstacle for the proteome analyses of *in vitro* infected cells is the strict cell-associated nature of MDV. This leads to rather low *in vitro* infection rates with usually below 5 % infected cells. Therefore, analysis of infected cells compared to mock-infected cells is difficult, as infected cells have to be enriched from the inoculated cell batch.

Recently, Schermuly *et al.* [61] developed a cultivation protocol which allows the prolonged cultivation of primary lymphocytes in the presence of soluble CD40 ligand for B cells and TCR-2 antibodies for T cells. Using this protocol, infection rates with MDV could be increased up to 20-50 %. This *in vitro* system successfully mimics a natural infection allowing the investigation of different aspects of MDV *in vivo* infection in a simple and accessible system [61]. My collaboration partners used this cultivation system to infect primary B lymphocytes, which were the basis for the present quantitative comparative analysis of the T- and B cell proteomes after infection with the very virulent MDV strain RB-1B and the vaccine strain CVI988/Rispens.

1.4.5. The role of lymphocytes in MD

Lymphocytes belong to the adaptive immune system and their main function is the specific recognition of antigens by antigen-receptors [62]. Hence, lymphocytes are central players for the host immune system during infections, as they produce antibodies, release interferons after contact with specific protein antigens and elicit cell-mediated immunity [63, 64]. As a consequence of contact between lymphocyte receptor and antigens, an intracellular cascade is triggered which results in the activation of the transcription factor NFκB [64]. This transcription factor is involved in the synthesis of many pro-inflammatory factors, mediators promoting proliferation and maturation of lymphocytes [64]. There are two types of lymphocytes, B and T lymphocytes. In general, after contact of foreign antigens with B cell receptors (BCR), B cells mature to antibody producing plasma cells and the secreted antibodies specifically target the antigen. In contrast, T cells proliferate into one of several functional effector cells

after binding of antigen to T cell receptor (TCR), in order to kill infected cells as cytotoxic T cells, activate B cells and macrophages as helper T cells or regulate activity of other lymphocytes as regulatory T cells [62]. The different functions suggest significant differences also between the protein expression profiles of B- and T cells. Although B cells and their function in antibody production was first described in chickens [62], knowledge about their natural protein expression profiles in chickens is sketchy. Many viruses including MDV target primary lymphocytes during infection. Viral infection of lymphocytes has far-reaching consequences on the functionality of the cells and the subsequent immune response. However, the impact of the infection on protein synthesis can vary from depression to stimulation depending on the virus and the susceptibility of each lymphocyte subpopulation [63]. In order to gain insights into the proteome of transformed T cells or infected B cells, the proteome of healthy naïve chicken lymphocytes had to be unraveled first. Transcriptomics was already applied to chicken bursal lymphocytes [65]. However, proteomic studies of chicken lymphocytes have so far mainly focused on B cells and their development in the bursa of Fabricius using two dimensional gel electrophoretic techniques [66, 67]. Proteomic characterization of the different compartments of the bursa of Fabricius was performed by McCarthy *et al.* using the differential detergents fractionation multidimensional protein identification technology focusing on the biology of the whole organ [68]. However, so far very little is known about the proteome of chicken T cells and no comparative studies between chicken B and T cells have been conducted yet.

1.5. Proteome analysis

The prerequisites for the present study were the new MDV infection system for primary lymphocytes described in [61], the availability of the annotated chicken genome sequence, proteome databases in public repositories and the possibility to analyze proteomes by mass spectrometry.

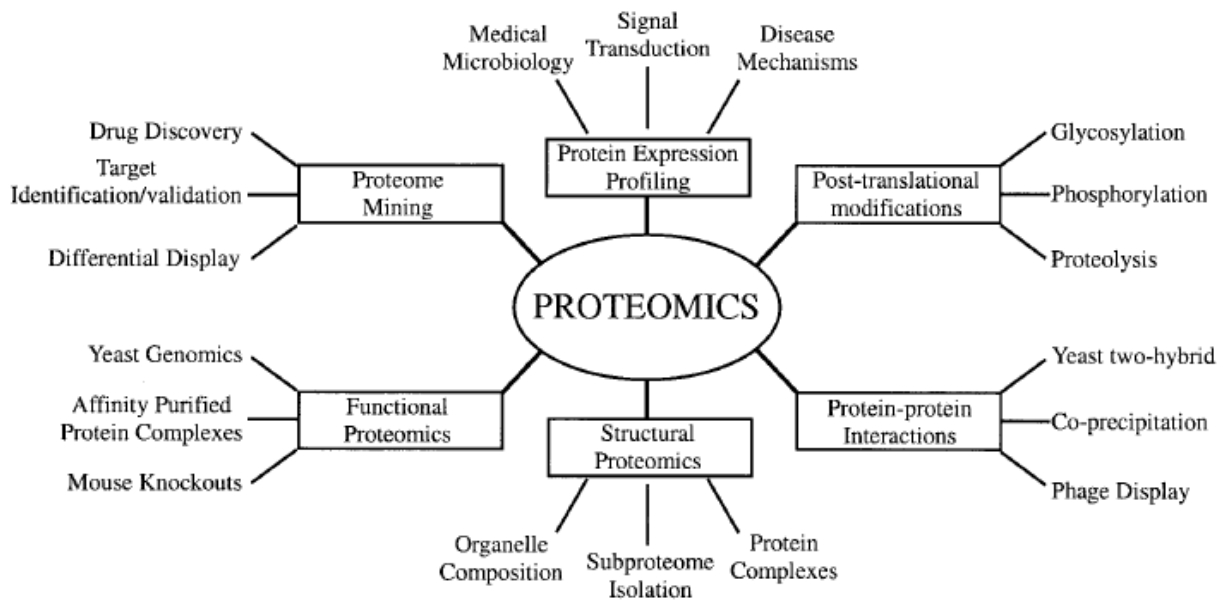


Figure 3 Different applications and fields of proteomics [69].

The proteome of a cell is the complement of proteins, which is expressed at a given time point under given conditions [69]. Proteome analysis, also called proteomics, is applied to characterize the proteomes of organelles, cells, tissues, or organisms. In contrast to the static genome, the proteome is highly dynamic and readily changes under different conditions [70]. Therefore, qualitative and quantitative changes of the proteome reflect adaptations of cellular functions and are highly meaningful to characterize the functional status of a cell. The number of proteins potentially expressed in a cell is greater than the number of genes, as different proteins can be expressed from different splice variants of one transcript and proteins with different post-translational modifications can be synthesized [70, 71], making proteome analysis a technical challenge. Other factors like protein abundance and cellular localization are also considered and the concentration of proteins to be analyzed usually exceeds the dynamic range of one single analysis [71]. Proteomics mainly aims at

obtaining a global and integrated view, studying all proteins of a cell at once and not only few selected proteins [69]. Proteomics includes diverse disciplines and study-areas (**Figure 3**) like characterization of post-translational modifications (PTM), protein-protein interactions, structural and functional analysis of proteins, and characterization of protein-expression profiles as response to a disease, an infection, or other stimuli [69]. Proteins are important mediators of all biochemical processes, hence de-regulation of proteins is a good indicator for infections and diseases [72]. It is known that various members of the *Alphaherpesvirinae* degrade mRNA directly or interfere with processing and synthesis of host proteins, a process known as viral host shut-off, to evade antiviral mechanisms of the cell. HSV infection for example leads to complete shutoff of host protein synthesis [73, 74] which is mediated by the viral host-cell shutoff (vhs) protein pUL41. Recently, Rutkowski *et al.* showed that HSV-1 possesses another *UL-41* independent host shut-off strategy, in which HSV-1 disrupts transcription termination leading to novel intergenic splicing variants between exons of neighboring genes. The cellular genes are still transcriptionally induced but the long read-through transcripts are not translated [75]. Similarly, Pseudorabies virus (PrV) possesses a virion host shutoff protein (vhs) that is encoded by *UL41* and acts as a mRNA-specific endoribonuclease [76] which is also identical for bovine alphaherpesvirus 1 (BHV-1) [77]. MDV also possesses a homologous vhs protein, the product of *UL41*, which is capable of degrading RNA, but does not seem to play a role in viral pathogenesis [78]. However, any virus infection affects and changes the host proteome due to interaction of viral proteins and cellular proteins. Proteomics allows to study the protein interactions involved in viral pathogenesis and to identify the function of viral proteins by analysis of the changes in the host proteome resulting from a virus infection [79]. In general, two different approaches for mass spectrometric based proteome analyses are known: top-down or bottom-up. During the top-down approach intact proteins are directly analyzed in the mass spectrometer, whereas peptides, generated through enzymatic or chemical digest, are the basis for the bottom-up proteome analysis [80, 81]. The top-down approach can provide information about the primary sequence and all modifications [80]. The major challenge of the top-down approach is the fact that to-date only simple protein mixtures can be efficiently

analyzed. For the analysis of highly complex protein samples, the bottom-up approach is the better choice. In this case, the proteins are digested by a proteolytic enzyme, followed by separation of the peptides by liquid chromatography and analysis by mass spectrometry. This 'shotgun' proteomic approach can be used for large-scale analysis [81, 82]. However, information might be lost through the conversion of peptides from proteins, which could lead to incorrect identification. Moreover, peptides shared between different proteins complicate peptide-based quantification of proteins. For the present study, the bottom-up proteomic approach was chosen.

1.5.1. Principles of mass spectrometry

Mass spectrometry allows determination of the mass-to-charge ratio (m/z) of an analyte. Current mass spectrometers usually have three components, an ion source where the molecules of interest are ionized and transferred into the gaseous state, the analyzer where molecules of different m/z values are separated, and a detector [83-85]. Early mass spectrometric techniques have used thermal vaporization to transfer small molecules into the gas phase. However, biopolymers and nonvolatile or thermally unstable molecules, such as peptides, proteins and nucleic acids cannot be transferred into the gaseous phase by thermal vaporization. Several decades after the development of the first mass spectrometers, new soft ionization methods were developed, which could also be used to transfer large, thermally labile molecules into gases. Presently, two soft ionization techniques are mainly used, which can produce intact molecular ions of larger molecules, i.e. electrospray ionization (ESI) and matrix-assisted laser desorption ionization (MALDI). In 2002, Koichi Tanaka received the Nobel prize for the development of the matrix-assisted laser desorption ionization technique, although Michael Karas and Franz Hillenkamp simultaneously developed MALDI with a different experimental setup which is preferably used nowadays [83]. In the MALDI process, analyte ions are formed after excitation of the matrix molecule with an intense pulsed UV laser beam [80] and transfer of the charge to the analyte. For efficient ionization and desorption, the sample is embedded in excess of matrix, which separates sample molecules and absorbs the energy of the laser leading to an explosive breakdown of the matrix-analyte mix, transferring both molecules into the gaseous phase. During the laser pulse-

induced evaporation of matrix and analytes, the matrix molecules collide with analyte molecules, transferring (in the positive ionization mode) a proton from the matrix to the sample [83, 85]. Matrices routinely used for UV lasers with 337 nm include sinapinic acid (SA), 2,5-dihydroxybenzoic acid (DHB) and α -cyano-4-hydroxycinnamic acid (CHCA). Different matrixes transfer different amounts of energy to the sample, leading to different degrees of fragmentation. Less efficient fragmentation is achieved with 'cold' matrices, such as DHB, while more fragmentation is obtained with 'hot' matrices, such as CHCA [80]. The sample molecules usually gain a single positive charge. A schematic representation of the MALDI process is shown in **Figure 4**. The ions produced in the ion source are transferred to the analyzer, which separates the ionized samples based on mass-to-charge ratios (m/z) and directs them to the detector. Hence, the sensitivity, resolution and mass accuracy depend highly on the analyzer. There are several different types of analyzers, including the ion trap (IT), time-of-flight (TOF), quadrupole, Orbitrap, and Fourier transform ion cyclotron resonance (FTICR). MALDI instruments are usually equipped with TOF analyzers, which offer an unlimited mass range and high ion transmission [86]. The ions are accelerated in an electrical field and thus, all ions receive the same energy per charge. Hence, the velocity of the ion after acceleration and the time of flight within the analyzer is inversely correlated to their m/z . This simple principle of TOF MS has been refined by advanced technologies that have immensely improved the performance of current MALDI-TOF mass spectrometers. For example, introduction of mass reflectors and the delayed extraction technology has significantly improved mass accuracies [87], and lasers with repetition rates of up to 10 kHz have shortened analysis times and enabled new technologies such as imaging mass spectrometry, molecular microscopy for the new age of biology and medicine [88, 89].

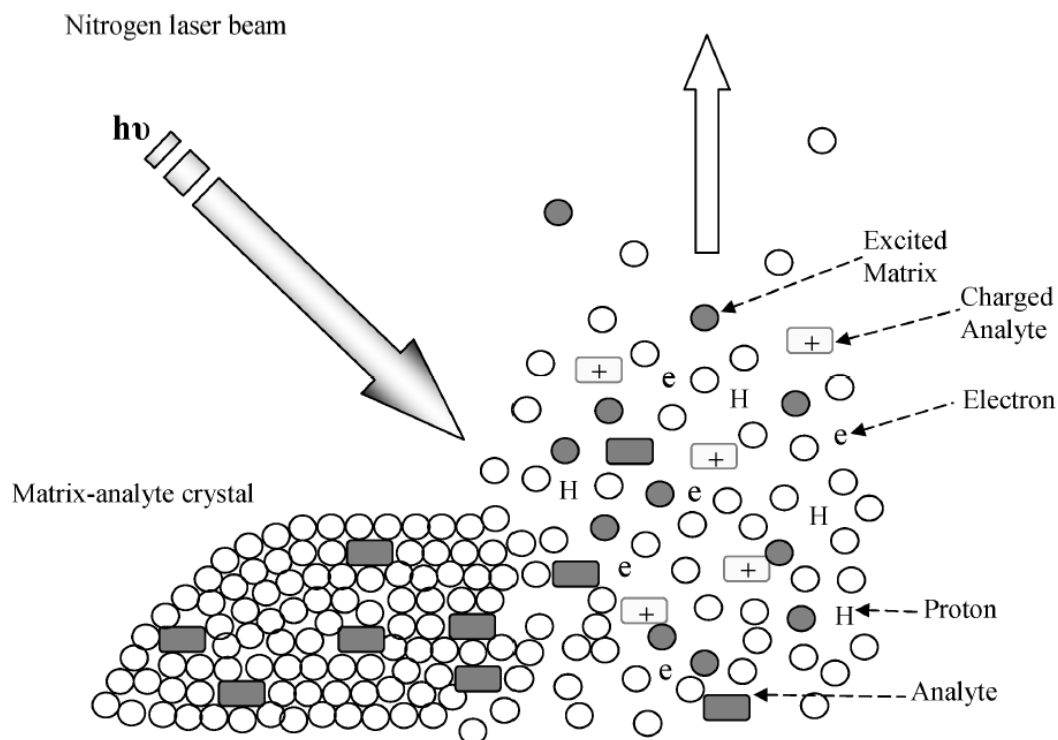


Figure 4 Schematic principle of matrix-assisted laser desorption ionization taken from El-Aneel *et al.* [90].

With the ESI method, ions are formed in the source at atmospheric pressure. A continuous flow of solvent, usually the outlet of a nano-HPLC, is pumped into the source through a fine capillary needle, which is held at high potential compared to adjacent sampling plate. Hence, a fine spray, containing droplets with high surface charge densities, is produced. The solvent is evaporated by application of heat or dry gas. This leads to a reduction in droplet size and increases the charge density. Subsequently, an explosive fragmentation of the droplets leads to formation of gas-phase ions that are directed to the analyzer [84, 85]. The schematic representation of ESI can be seen in **Figure 5**. ESI does not show the preference for singly charged ions like MALDI, but also produces multiply charged ions. ESI can be combined with a variety of different analyzers, but typically, a quadrupole mass analyzer is used. The major advantages of a quadrupole analyzer are its robustness and the fact, that less demanding vacuum conditions are sufficient. The detectable mass range is $< 4000\text{ m/z}$, which is compatible with ESI, which usually produces ions in the range of $500\text{--}2000\text{ m/z}$ [85]. The formation of multiply charged ions brings several advantages for ESI, as first, mass analyzers with a small m/z range, such as

quadrupole can be used to detect also high molecular weight molecules and second, more accurate molecular weights can be determined from the distribution of multiple charged peaks [84].

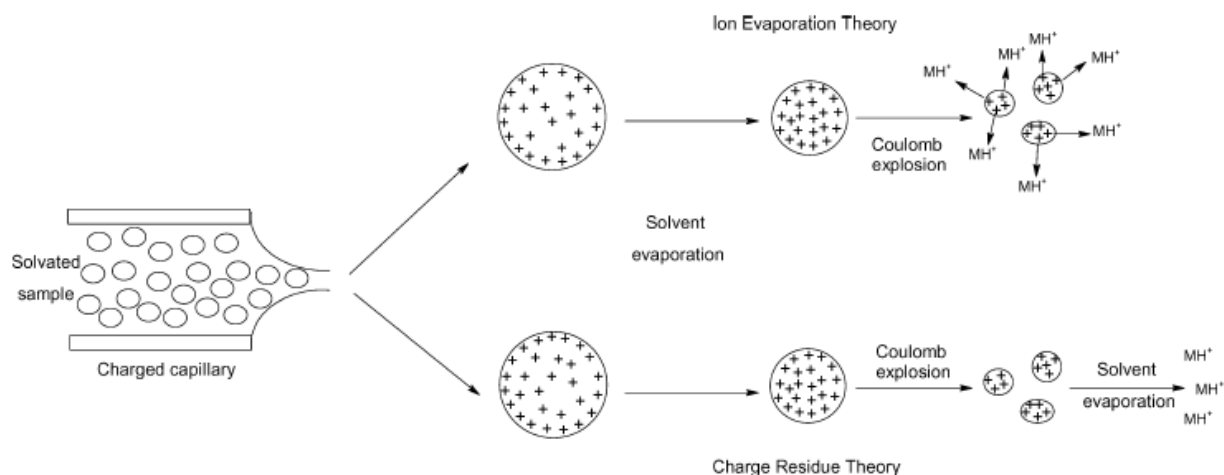


Figure 5 Schematic representation of ESI ionization taken from El-Aneed *et al.* [90].

Table 1 Advantages and disadvantages of MALDI and ESI according to [90] and [91].

| Ionization technique | Advantages | Disadvantages |
|----------------------|---|--|
| MALDI | Archive sample target => reanalyze samples under optimized conditions | |
| | Decoupling MS from LC separation increases time for spectra acquisition | Reduced throughput |
| | High sensitivity (detection into femtomol range) and tolerant to contaminations | Low resolution and sensitivity for large proteins with molecular weight of $\geq 30\text{kDa}$ |
| ESI | High sample throughput and efficiency | Contaminants from the tubes compete with analyte molecules |
| | High accuracy and high resolution | |

1.5.2. Protein and peptide fractionation techniques

In-depth analyses of whole proteomes can be difficult as the protein mixtures are highly complex and the large differences of the abundances of individual proteins add to the analytic challenge. To reduce complexity of the protein sample an additional chromatographic or electrophoretic fractionation step prior to the mass spectrometric analysis is often beneficial to achieve high yields in proteomic analyses

[92]. Several convenient workflows are at hand. Size-based fractionation of proteins by SDS-PAGE can be combined with in-gel digest of gel slices prior to LC-MS analysis ('geLC-MS'). Gel-free 'OFFGEL' isoelectric focusing (OG IEF) separates proteins on the basis of their isoelectric points. The side chains of amino acids carry different positive and negative charges depending on the pH of the milieu, thus defining peptides and proteins as amphoteric molecules. During OG IEF the macromolecules are present in a liquid phase and have to migrate through a stationary gel phase towards the compartment carrying the correct pH value for their isoelectric point (pI). Once this compartment is reached, the proteins/ peptides are retained in the liquid phase, as their net charge is equivalent to zero. The peptides are easily recovered in the solution [93]. OG IEF of proteins avoids the in-gel digestion step, it is highly scalable and can also be applied to separate peptides after the proteolytic digest and before LC-MS [94]. As peptide fractionation by OG IEF has been shown to provide excellent separation [95, 96] and thus avoids redundant analysis of peptides in the following LC-MS analysis, this approach was chosen for the present study where appropriate.

1.5.3. Quantitative mass spectrometry

Viral infections affect host protein synthesis, modifications and degradations of proteins, which leads to qualitative and quantitative differences in the proteomes of infected compared to healthy cells. Thus, quantitative MS is required to record changes of protein abundances that have been induced by a viral infection. One option for quantitative MS is the introduction of a stable isotope label into the sample representing a certain biological state (e.g. after infection) followed by the analysis of the samples as a mixture with the unlabeled samples representing e.g. the mock infected state. One well-established labeling method is stable isotope labeling by amino acids in cell culture (SILAC) [97]. With this technique, the relative protein abundances can be determined between two or more differentially stable isotope labeled cell cultures. The principle of SILAC was extended to *in vivo* studies and several SILAC mice have been generated [98, 99]. The isotopes are introduced by passaging of the cell cultures in media with isotopomers of essential amino acids. If trypsin is used as protease, labeling with lysine and arginine residues will, with the exception of the carboxy-terminal peptide, produce exclusively

labeled peptides as trypsin will cleave proteins at the carboxy terminus of these essential amino acids. As soon as the exchange of the isotope labeled amino acids in the proteins is complete, the infection experiments can be conducted. Infected and mock-infected cells are harvested and mixed in equal amounts. Thus, a global internal standard is established early in the proteomic workflow and the risk to introduce any quantitation artifacts during the downstream analyses is minimized. After MS analysis of the peptides the ratio of peak intensities of labeled peptides can be used to quantitate the relative protein expression level in the different cell batches. For samples that cannot be isotope labeled metabolically such as tissue sections or certain primary cells which cannot be passaged, the isotope label has to be introduced by a chemical reaction, e.g. by reductive alkylation [100] of the proteolytic peptides. Primary amino groups, hence all unmodified protein or peptide N-termini and the ϵ -side chains of lysine residues, can be labeled by reductive dimethylation using isotopomers of formaldehyde and sodium cyanoborohydride (**Figure 6**) [101]. After formation of the Schiff base between the primary amino group and the aldehyde, reduction with cyanoborohydride results in the formation of a methylated product which is similarly converted into the dimethylated form.

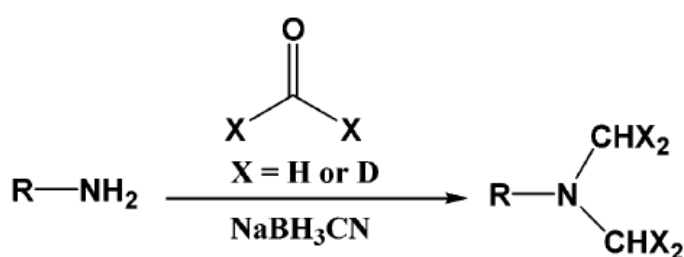


Figure 6 Dimethyl labeling reaction (taken from Hsu *et al.* [100]). Formaldehyde reacts with primary amino groups to form a Schiff base, which is reduced by sodium cyanoborohydride to a secondary amine, which readily reacts with another formaldehyde to form a dimethyl amino group.

The precision of isotope-based quantitation depends on the point in the analytical workflow where the samples are differentially labeled and mixed and the global internal standard is established. Hence,

the major disadvantage of reductive demethylation is the introduction of the label at one of the last steps of analysis. This makes the method slightly more imprecise than SILAC, but the chemical reaction is robust, economic and more flexible than the metabolic incorporation [101, 102].

MS-based quantitation of protein expression can also be carried out without isotope label [103] for estimation of protein abundance in the analyzed samples. For label-free quantitation, the different samples are analyzed separately and the amount of protein can be calculated on basis of different chromatographic or mass-spectrometric parameters such as the chromatographic peak intensity, spectral counting, or algorithms based on the sequence coverages of the proteins in the different samples [104]. The spectral counting method relies on comparison of the number of identified MS/MS spectra for the same proteins and gives an indication of the relative protein abundance, as for higher abundant proteins more proteolytic peptides are identified, which results in higher total number of identified MS/MS spectra [104]. Similar methods include the counting of precursor or fragment ion signals in the MS/MS spectra associated with the identified proteins [103]. The protein abundance index is calculated by dividing the number of measured peptides by the number of theoretical possible peptides for the protein. The precision of the PAI can be improved by conversion to the exponentially modified protein abundance index (emPAI), which has been defined as $10^{PAI}-1$ [105]. Calculation of a modified emPAI using 6.5 as exponential base has been shown to be even more precise [106]. The emPAI can be used to calculate the mole percentage of every protein that has been identified in a mixture on basis of the following formula:

$$protein\ content\ [mol\ \%] = \frac{emPAI}{\sum(emPAI)} \times 100.$$

The calculation of the emPAI is implemented in different proteomic softwares.

1.5.4. Quality of database

The quality of the results of a mass spectrometric proteome analysis does not only depend on the optimal sample preparation, fractionation technique and mass spectrometer, but also on the sequence

database that is used by the search engines, for example the Mascot software used in this study. Protein databases are in large parts calculated from genomic sequences by application of bioinformatic software. The identification process relies on the quality of the calculated protein sequences, which for many farm and companion animals lags behind the better established databases for *Homo sapiens* and some small animal models like *Mus musculus*. Recently, also RNA sequencing data are used to support and improve existing genomic databases with transcriptome data or even generate databases for organisms for which so far no complete genomic DNA sequences are available, which are then used in proteomic analysis [107]. This approach is referred to as ‘proteomics informed by transcriptomics’ (PIT).

Insufficient database quality is also an issue concerning the functional annotation of genes that can be found in the Gene Ontology (GO, [108, 109]) knowledgebase, which is used to identify pathways involved in the infection or transformation process. While 1,020,731 annotations are assigned to 97,713 human proteins, and 879,061 annotations to 65,106 murine proteins, only 189,307 annotations are found for 16,555 chicken proteins (information retrieved from <https://www.ebi.ac.uk/QuickGO/> [110], accessed 22.11.2016). Hence, for the evaluation of proteomics results from less well characterized species by Gene Ontology term enrichment analysis, e.g. with the Search Tool for the Retrieval of Interacting Genes/Proteins (STRING, [111]), the identified proteins have to be cross-referenced to the corresponding human orthologs, which are then used as input for the analyses. However, one has to keep in mind that not all identified proteins have human orthologs or some may have different functionality in the different species so that some information might be lost or results may be misleading.

1.6. Difficulties with proteomic analysis of MD tumors

In the past, several studies have investigated the host response and changes in the host proteome during infection and transformation with MDV. Yet, the characterization of the protein expression profiles of transformed cells was mainly based on analyses of whole organs which are a mixture of

different cell types including healthy and transformed cells, connective tissue and several different cell types [55, 60, 112, 113]. The infection by MDV is highly asynchronous and the tumors are present in different stages and sizes. Usually the normal organ cells are highly abundant in comparison to tumor cells, leading to a dilution of tumor-specific proteins with proteins from unaffected cells in the extract and thus, to a low sensitivity for the detection of tumor markers. In addition, the tumors originate from transformed T cells and not from the affected organ itself. Thus, differences between transformed and naïve T cells have to be differentiated from the different protein expression profiles in T cells and cells from the affected organ.

1.6.1. Laser-capture microdissection

Non-contact laser capture microdissection (LCM) can be used to specifically excise under direct microscopic visualization areas of interest from tissue sections with as little as possible contamination from surrounding tissue. The LCM technology consists of three basic components: the visualization of target cells in a microscope, the transfer of laser energy to a thermolabile polymer or photo volatilization of cells surrounding the region of interest and finally, the capture of the targeted area from the tissue section triggered by a laser pulse. The Zeiss P.A.L.M. Microbeam uses a UV laser to dissect the region of interest from a polyethylene tetrathalate (PET) membrane slide. The dissected area is then catapulted into an adhesive cap of a microcentrifuge tube placed above the cut area (**Figure 7**) [114].

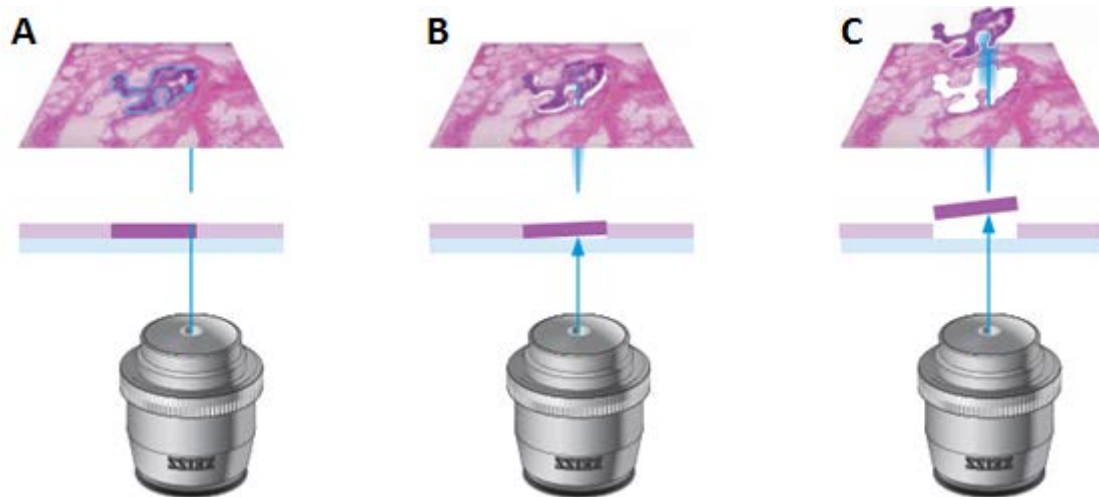


Figure 7 Schematic picture of non-contact LCM with Zeiss P.A.L.M. microbeam. A) The laser cuts the region of interest without contamination from surrounding tissue. **B)** The non-contact transfer is triggered with a single laser pulse. **C)** The region of interest is lifted from the membrane slide into the capture device.

Taken from the Zeiss website:

([https://applications.zeiss.com/C125792900358A3F/0/6C2B4E91AA6FD4C7C12579E500342F41/\\$FILE/60-3-0001_PALM-Familie_d.pdf](https://applications.zeiss.com/C125792900358A3F/0/6C2B4E91AA6FD4C7C12579E500342F41/$FILE/60-3-0001_PALM-Familie_d.pdf))

LCM is a versatile technique that can be applied to tissue sections irrespective of most prior treatments like hematoxylin and eosin (H&E) staining, formalin fixation, or paraffin embedding [115, 116]. After dissection and capture of the cells of interest, DNA, RNA, or proteins can be extracted, depending on the intended downstream analysis. These characteristics made LCM the method of choice for preparation of the MD tumors for the proteomic analysis conducted in this thesis.

2. Objectives and analytic strategy

The aim of this study was to unravel the molecular mechanisms during infection and transformation of lymphocytes by Marek's disease virus using MALDI TOF/TOF mass spectrometry. Infection with MDV can be divided into two major phases, the lytic phase and the latent phase, which includes the transformation of T lymphocytes. This study aimed at the characterization of the proteomes of MDV-infected lymphocytes during these two phases.

The recently improved *in vitro* cultivation system for primary lymphocytes [61] and the availability of MDV deletion mutants constructed using the BAC technology were the basis for the quantitative mass spectrometric studies presented here.

The first part of this doctoral thesis focused on the quantitative proteome analysis of infected primary B cells, the first target of lytic MDV infection. The aim was to identify potential infection markers in the natural target cells, which can give indications on the cellular processes involved in MDV infection. As MDV infection rates *in vitro* are rather low, my collaboration partner at the FU Berlin, Luca Bertzbach, used GFP labeled recombinant viruses that allowed the isolation of infected cells by FACS before proteome analysis.

The second part of the thesis focused on the latency and transformation phase of MDV infection. The major objective was the proteome analysis of MD tumors in visceral organs. The primary aim was to identify possible transformation markers in tumors that had developed in the livers of *in vivo* infected animals. In addition, the role of the viral telomerase RNA during transformation was to be elucidated by comparison of tumors that had formed after infection with WT-virus or a telomerase RNA negative mutant. Tumor samples were prepared from tissue sections using the LCM technology in order to minimize any contamination from the surrounding organ tissue.

For both parts of the thesis, the analysis of infected B cells and of micro-dissected tumor samples, efficient proteomic workflows were developed, which consisted of a filter-aided digest of the extracted

proteins, followed by differential dimethyl chemical labeling of the peptides for quantitative evaluation prior to LC-MALDI TOF/TOF mass spectrometry.

3. Materials

3.1. Animals

All the animals used in this study were healthy White Leghorn chickens hatched from SPF eggs (Valo Biomedia). All animal work was approved by the appropriate government agencies (Landesamt für Gesundheit und Soziales (LAGeSO, approval numbers G0218-12 and T0245-14).

3.2. Chemicals

All chemicals were of highest purity available suitable for chromatography and mass spectrometry.

| Chemicals/materials | Company |
|---|------------------------|
| α -cyano-4-hydroxycinnamic acid (Cat.nr.: 70990-1G-F) | Fluka Analytical |
| Acetonitrile (Cat.nr.: 34967-1L) | Fluka Analytical |
| Acrylamide (Cat.nr.: 7871.2) | Carl Roth |
| Agarose (Cat.nr.: 850111) | Biozym Scientific GmbH |
| Ammonia solution (Cat.nr.: 105426) | Merck |
| Ammonium hydrogen carbonate (Cat.nr.: 101131) | Merck |
| Ammonium peroxodisulfate (Cat.nr.: 101201) | Merck |
| Ammonium sulfate (Cat.nr.: 101216) | Merck |
| Aquatex (Cat.nr.: 108562) | Merck |
| Boric acid (Cat.nr.:5935.1) | Carl Roth |
| Bovine serum albumin (BSA, Albumin fraction V, Cat.nr.: 112018) | Merck |
| Bromophenol blue sodium salt (Cat.nr.: B8026) | Sigma-Aldrich |
| Coomassie® brilliant blue G-250 (Cat.nr.: 17524) | Serva |
| DL-Dithiothreitol (DTT; Cat.nr.: D9779-25G) | Sigma-Aldrich |
| Eosin G (Cat.nr.: 115935) | Merck |
| Ethanol (Cat.nr.: 9065.3, 1l) | Carl Roth |
| Ethidium bromide solution (Cat.nr.: 2218) | Carl Roth |

| | |
|--|------------------|
| Ethylenediamine-tetraaceticacid 2N 2H ₂ O (Cat.nr.: 8043.2) | Carl Roth |
| Eukitt® quick hardening mounting medium (Cat.nr.: 03989) | Sigma-Aldrich |
| Formaldehyde solution (37 wt. % in H ₂ O, Cat.nr.: 252549-100ml) | Sigma-Aldrich |
| Formaldehyde-d ₂ solution (20 wt. % in D ₂ O, Cat.nr.: 492620-20G) | Sigma-Aldrich |
| Formic acid (Cat.nr.: 84865.260, 500ml) | VWR Chemicals |
| Glycerol (Cat.nr.: 3783.1) | Carl Roth |
| Hydrochloric acid, fuming (Cat.nr.: 4625.1) | Carl Roth |
| Hydrogen peroxide (31 %, Cat.nr.: HN69.1) | Carl Roth |
| Hematoxylin (Cat.nr.: 517-28-2) | Merck |
| Isopropanol (Cat.nr.: 6752.3) | Carl Roth |
| Iodoacetamide (IAA, Cat.nr.: I1149) | Sigma-Aldrich |
| Methanol (Cat.nr.: 4627.4) | Carl Roth |
| N,N'-Methylene-bis-acrylamide (Cat.nr.: 7867.1) | Carl Roth |
| N,N,N',N'-Tetramethylethylenediamine (Cat.nr.: T9281-25ml) | Sigma-Aldrich |
| Ortho-phosphoric acid (Cat.nr.: 100573) | Merck |
| Phloxine B (Cat.nr.: 115926) | Merck |
| Sodium dodecyl sulfate (SDS, Cat.nr.: 2326.2) | Carl Roth |
| Sodium cyanoborohydride (Cat.nr.: 71435-10G) | Fluka Analytical |
| Tetramethylethylenediamine (TEMED, Cat.nr.: GE17-1312-01) | Sigma-Aldrich |
| Trichloromethane (Cat.nr.: 3313.1) | Carl Roth |
| Triethylamine (Cat.nr.: 808352) | Merck |
| Trifluoroacetic acid (TFA, Cat.nr.: T6508-5x10AMP) | Sigma-Aldrich |
| Tris(2-carboxyethyl)phosphine hydrochloride (TCEP, Cat.nr.: C4706-24) | Sigma-Aldrich |
| UltraPure™ Tris (Cat.nr.: 15504-020) | Invitrogen |
| Urea (Cat.nr.: 75826) | USB Corporation |
| Xylene (Cat.nr.: 4436.1) | Carl Roth |

3.3. Viruses

Recombinant viruses expression GFP under the control of the HSV-1 TK promoter were previously generated based vaccine strain CVI988 Rispens (vCVI988-TK-GFP) and the very virulent RB-1B (vRB-1B-TK-GFP) [50, 53]. Primary lymphocytes were infected with vCVI988-TK-GFP and vRB-1B-TK-GFP were reconstituted and propagated by Luca Bertzbach (FU Berlin). The Δ vTR RB-1B mutant used in the *in vivo* studies was constructed as described by Kheimar et al. [54].

3.4. Enzymes, antibodies and size markers

| Enzymes/size markers | Company |
|---|--------------------------|
| 50 bp DNA ladder (Cat.nr.: M-213-S) | Jena BioScience |
| AEC+ substrate chromogen (Cat.nr.: K346111-2) | Agilent (Dako) |
| Biotinylated Goat anti-rabbit IgG antibodies (Cat.nr.: BA-1000) | Vector laboratories |
| CD3 (polyclonal rabbit anti-human, Cat.nr.: GA50361-2) | Agilent (Dako) |
| PageRuler™ prestained protein ladder (10-180 kDa, Cat.nr.: 26616) | ThermoFischer Scientific |
| Trypsin (Cat.nr.: V511A) | Promega Corporation |

3.5. Buffers

3.5.1. Buffers for SDS-PAGE

| Buffer | Supplier/ reference | Composition |
|---|-----------------------------|---|
| 4x protein sample buffer | prepared according to [117] | 0.5 M Tris-HCl (pH 8.6) 8 % SDS 0.16 % bromophenol blue 40 % glycerol 2 % DTT |
| Ammonium sulfate/phosphoric acid stock solution | prepared according to [118] | 10 % ammonium sulfate 2 % phosphoric acid (w/vol) in deionized water |

Materials

| | | |
|--|-----------------------------|--|
| Coomassie stain solution | prepared according to [118] | 1 ml CBB stock solution 20 ml methanol Ammonium sulfate/phosphoric acid stock solution was added to 100 ml |
| Coomassie (CBB) stock solution | dto. | 10 % Coomassie® blue G250 (w/vol) in 50 % methanol |
| Separating buffer for SDS-PAGE 7.5 % gel | prepared according to [117] | 40 ml for 13 gradient minigels: 19.5 ml deionized water 10 ml Tris (1.5 M, pH 8.8) 10 ml Acrylamid/Bisacrylamid (30 %/1 %) 400 µl SDS solution (10 %) 20 µl TEMED 200 µl AMPS solution (10%) |
| Separating buffer for SDS-PAGE 15 % gel | dto. | 40 ml for 13 gradient minigels: 9.5 ml deionized water 10 ml Tris (1.5 M, pH 8.8) 20 ml Acrylamid/Bisacrylamid (30 %/1 %) 400 µl SDS solution (10 %) 20 µl TEMED 200 µl AMPS solution (10%) |
| Stacking gel for SDS-PAGE 4 % | dto. | 40 ml (for 13 minigels): 24.4 ml deionized water 10 ml Tris (0.5 M, pH 6.8) 5.2 ml Acrylamid/Bisacrylamid (30 %/1 %) 400 µl SDS solution (10 %) 40 µl TEMED 200 µl AMPS solution (10 %) |

3.5.2. Buffers for cell lysis and digestion

| Buffer | Supplier/ reference | Compostion |
|------------------------------|-----------------------------|------------------------------------|
| Iodoacetamide (IAA) solution | Prepared according to [119] | 0.1 M iodoacetamide in urea buffer |

| | | |
|--|-----------------------------|--|
| Lysis buffer | prepared according to [120] | 0.1 M Tris (pH 8.0 adjusted with HCl) 0.1 M DTT 2 % SDS |
| RapiGest™ SF (Cat.nr.: 186001861) | Waters, Eschborn | |
| Triethyl ammonium bicarbonate (TEAB) | | 1M triethylamine was titrated to pH 8.0 by introduction of CO ₂ and was diluted to 0.1 M immediately before use |
| Trypsin resuspension buffer (Cat.nr.: V542A) | Promega | 50mM acetic acid |
| Urea buffer (UB) | Prepared according to [119] | 8M Urea in 0.1 M Tris-HCl (pH 8.5) |

3.5.3. Buffers for OFFGEL IEF

| Buffer | Supplier/ reference | Composition |
|---|----------------------------|--|
| OFFGEL/ IPG buffer (ampholytes, pH 3-10, Cat.nr.: 17-6000-87) | GE Healthcare | |
| OFFGEL resuspension buffer | Prepared according to [95] | 20 % methanol, 1 % IPG buffer in deionized water |

3.5.4. Buffers for agarose gels

| Buffer | Supplier/ reference | Composition |
|--|-----------------------------|---|
| 6x DNA loading dye (R0611) | Thermo Scientific | 10 mM Tris-HCl (pH 7.6) 0.03 % bromophenol blue 0.03 % xylene cyanol FF 60 % glycerol 60 mM EDTA |
| Tris-borate-EDTA buffer (TBE-buffer, 10 x) | Prepared according to [121] | 55.03 g Boracic acid (0.89 M) 7.44 g EDTA-Na ₂ (0.02 M) 107.81 g Tris base (.089 M) in 1l deionized water |

3.5.5. Buffers for Immunohistochemistry

| Buffer | Supplier/ reference | Composition |
|----------------------|-----------------------------|--|
| 10 x TBS | dto. | 60.57 g Tris-HCl 80.0 g NaCl In 500 ml deionized water pH adjusted to 7.65 with HCl |
| Citrate buffer | dto. | 3.94 g NaCl 4.2 g Citric acid 0.372 g KCl Deionized water was added to 500 ml |
| Eosin/Phloxine | Prepared according to Mayer | 20 ml eosin 2 ml phloxine 156 ml ethanol 0.8 ml acetic acid |
| Hematoxylin solution | Prepared according to Mayer | 10 g hematoxylin 200 mg Sodium iodate 50 g potassium alum 50 g chloral hydrate 1 g citric acid in 1 l deionized water |

3.6. Kits

The following kits were used for immunohistochemistry, RT-PCR and RNA sequencing and were purchased from Vector Laboratories (Vectastain Elite® ABC HRP kit (Cat.nr.: PK-6100)), [Qiagen](#) (RNeasy Mini Kit (Cat.nr.: 74104), RNase-free DNase set (Cat.nr.: 79254), QIAquick Gel Extraction Kit (Cat.nr.: 28104), GeneRead™ DNA (L) Amp Kit (Cat.nr.: 180485)), [Invitrogen](#) (SuperScript III One-Step RT-PCR with Platinum *Taq* (Cat.nr.: 12574-026)), [Agilent technologies](#) (Agilent DNA 7500 Kit (Cat.nr.: 5067-1506), Agilent RNA 6000 Pico Kit (Cat.nr.: 5067-1513), [Life technologies](#) (IonXpress RNA-Seq Barcode 01-16 Kit (Cat.nr.: 447585), Ion Total RNA-seq Kit v2 (Cat.nr.: 4475936), Dynabeads mRNA DIRECT MicroKit (Cat.nr.: 61021), (Ion 540™ Kit-OT2 Kit (Cat.nr.: A27753), KAPA Library Quantification Kit (Cat.nr.: KK4824)), [Beckman Coulter](#) (Agencourt AMPure XP Kit (Cat.nr.: A63881)) and [VWR](#) (qScript™

One-Step SYBR® Green qRT-PCR Kit (Cat.nr.: 733-2080)). All reagent sets were used according to the manufacturers recommendations, which are described in more detail in the methods part.

3.7. PCR Primers

The primers used in this study were designed using the NCBI tool ‘Primer-BLAST’ (<https://www.ncbi.nlm.nih.gov/tools/primer-blast/>) [122] and the primer design tool from Eurofins genomics (<https://www.eurofinsgenomics.eu/de/ecom/tools/pcr-primer-design.aspx>).

| NCBI Reference Sequence | Gene Name | Primer Sequence | Product size |
|-------------------------|--|---------------------------------|--------------|
| NM_205518.1 | actin, beta (ACTB) | F: 5'-GAGAAATTGTGCGTGACATCA-3' | 152 bp |
| | | R: 5'-CCTGAACCTCTCATTGCCA-3' | |
| | | F: 5'-TGCTACGTCGCACTGGATTT-3' | 149 bp |
| | | R: 5'-AAAGATGGCTGGAAGAGGGC-3' | |
| NM_204305.1 | glyceraldehyde-3-phosphate dehydrogenase (GAPDH) | F: 5'-AATGGCTTCCGTGTGCCAACC-3' | 223 bp |
| | | R: 5'-ATTCAGTGCAATGCCAGCACCC-3' | |
| NM_001012576.1 | heat shock protein family A member 4 like (HSPA4L) | F: 5'-TGGCGACAACCTCCAAAGTGA-3' | 129 bp |
| | | R: 5'-TCAGTATCCATCGCTGCGTC-3' | |
| NM_205041.1 | 2'-5'-oligoadenylate synthetase like (OASL) | F: 5'-AGGTCCTGGTGAAGGACAGT-3' | 145 bp |
| | | R: 5'-TCCAGCTCCTTGGTCTCGTA-3' | |
| NM_001135968.1 | transporter 1, ATP-binding cassette, sub-family B (TAP1) | F: 5'-ACGACTTCATCACTCGCCTGC-3' | 280 bp |
| | | R: 5'-TCCAACACCACCACTCGTTGTG-3' | |
| XM_418246.5 | interferon gamma-inducible protein 30 (IFI30) | F: 5'-CGCTCAGGAGAGGAATGTCT-3' | 181 bp |
| | | R: 5'-GCAAGCCTTCAGATTCTTGG-3' | |
| XM_004936995.2 | p21 protein (Cdc42/Rac)-activated kinase 2 (PAK2) | F: 5'-CTCCATGCCAACCAGGTCAT-3' | 179 bp |
| | | R: 5'-TTCCGTGTGACGACTTCAGG-3' | |
| NM_001031451.1 | FYN binding protein (FYB) | F: 5'-GCCCCAAAACGGAAGTCTTTGC-3' | 256 bp |
| | | R: 5'-TGGGCTTGACATTTCTGGGCG-3' | |
| NM_001030753.1 | H2A histone family, member J (H2AFJ) | F: 5'-AGGCCAAGTCGCGTTCATC-3' | 148 bp |
| | | R: 5'-ATCTCGGCCGTCAGGTACT-3' | |
| XM_015296999.1 | regulator of chromosome condensation 2 (RCC2) | F: 5'-CTGGTTGTAGGCTTGAGCA-3' | 146 bp |
| | | R: 5'-TGAGGAAGGAGGGTGGGAAA-3' | |
| NM_205342.1 | lamin B receptor (LBR) | F: 5'-GCAAACAAGATGACCCCAGC-3' | 150 bp |
| | | R: 5'-GGCCTTCCACAACCTTCTCT-3' | |
| XM_001231970.4 | glutathione S-transferase theta 1-like (GSTT1L) | F: 5'-AACAGGCCAGGGTTGATGAG-3' | 137 bp |
| | | R: 5'-AGCACCTTCCACTTTCTCCG-3' | |

| | | | |
|-----------------------|---|--|--------|
| XM_015298483.1 | interleukin enhancer binding factor 2 (ILF2) | F: 5'-ATCAGACACGCTCGTTGGTT-3' R: 5'-TAGTGCCCCAGCAAATCCAG-3' | 140 bp |
| NM_001292069.1 | proteasome 26S subunit, ATPase 5 (PSMC5) | F: 5'-TGAGTTGCCAGTCAAGCACCC-3' R: 5'-ATCACAAACAGCTCCCGCACC-3' | 216 bp |
| XM_417710.4 | interferon-induced guanylate-binding protein 1-like (LOC419563) | F: 5'-AGTCAGGGAGGCAGAGGTAG-3' R: 5'-CTGATGTTCTTCAGGCGGT-3' | 151 bp |
| M75729 | Marek's disease virus 175 kDa protein (ICP4) gene | F: 5'-TTTCTAGCAAGGAGCGACGC-3 R: 5'-CTGACTTGCGCTTACGGGAA-3 | 81 bp |

3.8. Apparatus and equipment

| Apparatus/equipment | Company |
|---|--------------------------|
| 1536 BC Anchor chip target | Bruker |
| 2720 Thermal Cycler | Applied Biosystems |
| 384 MTP Anchor chip target (800 anchor) | Bruker |
| 3100 OFFGEL fractionator | Agilent Technologies |
| Acclaim PepMap100 (75 µm x 15 cm, C18, 3 µm, 100 Å, analytical column, Cat.nr.: 160321) | ThermoFischer Scientific |
| Agilent 2100 Bioanalyzer | Agilent Technologies |
| BD FACSAria™ Fusion cell sorter | BD Biosciences |
| Bio-Rad Gel Doc™ XRt Molecular imager | Bio-Rad |
| Branson digital sonifier 450D | G.Heinemann |
| C1000™ Thermal Cycler | Bio-Rad |
| Cell strainer (Falcon™, 100µm micron pores, nylon mesh) | ThermoFischer Scientific |
| Centrifuge 5430 R | Eppendorf |
| CFX96 Touch™ Real-Time PCR Detection System | Bio-Rad |
| Chip Priming station (Cat.nr.: 5065-4401) | Agilent Technologies |
| Cryostat HM 560 Cryostar | Microm International |
| DNA/RNA UV-Cleaner UVC/T-M-AR | BioSan |
| EASY-nLC II chromatographic system | Bruker |

| | |
|--|-----------------------------|
| Galaxy Mini | VWR |
| Heraeus Pico17 Centrifuge | Thermo Electron Corporation |
| Ion S5™ XL next-generation sequencing System | ThermoFischer Scientific |
| Mastercycler epgradient S | Eppendorf |
| NS-MP-10 pre-column (C ₁₈ -modified Silica gel matrix, 5 µm bead size, inner diameter 100 µm, length 20 mm) | BioSphere |
| PALM MicroBeam instrument | Zeiss, Jena |
| Primus 96 Plus Thermal cycler | MWG-Biotech |
| Proteineer fcll sample spotting robot | Bruker |
| Rotisserie (Laquake Shaker/Rotisserie, Cat.nr.: 3,625,485) | Barnstead Thermolyne |
| Thermomixer comfort | Eppendorf |
| UltrafleXtreme MALDI-TOF/TOF mass spectrometer | Bruker |
| Univapo vaccum concentrator centrifuge (150H) | UniEquip |
| Vacuum system (BVC 21 NT, max. vacuum: 150 mm Hg) | Vacuubrand |
| Vortex-Genie 2 | Scientific Industries |

3.9. Consumables

| Consumables | Supplier |
|---|------------------------|
| AdhesiveCap (200 µl, opaque (D) PCR tubes, Cat.nr.: 415190-9181-000) | Zeiss |
| Capillary tips (200 µl, 0.57 mm AD, for gel pockets ≥ 0.6 mm, Cat.nr.: 728204) | Biozym |
| Conical tubes (15 ml, non-pyrogenic, polypropylene, Cat.nr.: 16.554.502) | Sarstedt |
| Conical tubes (50 ml, DNA- , DNase, RNase free, non-pyrogenic, Cat.nr.: 62.547.254) | Sarstedt |
| Disposable cuvettes (1.5 ml semi-micro, 759115) | BRAND GmbH |
| Empore™ Solid Phase Extraction Cartridges (C18-SD, 7mm/3ml, Cat.nr.: 4215SD) | Supelco, Sigma-Aldrich |
| Filter tips PP (0.1-10 µl, long, Cat.nr.: 07-612-8300) | Nerbe plus |

| | |
|--|-------------------------------|
| Filter tips PP (0-100 µl, Cat.nr.: 07-642-8300) | Nerbe plus |
| Filter tips PP (100-1000 µl, Cat.nr.: 07-693-8300) | Nerbe plus |
| Gloves (ecoSHIELD™, Eco Nitril, PF250, Cat.nr.: 62 5122) | SHIELD Scientific |
| Immobiline DryStrip (pH 3-10, 13cm, Cat.nr.: 17-6001-14) | GE Healthcare |
| Low bind reaction tubes (1.5 ml, Cat.nr.: 04-210-1100) | Nerbe plus |
| MembraneSlide 1.0 PEN (25 x 75 mm, Cat.nr.: 415190-9041-000) | Zeiss |
| Micro tips premium (10 µl, Cat.nr.: 720011) | Biozym |
| PCR caps (Optical Flat 8-cap strips, for 0.2 ml tube strips, Cat.nr.: TCS0803) | Bio-Rad |
| PCR tubes (individual, 8-tube strip, clear, Cat.nr.: TLS0801) | Bio-Rad |
| Pipette tips (10-200 µl, universal, Cat.nr.: 739290) | Greiner Bio-One International |
| Pipette tips (200-1000 µl, blue, Cat.nr.: 686290) | Greiner Bio-One International |
| Safe lock tubes, 1.5 ml tubes® (Cat.nr.: 0030120.086) | Eppendorf |
| UVette® routine pack (Cat.nr.: 952010069) | Eppendorf |
| Vinyl 2000 PF gloves (non-powdered, latex-free, Cat.nr.: 1251S) | Meditrade |
| Vivacon® 500, 10.000 Da, hydrosart membrane (Cat.nr.: VN01H02) | Sartorius, Göttingen |
| Vivacon® 500, 30.000 Da, hydrosart membrane (Cat.nr.: VN01H22) | Sartorius |
| Pierce™ C ₁₈ tips (Cat.nr.: 87782) | ThermoFischer Scientific |

3.10. Softwares

| Software/database | Supplier/websites |
|---------------------------------------|--------------------------------|
| 2100 Expert Software version C.01.069 | Agilent Technologies |
| Aida Image Analyzer v5.0 | Raytest Isotopenmeßgeräte GmbH |
| BD FACSDiva v6.2 | BD Biosciences |
| Bio-Rad CFX Manager 3.1 | Bio-Rad |
| FlexAnalysis v3.4 | Bruker |
| FlexControl v3.4 | Bruker |

| | |
|--|---|
| g:profiler/g:cacao | http://biit.cs.ut.ee/gprofiler/ http://biit.cs.ut.ee/gprofiler/gcocoa.cgi [123] |
| HALO™ Image Analysis System v.1.90.61.2327 | Indica Labs |
| HyStar v3.2 | Bruker |
| Image Lab v5.2.1 | Bio-Rad |
| Torrent Suite v5.6.0 | ThermoFischer Scientific |
| Ion Torrent S5 XL Server | ThermoFischer Scientific |
| Mascot Server v2.4.1 | Matrix Science |
| PALM® RoboSoftware v4.5 | Zeiss |
| ProteinScape software v3.0 | Bruker |
| QuickGO | https://www.ebi.ac.uk/QuickGO/ [110] |
| RStudio v1.0.143 | RStudio, Inc [124] |
| R | |
| SigmaPlot v11.0 | Systat Software, Inc. |
| STRING protein-protein interaction | http://string-db.org/ [125] |
| Warp-LC v1.3 | Bruker |

4. Methods

4.1. Proteome analysis of naïve primary chicken lymphocytes

Primary B and T cells were isolated from the bursa of Fabricius or thymus, respectively, of three 8 to 14 week-old healthy chickens by my collaboration partner Luca Bertzbach at the FU Berlin. The cells were obtained by grinding the organs mechanically through 0.4 μm cell dissociation sieves. B and T cells were isolated by centrifugation on Biocoll separating solution (density 1.077 g/ml) for 12 min at 650 x g at room temperature (rt). The lymphocyte layer was removed and washed twice with PBS. Aliquots with 3×10^6 to 10^7 lymphocytes, were prepared and stored at -80°C before analyses.

4.1.1. In-solution digestion

For in-solution digestion 3×10^6 cells of each cell type were lysed in 20 μl 0.1 % RapiGestTM SF according to manufacturer's protocol. Samples were heated for 1 h at 60°C and subsequently sonicated for 5 min in 10 sec intervals with an amplitude of 85 % (Branson digital Sonifier 450D). DL-Dithiothreitol (DTT) was added to a final concentration of 5 mM and samples were incubated for 45 min at 60°C . Subsequently, iodoacetamide (IAA) was added to a final concentration of 15 mM and the samples were incubated for 30 min in the dark. Trypsin was added in an enzyme: substrate ratio of 1:50 and the samples were digested for 16 h at 37°C . After the digest, the RapiGest was removed by acidifying the samples to pH 2 with 10 % trifluoroacetic acid (TFA) followed by centrifugation. The peptides in the supernatant were desalted with C₁₈-tips according to the standard protocol.

4.1.2. Desalting of the labeled peptides with PierceTM C18 Tips

Acidified samples were desalted using 100 μl PierceTM C18 tips for up to 80 μg of peptide samples. Tips were wetted twice with 100 μl 50 % acetonitrile (ACN) and equilibrated twice with 100 μl 0.1 % TFA. Subsequently, the sample was loaded onto the tip by pipetting up and down ten times. Excess salt was removed by washing the sample twice with TA05 (5 % ACN/ 0.1 % TFA). The sample was eluted into a

new reaction tube with 100 µl TA65 (65 % ACN / 0.1 % TFA) by aspirating and dispensing in three cycles.

The samples were concentrated *in-vacuo*.

4.1.3. Lysis of cells and protein extraction

Equal amounts (2×10^7 cells) of each isolated T or B cells were lysed in 400 µl lysis-buffer (0.1 M DTT, 2 % SDS, 0.1 M Tris-HCl, pH 8.0). Samples were heated for 10 min at 95 °C and sonicated for 5 min in 10 sec intervals with an amplitude of 85 %. The samples were centrifuged for 5 min at 14,000 x g and rt. The supernatant was carefully removed and used in the following FASP digest.

4.1.4. Filter aided sample preparation (FASP) digest

Duplicate samples for each lymphocyte type were processed. The FASP digest was carried out according to standard protocol [119] with minor changes. Divergent from the standard FASP protocol, ammonium bicarbonate was replaced by 0.1 M TEAB in the digestion buffer for compatibility with the following dimethyl labeling. Filter units (Vivacon® 500, 30.000 Da) were used together with porcine sequencing grade modified trypsin in an enzyme: substrate ratio of 1:50. In short, the extracted proteins were loaded into separate Vivacon filter units and centrifuged for 15 min at 20,000 x g at 20 °C. These centrifugation conditions were used for all following concentration and washing steps. The samples were washed thrice with UB (Urea buffer, 8 M Urea in 0.1 M Tris-HCl [pH 8.5]) and alkylated by resuspension in 100 µl 0.1 M IAA (iodoacetamide in 8 M UB) for 20 min in the dark. Excess IAA was removed by centrifugation and washing twice with 100 µl UB. The buffer was changed in two washing-centrifugation steps to 0.1 M triethyl ammonium bicarbonate buffer (TEABB) for digestion followed by dimethyl labeling. Trypsin was added to an enzyme: substrate ratio of 1:50 and additional 40 µl TEABB were added to filter units. The samples were digested for 16 h at 37 °C. The peptides were retrieved by centrifugation into clean reaction tubes. Fifty µl 0.1 M NaCl was added to the filter units to dissolve residual peptides, which were also recovered after a short incubation by centrifugation.

4.1.5. Dimethyl labeling

For quantitative mass spectrometry (MS) the peptides from primary B and T cells were differentially dimethylated with conventional and isotope labeled formaldehyde using the protocol by Boersma [101] with slight adjustments. Samples of both celltypes were labeled with either isotopomer and each MS analysis was carried out with two independent technical replicates with inverse labeling.

For the labeling reaction, the samples were diluted in 100 μ l TEABB and for every 25 μ g of peptides, 4 μ l 4 % formaldehyde isotopomer solution were added. After mixing, 4 μ l 0.6 M CNBH was added to reduce the formed Schiff base. The samples were incubated for 1 h at room temperature with gentle shaking. The reaction was stopped by addition of 16 μ l 1 % ammonia solution (32 %, EMPLURA®) and the samples were acidified by adding 10 μ l 10 % TFA to reach a $\text{pH} \leq 3$. Finally, the peptides were desalted on Empore™ Solid Phase Extraction Cartridges.

4.1.6. Modified FASP digest and dimethyl labeling as one-pot reaction

In order to reduce the risk of sample loss during the long workflow, we optimized the handling that digest and labeling reaction can be conducted in one filter unit. The FASP digest was performed as described under **4.1.4 Filter aided sample preparation (FASP) digest**. Following the FASP digest, the peptides were not retrieved by centrifugation but the dimethyl reagents were directly added to the filter units. Similar to the aforementioned protocol, for every 25 μ g of proteins 4 μ l 0.6 M sodium cyanoborohydride were added to both filtrates and 4 μ l 4 % formaldehyde solution (CH_2O for light label) or 4 μ l 4 % formaldehyde- d_2 -solution (CD_2O for heavy label) were added. The samples were incubated for 1 h at 23 °C with gentle shaking at 300 rpm. The reaction was stopped by addition of 16 μ l 1 % ammonia solution and the samples were acidified to a final pH lower than 3 by addition of 10-15 μ l 10 % TFA. After stopping the labeling reaction, the labeled peptides were retrieved by centrifugation. Thus, the samples were centrifuged for 15 min at 20,000 x g at 20 °C. Subsequently, in order to reduce sample loss 50 μ l 0.1 M TEABB was added to filter units and the samples were again centrifuged for 15 min at 20,000 x g at 20 °C.

4.1.7. Desalting of the labeled peptides with Empore™ Cartridges

The labeled peptides were desalted with Empore™ Solid Phase Extraction Cartridges (C18-SD) [119] placed in 15 ml conical tubes according to manufacturer's instructions with slight changes. The C18-SD membrane was wetted with 1 ml methanol, washed with 500 µl TA65 (65 % acetonitrile, 0.1 % TFA in deionized water (v/v/v)) and equilibrated in 500 µl 0.1 % TFA, each followed by centrifugation for 1 min at 1,000 x g. Samples were loaded to the membrane by centrifugation (800 x g for 1 min). For more complete sample binding, the flow-throughs were reloaded and passed through the membrane thrice by centrifugation (500 x g or 200 x g for 1 – 3 min). The membrane was washed twice with 500 µl 0.1 % TFA and the peptides were eluted by consecutive addition of 500 µl TA65 (200 x g for 3 min) and 200 µl TA65 (200 x g for 2 min). The combined eluates were concentrated by vacuum centrifugation.

4.1.8. OFFGEL Isoelectric focusing of labeled peptides

The light and heavy labeled desalted peptides were resuspended separately in 900 µl 20 % methanol, 1 % IPG buffer (suitable for pH 3-10, GE Healthcare) and then equally mixed (1:1 (v:v)). In total about 300 µg peptides were fractionated with a 3100 OFFGEL Fractionator (Agilent) following the manufacturer's recommendations. Briefly, peptides were equally distributed over the 12 chambers of the device and focused on Immobiline DryStrips (13 cm, pH 3-10, GE Healthcare) and focused by application of a maximum voltage of 4500 V, a maximum current of 50 µA per strip, and a maximum of 20kVh. After focusing, the fractions were concentrated in a vacuum centrifuge.

4.1.9. Comparison of OG IEF fractionation efficiency of labeled and unlabeled peptides

In order to evaluate the OG IEF fractionation efficiency of dimethyl labeled peptides, unlabeled and dimethyl labeled laser-dissected liver material were fractionated separately. Ten 5mm² cuts of a 20µm section were prepared as described in greater detail in section **4.3.5 Laser capture microdissection**. The tissues were lysed as described in **4.1.3 Lysis of cells and protein extraction** but 30 µl lysis buffer were added instead of 400 µl. The supernatants of the 5 aliquots were combined and 2 x 120 µg of proteins were digested with the FASP protocol described in **4.1.4 Filter aided sample preparation (FASP) digest**.

The peptides of one digest were split in two aliquots, and differentially labeled as described in **4.1.5** *Dimethyl labeling*. Both unlabeled and dimethyl labeled peptides were desalted as described in **4.1.7** *Desalting of the labeled peptides with Empore™ Cartridges* prior to OG IEF fractionation. The unlabeled and labeled peptides were fractionated on separate strips according to protocol described in **4.1.8** *OFFGEL isoelectric focusing of labeled peptides*.

4.1.10. Liquid chromatography and mass spectrometry

The in-solution digested samples and the OFFGEL fractions containing labeled and unlabeled peptides were analyzed on a nLC-MALDI-TOF/TOF platform. Peptides were separated based on hydrophobicity by nano liquid chromatography (EASY-nLC II, Bruker), spotted to a MALDI target by a connected Proteineer fcll sample spotting robot (Bruker), and analyzed with an UltrafleXtreme MALDI-TOF/TOF mass spectrometer (Bruker). Aliquots of each IEF fraction containing approximately 8 µg of protein were dissolved in 20 µl 0.1 % TFA and injected for desalting and concentration of the peptides on a NS-MP-10 pre-column with a C₁₈-modified silica gel matrix (5 µm bead size, inner diameter 100 µm, length 20 mm) and fractionated on the analytical column (Acclaim PepMap100, 75 µm x 15 cm, C₁₈, 3 µm, 100 Å) with a constant flow rate of 300 nl/min and a gradient of 2-45 % acetonitrile. The eluted peptides were mixed with saturated α-cyano-hydroxycinnamic acid (CHCA) matrix (Sigma-Aldrich) at a flow rate of 150 µl/h. For the T or B cell peptides from the in-solution digest the gradient was collected in 1360 fractions on a 1536 BC Anchor chip target (Bruker), whereas the gradient for the separate OFFGEL fractions was collected in 226 fractions. The fractions were then analyzed by mass spectrometry.

Acquisition was performed in positive mode and in the m/z range 700-3,500 Da. For each spot 40 fragment spectra were acquired for peaks with a signal-to-noise ratio (S/N) of at least 7. The spectra were processed by Flexanalysis software and identified using the Mascot software (version 2.4.1, Matrix Science, www.matrixscience.com). The query was sent to the ProteinScape software (Version 3, Bruker). The acquired spectra were matched against a database containing the protein sequences

from the complete *Gallus gallus* genome, complete MDV RB-1B gene sequences and common contaminants, such as keratin from human and sheep (sequences retrieved from ENSEMBL website on 29th of July 2016). The cut-off of missed cleavage of trypsin-digested samples was set to one. Oxidation of methionine, acetylation of protein N'-termini and the two forms of dimethylation of lysine and the N'-termini were set as variable modification, whereas the carbamidomethylation of cysteine was set as fixed modification. Identification results were sent from the Mascot server to the ProteinScape software (Version 3, Bruker) for further evaluation.

4.1.11. Statistical evaluation

4.1.11.1. Label-free quantitation

Label-free quantitation of the identified proteins was carried out on basis of the exponentially modified protein abundance index (emPAI, [105]) calculated by the Mascot software. The emPAI is used to estimate the amounts of proteins in a complex mixture by dividing the number of identified peptides by the number of observable peptides for every protein [105]. Since the PAI shows a linear relationship with the logarithm of protein concentration, the PAI is converted to the emPAI, the exponentially modified PAI, which gives a better estimation of the absolute abundance of one protein. For the calculation of the mole percentages of proteins the formula published by Ishihama et al. [105] was implemented using an in-house R script [124]. With differences in emPAI and correlating mole-% an estimation of the quantitative differences of the proteins in the two different lymphocyte populations were given.

4.1.11.2. Quantification based on isotope ratio

The quantitatively up- or down-regulated proteins were retrieved from the protein lists generated by ProteinScape. To facilitate the identification of truly regulated protein candidates an in-house R script was used, which removed peptides with irregular labeling from the peptide result lists calculated by Proteinscape software and indicated outlying isotope ratios probably caused by shared peptides. On

basis of a corrected median of peptide isotope ratios protein candidates that were characterized by at least 2-fold up or down regulation were identified and chosen for further manual analysis.

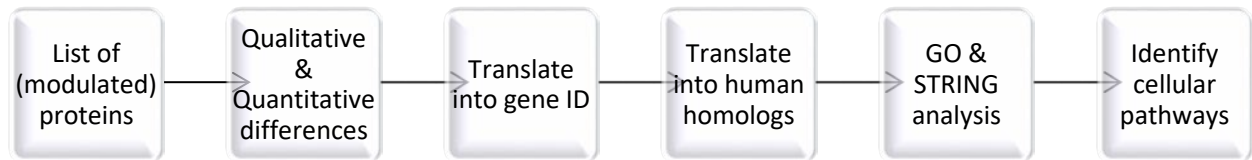


Figure 8 Analytical workflow: From obtaining lists of regulated proteins after MS, up to identification of cellular pathways.

4.1.12. Gene Ontology analysis

After determining the qualitative and quantitative differences, the identifiers of the differentially expressed proteins were cross-referenced to the *Gallus gallus* gene IDs and the gene IDs of the human orthologs using data retrieved from the ENSEMBL biomart [126] website on 15th of November 2016 (**Figure 8**). Gene Ontology (GO) analysis was carried out using the web based softwares g:profiler/g:cacao (<http://biit.cs.ut.ee/gprofiler/>, <http://biit.cs.ut.ee/gprofiler/gcocoa.cgi> [127], QuickGO from the European Bioinformatics institute (<https://www.ebi.ac.uk/QuickGO/>, [110] and STRING protein-protein interaction database (<http://string-db.org/> [111].

4.2. Proteomic analysis of primary B lymphocytes infected with MDV

In vivo and *in vitro* infection experiments were conducted in the group of Prof. Benedikt Kaufer at the FU Berlin. Primary B cells were prepared from the bursa of Fabricius of 6 to 11 week-old chickens by dissociation of the organ and subsequent isolation of the cells by density gradient centrifugation. B cells were maintained in RPMI 1640 medium supplemented with 10 % FBS and 1 % penicillin/streptomycin at 40 °C and activated using recombinant soluble chicken CD40 ligand (chCD40L) [128]. Isolated B cells were infected by overlay and co-cultivation with MDV infected chicken embryo cells (CECs). CECs infected with GFP-expressing recombinants of MDV strains CVI988 [53], or RB-1B [50] (5×10^4 pfu) and mock- infected controls were co-cultured with 10^6 B cells per well on 24-

well-plates in the presence of CD40L for 16 hours at 41°C. As both MDV recombinants express GFP under the control of the early HSV-1 TK promoter, infected B cells could be isolated by fluorescence activated cell sorting (FACS) based on the GFP signal. Cell viability was determined using the eFluor780 (Affymetrix eBioscience) fixable viability dye. Fluorescence labeled monoclonal antibodies (MAb) specific for chicken Bu1 (clone AV-20) were used to further discriminate B cells. FACS of 10^6 cells per sample was performed on a FACS Aria III using the FACSDiva software (Becton Dickinson). Three independent infection experiments were conducted. The workflow for the quantitative proteome analysis comparing MDV- infected and mock- infected primary B cells is described in **Figure 9**.

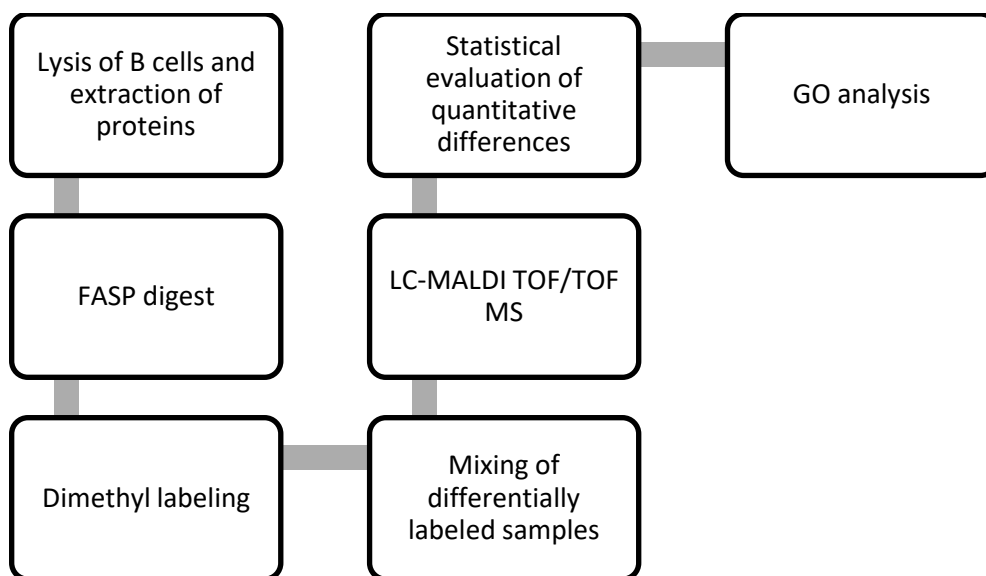


Figure 9 Overview of the workflow for the proteomic analysis of MDV-infected primary B cells.

4.2.1. Lysis of cells and extraction of proteins

Per experiment 10^6 cells of each CVI988- or RB-1B-infected (GFP +) and mock-infected B cells were lysed in 100 μ l of lysis buffer containing 0.1 M DTT and 2 % SDS in 0.1 M Tris-HCl (pH 8.0). Samples were heated for 10 min at 95 °C and then sonicated for 5 min in 10 sec intervals with an amplitude of 85 % at 4 °C. The samples were centrifuged for 5 min at 14,000 x g and RT.

4.2.2. Determination of protein content of primary chicken B cells

Protein content of the samples was determined by densitometry after SDS-PAGE with BSA (1, 2, 4, 8 and 10 µg per lane) as standard. Briefly, aliquots of the protein extracts of infected and mock infected cells were electrophoresed for 45 min at 200 V on a hand-cast gradient polyacrylamide gels (7.5 -15 %) [129] and the gels were stained overnight (ON) with Coomassie brilliant blue stain solution [118]. Stained gels were scanned and evaluated with AIDA Image Analyzer v5.0.

4.2.3. Filter aided sample preparation (FASP) digest

After lysis, 20 µg aliquots were digested using the FASP protocol as described in section **4.1.4** *Filter aided sample preparation (FASP) digest*.

4.2.4. Dimethyl labeling

Two sample pairs were compared at a time as a dual (not multiplexed) isotope label was used. Dimethyl labeling was carried out as described in section **4.1.5** *Dimethyl labeling*. For each of the three samples (mock infected, CVI988- and RB1B-infected) two independent technical replicates with inverse labels were prepared. Desalting was carried out as described in section **4.1.7** *Desalting of the labeled peptides with Empore™ Cartridges*.

4.2.5. LC-MALDI TOF/TOF mass spectrometry

For each pair of differentially labeled samples a 1:1 mix (v:v) was analyzed in a preliminary experiment in order to determine the proper mixing ratio for the following analysis. If necessary, the mixing ratios were adjusted accordingly.

Nano-LC MALDI-TOF/TOF MS and evaluation of the data was essentially carried out as described in section **4.1.9** *Liquid chromatography and mass spectrometry*, section **4.1.10.2** *Quantification based on isotope ratio* and section **4.1.12** *Gene Ontology analysis*.

4.2.6. Confirmation of infection markers by RNA sequencing

For confirmation of the potential infection markers that were identified in the proteomic analysis of infected B cells, we performed RNA sequencing in order to determine expression levels in the transcriptome. The bursa of Fabricius was isolated from three different chickens and the B cells were prepared by density gradient centrifugation as described above under **4.1 Proteomic analysis of naïve primary chicken lymphocytes**. B cells were maintained in RPMI 1640 medium supplemented with 10 % FBS and 1 % penicillin/streptomycin at 41 °C and activated using recombinant soluble chCD40L. Isolated B cells were infected via overlay infection and co-cultivation with infected chicken embryo cells (CECs). Briefly, vRB-1B and vCVI988 (5×10^4 pfu each) and mock- infected by overlay infection of 1×10^6 B cells on infected CECs per well on 24-well plates in the presence of CD40L for 16 hours at 41°C. For each infection batch, 1.5×10^5 cells were sorted and snap-frozen.

4.2.6.1. RNA isolation

The RNA was isolated from cells with the RNeasy® Mini Kit (QIAGEN) following the manufacturer's instructions. Shortly, the B cells were lysed with 350 µl RLT buffer containing 2 % 2 M DTT and incubated for 30 min at RT. The samples were centrifuged for 3 min at 14,000 x g, the supernatants transferred to new reaction tubes, mixed with 350 µl 70 % ethanol and loaded onto spin columns. After centrifugation for 15 sec at 10,000 x g, 350 µl RW1 buffer was added and the column was centrifuged again for 15 sec at 10,000 x g. Contaminating DNA was removed by DNase I digest (RNase-free DNase set, QIAGEN). The stock DNase I solution was diluted 1:8 in DNase buffer. To each column 80 µl of the diluted DNase I were added, the column was allowed to stand at rt for 15 min and 350 µl RW1 buffer was added before centrifugation for 15 sec at 10,000 x g. Centrifugation was repeated after addition of 500 µl RPE buffer. Again, 500 µl RPE buffer were added and centrifuged for 2 min at 10,000 x g. The columns were transferred to new reaction tubes and centrifuged for 1 min at 10,000 x g to remove residual ethanol. The columns were then transferred to new reaction tubes and the RNA was eluted with 30 µl RNase-free water. The RNA content was determined by photometry (P330, Implen).

4.2.6.2. Quality assessment of isolated RNA

The quality of total RNA was evaluated with the Agilent RNA 6000 pico kit following the manufacturer's instructions. The samples were denatured prior to the quality assessment by incubating at 70 °C for 2 min. For each sample, 1 µl of the isolated RNA was tested. The chip was vortexed for 1 min at 2,400 rpm and immediately analyzed in the Agilent 2100 Bioanalyzer with 'eukaryote total RNA Pico' class.

4.2.6.3. Isolation of mRNA from purified total RNA

For the preparation of the transcriptome library, mRNA was isolated with the DynaBeads mRNA DIRECT™ Micro Kit (life technologies). The RNA samples were brought to a volume of 48 µl with nuclease-free water and 2 µl (1:100) ERCC Spike-In control mix was added to each sample. The RNA samples with ERCC control mix were heated to 70 °C for 2 min. To each sample 50 µl lysis buffer was added, the mixture was vortexed and collected by centrifugation. The mRNA was isolated by two rounds of binding the mRNA to magnetic beads, washing the mRNA with appropriate buffer and elution in pre-warmed (80 °C) nuclease-free water according to manufacturer's instructions. Finally, the mRNA was eluted from the beads by mixing with 12 µl pre-heated (80 °C) nuclease-free water in a pipette and replacing the tubes on the magnetic stand. After the supernatant had cleared, at least 10 µl of the solutions were recovered and transferred to new safe-lock reaction tubes. The eluted mRNAs were stored at -80 °C.

4.2.6.4. Fragmentation of whole transcriptome RNA from total RNA samples and construction of whole transcriptome libraries

Preparation of the transcriptome libraries was performed with the Ion Total RNA-Seq kit v2 following the manufacturer's instructions.

For enzymatic fragmentation of the mRNA, 10 µl of the mRNA samples were mixed with 1 µl 10x RNase III reaction buffer and 1 µl of RNase III by pipetting up and down five times. The samples were incubated at 37 °C for 3 min, mixed with 20 µl nuclease-free water and cooled on ice. The fragmented RNA was purified with the magnetic bead cleanup module according to manufacturer's instructions.

The fragmented RNA was eluted by addition of 5 µl pre-warmed (37 °C) nuclease-free water and incubated for 1 min on the magnetic stand. After clearing of the solution, the supernatants containing the fragmented RNA were transferred to new reaction tubes.

The transcriptome libraries were constructed immediately after the fragmentation. First, the RNA was hybridized and ligated. For each sample, the hybridization master mix was prepared separately by mixing 2 µl 'ion adaptor mix v2' with 3 µl hybridization solution into 0.2 ml reaction tubes. Four µl fragmented RNA preparation was added to 5 µl hybridization master mix and mixed by pipetting up and down ten times, followed by a short centrifugation. The samples were placed in a thermal cycler and incubated for 10 min at 65 °C, followed by incubation at 30 °C for 5 min. Ten µl of 2X ligation buffer and 2 µl ligation enzyme mix were added on ice to the hybridization reaction and mixed by pipetting up and down five times. The ligation reaction was incubated at 30 °C for 1 hour before reverse transcription. A master mix was prepared which per sample contained 2 µl nuclease-free water, 4 µl 10X RT Buffer, 2 µl 2.5mM dNTP mix and 8 µl ion RT Primer v2. The ligated sample was added to 16 µl of the master mix and briefly centrifuged. The samples were heated for 10 min at 70 °C and cooled on ice. Four µl of the 10X SuperScript III Enzyme mix were added to each sample and vortexed. Prior to incubation for 30 min at 42 °C, the samples were briefly centrifuged.

Following the reverse transcription step, the cDNA was purified with the magnetic bead cleanup module following the manufacturer's instructions. After binding of cDNA to beads and washing of the cDNA, the samples were eluted in 6 µl pre-warmed (37 °C) nuclease-free water. Thus, 7 µl pre-warmed (37 °C) nuclease-free water were added to each sample and incubated for 1 min on the magnetic stand. After clearing of the solution, 6 µl of the supernatants were transferred to new reaction tubes.

After purification, the cDNA was amplified and barcoded libraries were prepared with the Ion Xpress™ RNA-Seq Barcode 01-16 Kit. For each reaction, the master mix was prepared separately by pipetting 45 µl Platinum® PCR SuperMix High Fidelity into new 0.2 ml reaction tubes and adding 1 µl of ion Xpress™ RNA 3' Barcode Primer and 1 µl of the selected Ion Xpress™ RNA-Seq Barcode BC primer

(BC01-BC09). In order to avoid any cross contamination of the various barcodes, gloves were changed after pipetting each barcode. The samples were mixed by vortexing and shortly centrifuged. A PCR was run with the following thermal profile:

| Stage | Temp [°C] | Time |
|-----------|-----------|-------|
| Hold | 94 | 2 min |
| 2 cycles | 94 | 30 s |
| | 50 | 30 s |
| | 68 | 30 s |
| 16 cycles | 94 | 30 s |
| | 62 | 30 s |
| | 68 | 30 s |
| Fold | 68 | 5 min |

The amplified cDNA was again purified with the magnetic bead cleanup module. The cDNA was eluted in 15 µl pre-warmed (37 °C) nuclease-free water.

4.2.6.5. Quality assessment of transcriptome library

The quality of the cDNA libraries was evaluated with the Agilent DNA 7500 and the Agilent high sensitivity DNA kits according to the manufacturer's instructions. One µl of each sample was evaluated on a DNA 7500 chip and each 1 µl of one library of the mock, RB-1B and CVI988 infected B cells was tested on a DNA high sensitivity chip. The two chips were evaluated with the Agilent 2100 Expert Software.

4.2.6.6. Second purification and amplification

To increase concentration and quality a second round of purification and amplification of the libraries was performed. In order to remove fragments below 200 bp, the libraries were purified with Agencourt

AMPure XP kit. The libraries were mixed 1:1 with AMPure beads, thus 50 µl of beads were distributed in low binding reaction tubes, 50 µl of libraries were added and the tubes were shortly centrifuged. The samples were incubated for 15 min in the rotisserie at rt. Subsequently, the samples were placed on the magnetic stand for 3 min for the solution to clear. The supernatants were removed and the beads were washed twice by addition of 200 µl of 100 % ethanol, rotation on the magnetic stand and removal of the wash solution. After the second wash cycle, the beads were air-dried. The purified libraries were eluted in 22 µl nuclease-free water and used in a second round of high-fidelity amplification with the QIAGEN GeneRead DNA L Amp kit. The master mix was prepared for each sample by mixing 25 µl 2x Hifi PCR Master Mix, 1.5 10 µM Primer Mix, 5.5 µl RNase-free water. Eighteen µl of the purified samples were added to the Master Mix. The thermal cycling parameters were 98 °C for 2 min, followed by 10 cycles of 98 °C for 20 sec, 60 °C for 30 sec and 72 °C for 30 sec. After cycling the samples were incubated for 1 min at 72 °C.

Following the PCR, the amplified libraries were again purified two rounds with the AMPure beads. The libraries were mixed 1:1.2 with the beads (60 µl beads were mixed with 50 µl sample). The sample-beads mix was incubated and washed as described above. Finally, the purified libraries were eluted in 16 µl nuclease-free water.

4.2.6.7. KAPA PCR

In order to determine the exact number of molecules per library, a KAPA PCR was performed with the KAPA Library Quantification Kit (IonTorrent). The master mix was prepared by mixing 12 µl KAPA SYBR FAST qPCR MM + Primer mix with 4 µl nuclease-free water. The samples were diluted 1:10,000, 1:20,000, 1:40,000 (Mock 1), 1:200, 1:400, 1:800 (RB-1B 2, RB-1B 3) and 1:20,000, 1:40,000 and 1:80,000 (Mock 2-3, RB-1B 1 and CVI 1-3) for proper determination of molecule number. Four µl of the diluted libraries were added to 16 µl of the master mix and the PCR was run with the following thermal cycle parameters. The taq polymerase was activated at 95 °C for 5 min, followed by 35 cycles of denaturation at 95 °C for 30 sec and annealing and elongation at 60 °C for 45 sec.

4.2.6.8. Pooling of libraries

In order to obtain similar numbers of reads for each library the number of library molecules was calculated based on the determined molecule concentration [pM] for the weakest dilution as shown in **Table 2** and **Table 3**. Two different sequencing runs were performed. For each run, the pool was filled up with nuclease-free water to 100 µl and used for the One Touch reaction.

Table 2 Pooling scheme for first sequencing run of the libraries. Lib02429: mock 1, Lib02430: mock 2, Lib02431: mock 3, Lib02432: RB-1B 1, Lib02433: RB-1B 2, Lib02434: RB-1B 3, Lib02435: CVI988 1, Lib02436: CVI988 2, Lib02437: CVI988 3. MID: barcode number.

| Library | MID | % | pM | Dilution 1/x | Fmol | reads | µl |
|---------------|-----|-------------|-----------|--------------|----------|------------|--------------|
| lib02429 | 1 | 11.1 | 291,661.1 | 10,000 | 0,072215 | 8,888,000 | 2.48 |
| lib02430 | 2 | 11.1 | 195,913.7 | 20,000 | 0,072215 | 8,888,000 | 7.37 |
| lib02431 | 3 | 11.1 | 464,385.8 | 20,000 | 0,072215 | 8,888,000 | 3.11 |
| lib02432 | 4 | 11.1 | 130,356.3 | 20,000 | 0,072215 | 8,888,000 | 11.08 |
| lib02433 | 5 | 11.1 | 2,921.4 | 200 | 0,072215 | 8,888,000 | 4.94 |
| lib02434 | 6 | 11.1 | 1,303.1 | 200 | 0,072215 | 8,888,000 | 11.08 |
| lib02435 | 7 | 11.1 | 304,052.1 | 20,000 | 0,072215 | 8,888,000 | 4.75 |
| lib02436 | 8 | 11.1 | 137,809.6 | 20,000 | 0,072215 | 8,888,000 | 10.48 |
| lib02437 | 9 | 11.1 | 143,237.2 | 20,000 | 0,07228 | 8,896,000 | 10.09 |
| Actual | | 100 | | | 0,65 | 80,000,000 | 65.39 |
| Debit | | 100 | | | 0,65 | 80,000,000 | 100.00 |

Table 3 Pooling scheme for second sequencing run of the libraries. Lib02429: mock 1, Lib02430: mock 2, Lib02431: mock 3, Lib02432: RB-1B 1, Lib02433: RB-1B 2, Lib02434: RB-1B 3, Lib02435: CVI988 1, Lib02436: CVI988 2, Lib02437: CVI988 3. MID: barcode number.

| Library | MID | % | pM | Dilution 1/x | fmol | reads | µl |
|----------|-----|-------------|-----------|--------------|--------|------------|-------------|
| lib02429 | 1 | 43.0 | 291,661.1 | 10,000 | 0,2795 | 34,400,000 | 9.58 |
| lib02430 | 2 | 8.0 | 195,913.7 | 20,000 | 0,052 | 6,400,000 | 5.31 |
| lib02431 | 3 | 16.0 | 464,385.8 | 20,000 | 0,104 | 12,800,000 | 4.48 |
| lib02432 | 4 | 9.0 | 130,356.3 | 20,000 | 0,0585 | 7,200,000 | 8.98 |
| lib02433 | 5 | 5.0 | 2,921.4 | 200 | 0,0325 | 4,000,000 | 2.22 |
| lib02434 | 6 | 0 | 1,303.1 | 200 | 0 | 0 | 0.00 |
| lib02435 | 7 | 9.0 | 304,052.1 | 20,000 | 0,0585 | 7,200,000 | 3.85 |
| lib02436 | 8 | 6.0 | 137,809.6 | 20,000 | 0,039 | 4,800,000 | 5.66 |

| | | | | | | | |
|---------------|---|------------|-----------|--------|-------|------------|-------------|
| lib02437 | 9 | 4.0 | 143,237.2 | 20,000 | 0,026 | 3,200,000 | 3.63 |
| Actual | | 100 | | | 0,65 | 80,000,000 | 43.71 |
| Debit | | 100 | | | 0,65 | 80,000,000 | 100.00 |

4.2.6.9. OneTouch reaction and Sequencing of Libraries

Sequencing was performed on an Ion S5™ XL system with the Ion 540™ Kit-OT2 kit following the manufacturer's instructions. Prior to the sequencing run, the OneTouch reaction was performed (see chapter 4) to amplify single library molecules. During the OneTouch reaction an oil emulsion is created, in which each drop contains a single Ion Sphere™ Particle (ISP) to which a single library molecule is bound. In a second step, the bound library molecule is amplified. The library was vortexed for 5 sec and briefly centrifuged. For each sequence run 80 µl nuclease-free water, 120 µl Ion S5™ enzyme mix, 100 µl ISPs and 100 µl diluted library was added to 2 ml Ion S5™ Reagent Mix. The sample was transferred to a freshly prepared Ion OneTouch™ reaction filter and the reaction was automatically performed in the Ion OneTouch™ instrument.

After 16 hours the amplified library molecules were retrieved and prepared for the recovery of the template-positive ISPs. After final centrifugation, the supernatant was removed leaving 100 µl in the tube. The ISPs were resuspended by pipetting up and down five times. Hundred µl nuclease-free water was added to each recovery tube and the complete sample was transferred to a new low bind reaction tube, which was filled up to 1 ml with nuclease-free water. The ISPs were vortexed and centrifuged for 8 min at 15,500 x g. The supernatant was removed leaving 20 µl in the tube. The ISPs were filled up to 100 µl with resuspension solution, vortexed and briefly centrifuged. Subsequently, the template-positive ISPs were enriched following the protocols from chapter 5. The template positive ISPs contain biotin residues, which can be extracted automatically with Dynabeads™ MyOne™ Streptavidin C1 beads on the Ion OneTouch™ ES instrument, in order to obtain the ISPs with templates only. After the automated purification, the ISPs were centrifuged at 15,000 x g for 5 min. The supernatant was removed except for the last 10 µl. The ISPs were resuspended by pipetting up and down ten times and

again centrifuged for 5 min at 15,000 x g. The supernatant was removed except the last 10 µl and nuclease-free water was added to a total volume of 100 µl. The total sample was prepared for sequencing and loaded on an Ion 540TM chip as described in Chapter 7. Briefly, 5 µl control ISPs were added to the enriched template-positive ISPs and vortexed. The control-sample mix was centrifuged for 5 min at 15,000 x g and the supernatant except last 10 µl was carefully removed. Fifteen µl Ion S5TM annealing buffer and 20 µl Ion S5TM sequencing primers were added. The sample was incubated for 2 min at 95 °C followed by incubation at 37 °C for 2 min. Subsequently, 10 µl Ion S5TM loading buffer was added, the sample was vortexed and shortly centrifuged. The complete sample was added into a loading well of the Ion 540TM chip. The chip was centrifuged in the Ion ChipTM Minifuge for 10 min and loaded twice with annealing buffer. Fifty µl 50 % annealing buffer with 2 % foaming solution (10 % TritonTM X-100 solution) was foamed and 100 µl of foam was injected into the chip loading port. After addition of 55 µl of 50 % annealing buffer to the chip loading well, the chip was centrifuged for 30 sec. The chip was flushed by adding 100 µl flushing solution to the chip loading port two times. Subsequently, 100 µl of 50 % annealing buffer was added to loading port three times. 65 µl polymerase solution (6 µl Ion S5TM Sequencing polymerase was added to 60 µl 50 % annealing buffer) was added to the chip loading port. The chip was incubated for 5 min and sequenced in the Ion S5TM XL system.

4.3. Proteome analysis of MD tumors

Proteome analysis of MDV-induced tumors was carried out following the workflow outlined in **Figure 10**. All animal experiments were conducted by my collaboration partners in Berlin. Chickens (White leghorns) were infected with the MDV RB-1B strain and the recombinant RB-1B virus Δ vTR lacking viral telomerase (vTR) [54]. A BAC containing the RB-1B genome, which lacks most of the internal long repeat region, but can be restored by virus reconstitution, was used and the vTR region was completely deleted by two-step red mediated mutagenesis [54]. The organs of infected and healthy chickens were removed and snap-frozen in liquid nitrogen and stored at -80°C until further use. Tumors from chickens infected with WT RB-1B virus or with the Δ vTR-RB-1B mutant are further on referred to as WT tumor or Δ vTR tumor, respectively.

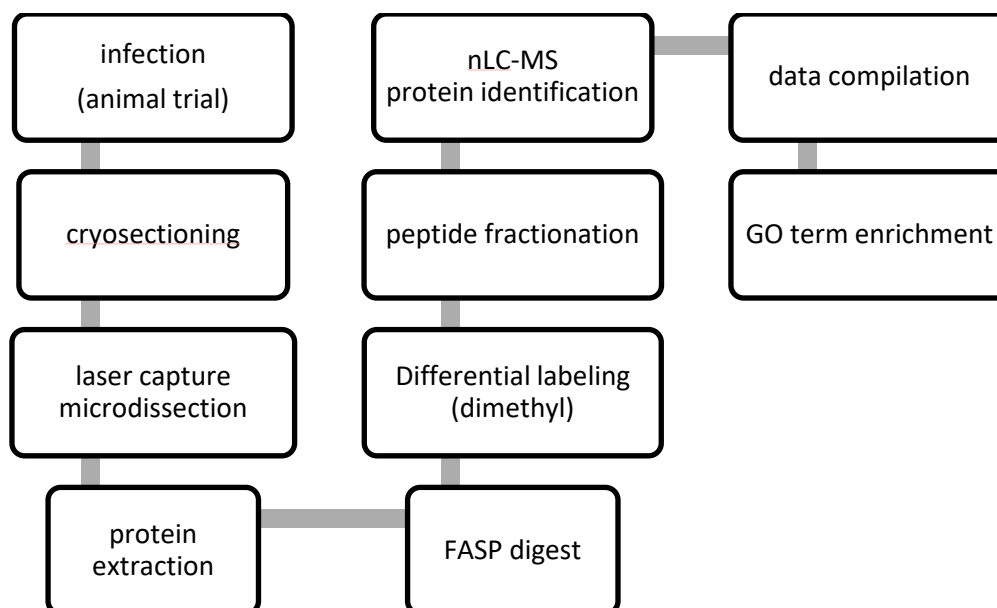


Figure 10 Overview of the workflow for the proteomic analysis of MD tumors.

4.3.1. Cryosectioning of snap frozen liver samples

20 μm cryosections were cut from the organ samples in a -20°C precooled cryostat (HM 560 Cryostar, Microm International) and carefully placed near the center of the PEN membrane on pre-cooled membrane slides (MembraneSlide 1.0 PEN, 25 x 75 mm, Zeiss) using a clean, soft brush and avoiding ruffles. For better adherence of the section to the membrane the slide was warmed to ambient

temperature for 1 min allowing it to melt. The cryosections were fixed by immersion in -20 °C 70 % ethanol for 1 min followed by a short second fixation step in cooled absolute ethanol (-20 °C). The cryosections were dried prior to laser dissection for 1 h at room temperature in mild vacuum (150 mm Hg) by placing the slide in a desiccator connected to a vacuum system (BVC 21 NT, Vacuubrand).

4.3.2. Hematoxylin and eosin staining and immunohistochemistry

For morphological examination of MDV-induced tumors, 8 µm thick organ sections were prepared from paraffin embedded liver from chickens infected with either WT-RB-1B or the Δ VTR mutant. Prior to H&E (hematoxylin and eosin) staining and immunohistochemical analysis of the sections, the paraffin was removed by sequential immersion in xylene (2x), isopropanol (2x), 96 % isopropanol, 80 % isopropanol 70 % isopropanol, 50 % isopropanol, and deionized water, for 3 min each.

For H&E staining the sections were immersed in acidic hematoxylin solution for 15 min, rinsed with deionized water and then placed in tap water to blue for 10 min. For the eosin stain, the sections were placed in eosin/phloxine B solution (1 % Eosin G, Merck, 1 % phloxine in ethanol and 0.5 % acetic acid) for 3 min and rinsed with tap water. The sections were dehydrated in an ascending alcohol series (70 % ethanol, 80 % ethanol, 90 % ethanol in deionized water (v/v), isopropanol) After two washes in xylene (3 min) the stained sections were covered with Eukitt® quick hardening mounting medium (Sigma Aldrich) for microscopy.

4.3.3. Immunohistochemistry

For immunohistochemistry, the sections were treated with the Vectastain Elite® ABC HRP kit (peroxidase standard, Vector laboratories). Endogenic peroxidases were inactivated with 3 % hydrogen peroxide in methanol (v/v) for 10 min. After dehydration with a descending ethanol series (80 %, 70 % and 50 %, 3 min each) the sections were rinsed with deionized water. The antigens were unmasked by incubation in 10 mM citrate buffer (pH 6.0) for 10 min at 110°C using a decloaking chamber. The slides were washed thrice in TBS (pH 7.65) for 3 min. Unspecific binding was reduced by incubation with a

goat antiserum for 30 min in a humid chamber. The sections were incubated with primary polyclonal rabbit anti-human CD3 antibody (1:200) in a humid chamber at 4 °C ON and washed thrice in TBS for 3 min. The sections were incubated with the secondary biotinylated goat anti-rabbit antibody (1:200, BA-1000, Vector laboratories) for 30 min in a humid chamber and washed thrice in TBS for 3 min. After incubation with the avidin-biotin-complex (Vector laboratories) for 30 min at room temperature and 3 washes with TBS for 3 min the AEC-substrate chromogen (3-amino-9-ethyl carbazol-staining reagent, DAKO) was used for detection of the CD3 antigen. The sections were counterstained with hematoxylin and covered with Aquatex® (Merck).

4.3.4. Quantitation of cell types with HALO™ imaging software

The main cell types in the tumor samples were quantified using the HALO™ imaging software (Indica Labs, Corrales, NM). In the WT- and Δ vTR-tumors CD3+ as well as CD3- lymphocytes, connective tissue and hepatocytes were defined and quantified. For each tumor type, three different tumors from different chickens were analyzed and in each tumor, six different areas were randomly selected for the quantitation. As control the same cell types were also quantified in liver from a non-infected control chicken tissue.

4.3.5. Laser capture microdissection

The microdissection was performed with a PALM® MicroBeam instrument operated with the PALM® RoboSoftware 4.5 (Zeiss, Germany) using the RoboLPC program with the 5x magnification of the microscope according to manufacturer's instructions. Fifteen identical rectangles with total area of 250000 μm^2 of each tumor or liver sections were collected in one cap of a 0.5 ml reaction tube (Safe-Lock Tubes, Eppendorf, Hamburg, Germany, article number: 0030 121.023) containing 40 μl deionized water (18 M Ω). The edges of the cryosections and the borders between tumor and healthy tissue were excluded. For each replicate, 10 tumor or liver aliquots (with 0.075 mm³ LCM material per aliquot) were prepared. The 20 aliquots were then collected by centrifugation (2 min at 15000 x g) and dried by vacuum centrifugation in a Univapo Vacuum Concentrator Centrifuge (150H, UniEquip).

4.3.6. Lysis of samples and protein extraction

Lysis of the dissected material and 1×10^7 control T cells was performed as described in section 4.2.1, except that the LCM dissected material was lysed in 30 μ l lysis buffer. The supernatants were recovered for FASP digest [119].

4.3.7. Densitometric determination of protein content

The estimation of the protein contents of lysed samples was carried out by densitometry of Coomassie stained SDS-PAGE gels as described in section **4.2.2. Determination of protein content of primary chicken B cells**. For calibration, samples containing 1, 2, 4, 8 and 10 μ g of bovine serum albumin were applied and the staining intensity was evaluated with AIDA Image Analyzer v5.0 in the 2D Densitometry mode.

4.3.8. FASP digest, dimethyl labeling and desalting of peptides

After lysis of LCM sections or naïve T cells, the proteins were digested using the FASP protocol as described above (**4.1.4 Filter aided sample preparation (FASP) digest**). The peptides from the different organ samples and T cells received a dimethyl label for comparative analysis (see **4.1.5. Dimethyl labeling**). The labeling was followed by desalting of the peptides with the Empore cartridges (see section **4.1.7 Desalting of the labeled peptides with Empore™ Cartridges**) and concentration *in vacuo* as described above.

4.3.9. OFFGEL Isoelectric focusing (OG IEF) of peptides

To ensure a balanced mix of the labeled peptides, the mixing ratio was determined before focusing by a LC-MS run with a small aliquot of the samples mixed on basis of the protein content as determined by BCA assay. The peptides were then mixed according to the median of isotope ratios of the preceding LC-MS run, dried, solubilized in 200 μ l 20 % methanol/1% IPG buffer (GE Healthcare) and sonicated for 15 min in a water bath. Focusing was carried out on a 3100 OFFGEL Fractionator (Agilent) using 13 cm Immobiline DryStrips (13 cm, pH 3-10, GE Healthcare) according to manufacturer's instructions (20

kVh, maximum voltage 4,500 V, maximum current 50 μ A per strip, maximum power 200 MW). After focusing was completed, the fractions were retrieved, dried in a vacuum centrifuge and solubilized in 0.1% TFA.

4.3.10. LC-MALDI TOF/TOF MS of IEF fractions

After IEF the peptide fractions were reconstituted in 0.1 % TFA and analysed by LC-MALDI TOF/TOF MS as described above (**4.1.9 Liquid chromatography and mass spectrometry**), but a shorter gradient resulting in 226 LC-MS fractions was applied. Quantitative evaluation was carried out as described in section **4.1.10.2. Quantification based on isotope ratio** based on the protein lists retrieved from ProteinScape. The lists of identified regulated proteins were again used as input for comparative analyses and gene ontology analyses (see section **4.1.12 Gene Ontology analysis** for more information). Potential transformation markers were further characterized by quantitative RT-qPCR.

4.3.11. RNA isolation for qPCR

The RNA from cells and tissue samples was isolated with the RNeasy® Mini Kit (QIAGEN) as described in **4.2.6.1 RNA isolation**. Finally, the RNA of the T cells and the LCM samples were eluted in 50 μ l and 30 μ l RNase-free water, respectively. The RNA content was determined with a nanophotometer.

4.3.12. Confirmation of potential transformation markers by qRT-PCR

Several selected potential transformation markers were confirmed in a one-step quantitative RT-PCR using the qScript™ One-Step SYBR® Green RT-qPCR Kit (Quantabio). Each reaction was performed along with GAPDH and 28S rRNA or β -actin as controls and non-template controls (NTC) for each primer reaction. Each gene was measured in duplicates in the Bio-Rad CFX96 Touch™ Real-Time PCR Detection System. Final reaction volumes of 20 μ l contained 1 ng isolated template RNA, 100 nM of each primer, 0.4 μ l 'qScript One-Step reverse transcriptase' and 10 μ l 2x SYBR Green master mix containing AccuStart Taq DNA polymerase. The thermal cycling parameters were 50 °C for 10 min, 95 °C for 5 min, followed by 42 cycles of 95 °C for 10 sec, 60 °C for 30 sec and 72 °C for 30 sec.

4.3.13. Quantification by one-step RT-qPCR

The expression of potential transformation markers in Δ vTR tumors compared to T cells and healthy liver tissue was calculated relative to expression of GAPDH, 28S rRNA and β -actin. The relative gene expression in tumor samples compared to T cells was calculated using the $2^{\Delta Ct}$ method [130].

5. Results

5.1. Proteomic characterization of naïve chicken B- and T lymphocytes

To analyze the protein expression profile of naïve chicken B and T cells, the bursa of Fabricius and thymus of white leghorn chickens were removed and the lymphocytes were purified in a Biocoll density gradient. FACS analysis of thymus cells and cells from the bursa of Fabricius determined a T cell or B cell population of 97.8 % and 98.2 %, respectively (data not shown). Aliquots of 3×10^6 to 10^7 lymphocytes were prepared and snap-frozen. For direct comparisons of T and B cells proteomes, we made use of the chemical dimethyl label. During the proteome analysis of naïve primary lymphocytes, the compatibility of FASP digest, dimethyl labeling and OFFGEL isoelectric focusing was tested and implemented into the workflow.

5.1.1. Proteomic analysis of unlabeled chicken B and T cells

In a first experiment one sample each of 3×10^6 B cells and T cells was lysed with RapiGest™, the proteins were extracted, digested with trypsin in-solution and 5µg of the digest were analyzed by LC-MALDI-TOF/TOF MS using the long gradient with 1360 fractions. In B cells and T cells, 1061 and 939 proteins were identified, respectively (Supptbl1 and Supptbl2. All supplements can be found on the accompanying CD).

Proteins were quantitated on the basis of the emPAI. To extract B cell or T cell specific proteins from the protein lists, the ENSEMBLE protein IDs in the Mascot reports (Supptbl 3 and 4 on the accompanying CD) were cross-referenced to gene IDs and subsequently compared according to the ENSEMBL gene IDs. Hence, 266 B cell specific and 146 T cell specific proteins were identified with at least two associated peptides per protein. While the proportions of most proteins, which were identified in both B and T cells, were quite similar, 214 and 120 proteins were at least 2-fold upregulated in B cells or T cells, respectively.

For the GO-term enrichment analysis, the identifiers of the differentially expressed proteins were cross-referenced to the *Gallus gallus* gene IDs and subsequently to the gene IDs of the human orthologs using data retrieved from the ENSEMBL biomaRt [126] (Supptbl 5 and 6 on the accompanying CD). The cutoff for up- or downregulation was set to fold-changes of 0.5 and 2, respectively. Using the results from the separate LC-MS runs of B cell- and T cell-lysates, a list of 334 regulated proteins (summarized in Supptbl 7 on the accompanying CD) was obtained, which served as basis for GO-term enrichment and KEGG analysis with g:profiler and g:cacao [127] (the original output for the separate GO analyses of quantitatively upregulated proteins in B or T cells can be found in Supptbl 8 and Supptbl 9, respectively, on the accompanying CD). Significance level (p-value) was set to 1 % for the enrichment analysis. Of the 214 upregulated B cell proteins 58 were associated with antigen processing and presentation (GO:0019882), 76 with mismatch repair (KEGG:03430), 70 with RNA degradation (KEGG:03018), 88 with RNA transport (KEGG:03013), and 57 with DNA replication (KEGG:03030). The upregulated proteins from the T cell samples were linked to housekeeping biological processes such as citrate cycle (15 proteins, KEGG:00020) and biosynthesis of amino acids (18 proteins, KEGG:01230).

5.1.2. Proteomic analysis of dimethyl labeled and OG IEF fractionated B and T cell peptides

To increase yields of identified proteins and refine the quantitative evaluation of differences between the protein expression profiles of B and T cells, a fractionation step and isotope labelling was included into the proteomic workflow. Samples containing 2×10^7 cells were digested using the FASP protocol and 150 µg of the resulting peptides for each T- and B cells were dimethyl labeled and fractionated by OG isoelectric focusing before LC-MALDI TOF/TOF MS analysis. Two technical replicates of every cell type were processed and each OG IEF fraction was measured once. In order to reduce sample loss, the FASP protein digest was extended by on-filter dimethyl labeling in the same filter device. This simplifies the workflow while the efficiency of dimethyl label and yields are not affected compared to separate FASP and dimethyl reaction. Although we expected that dimethylated peptides were separated by OG

IEF as well as unmodified peptides, the performance of OG IEF was tested in comparison to focusing of unmodified peptides. The fractionation efficiency of labeled and unlabeled peptides was tested with peptides derived from laser-dissected liver samples. To test the influence of dimethyl labeling on OG IEF, preparations of 120 µg of each labeled and unlabeled peptides were separately fractionated by OG IEF and the 24 separate fractions were analyzed by nLC-MALDI-TOF/TOF MS. The distribution of peptides was evaluated with an in-house script in the programming language R and the percentages of identified peptides were calculated over the number of fractions that they were identified in. When comparing the fractionation efficiency of labeled peptides with unlabeled peptides from liver similar peptide distributions were found. As an example, 82.2 % and 75.2 % of the peptides were detected in only one OG fraction for labeled and unlabeled material (**Figure 11**), respectively. This is consistent with the detection of about 70 % of iTRAQ labeled peptides [94, 131] and more than 80 % of unlabeled peptides of serum proteins in only one OG fraction [96].

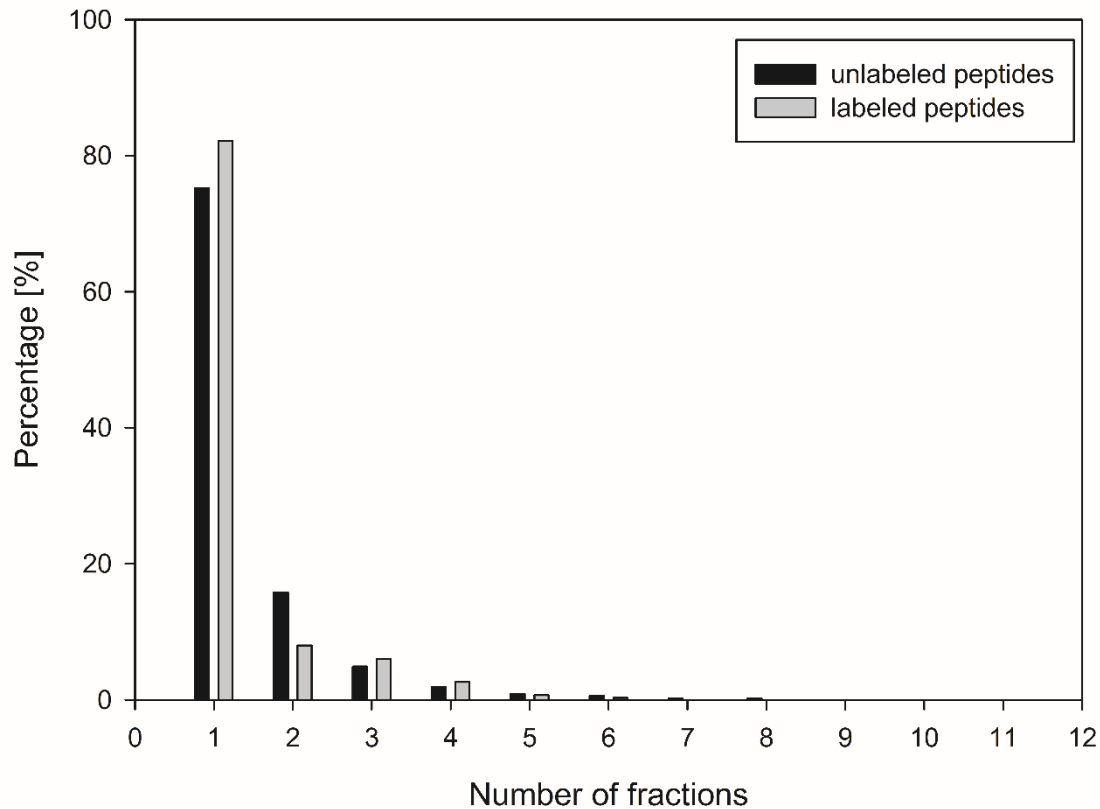


Figure 11 Comparison of the fractionation efficiency of labeled (black bars) and unlabeled (gray bars) peptides by OG-IEF.

Bars indicate the percentage of peptides identified in the number of fractions indicated on the x-axis.

For the comparison of the protein expression profiles of B and T cells, one biological replicate of each cell type was processed. Technical replicates of the FASP digest were inversely labeled and fractionated by IEF so that for the final compilation 24 LC-MS runs were available (12 of each mixture, one mixture with heavy B cell peptides, one with heavy T cell peptides).

The compilation of the results from the twelve OG fractions for each of the two independent OG IEF experiments resulted in a total of 1423 identified proteins for the first experiment and 1392 proteins for the inversely labeled replicate (Supptbl 10 and 11 on the accompanying CD). As a first qualitative evaluation of the experiment, B cell and T cell specific proteins were identified by running separate Mascot queries with light and heavy dimethylation as fixed modifications (Supptbl 12-15 on the accompanying CD). Comparison of the panels of identified proteins based on ENSEMBL gene IDs resulted in 129 B cell specific and 152 T cell specific proteins in the first experiment, and 120 B cell

specific and 137 T cell specific proteins in the inverse experiment. However, only the proteins listed in

Table 4 were consistently found in both independent experiments.

Table 4 Summary of T cell and B cell specific proteins, which were identified in both replicates. *H. sap.:* *Homo sapiens*.

T cell specific proteins

| Accession | Protein Name | <i>H. sap.</i> Gene ID |
|---------------------|---|------------------------|
| ENSGALP00000002252 | zeta-chain (TCR) associated protein kinase 70kDa | ENSG00000115085 |
| ENSGALP00000005944 | phospholipase C gamma 1 | ENSG00000124181 |
| ENSGALP00000003296 | lymphocyte cytosolic protein 2 | ENSG00000043462 |
| ENSGALP000000042659 | B cell lymphoma/leukemia 11B-like | ENSG00000127152 |
| ENSGALP000000042497 | RAR-related orphan receptor C | ENSG00000143365 |
| ENSGALP000000038576 | GTPase IMAF family member 7-like | ENSG00000179144 |
| ENSGALP000000014104 | Ras association (RalGDS/AF-6) and pleckstrin homology domains 1 | ENSG00000173166 |
| ENSGALP000000012883 | recombination activating gene 2 (RAG2) | ENSG00000175097 |
| ENSGALP000000042627 | granulysin (GNLY) | N/A |
| ENSGALP000000002866 | leucine-rich repeats and WD repeat domain containing 1 | ENSG00000161036 |
| ENSGALP000000004962 | tripartite motif containing 25 | ENSG00000121060 |
| ENSGALP000000005468 | 2' 3'-cyclic nucleotide 3' phosphodiesterase | ENSG00000173786 |
| ENSGALP000000032097 | CD5 molecule | ENSG00000110448 |
| ENSGALP000000011982 | CD3e molecule | ENSG00000198851 |
| ENSGALP000000013870 | X-prolyl aminopeptidase 1 soluble | ENSG00000108039 |
| ENSGALP000000019064 | DnaJ heat shock protein family (Hsp40) member C13 | ENSG00000138246 |
| ENSGALP000000025808 | ribonucleotide reductase M2 B (TP53 inducible) | ENSG00000048392 |
| ENSGALP000000040991 | MYC associated factor X | ENSG00000125952 |
| ENSGALP000000006708 | hexokinase 1 | ENSG00000156515 |
| ENSGALP000000042061 | phosphatidylinositol-5-phosphate 4-kinase type II alpha | ENSG00000150867 |
| ENSGALP000000028993 | Hsap of 1: ADP-ribosyltransferase 1 | ENSG00000129744 |
| ENSGALP000000038459 | tubulin folding cofactor D | ENSG00000141556 |
| ENSGALP000000002789 | no description available | ENSG00000257923 |
| ENSGALP000000038107 | squamous cell carcinoma antigen recognized by T cells 3 | ENSG00000075856 |
| ENSGALP000000032645 | DNA nucleotidylexotransferase | ENSG00000107447 |
| ENSGALP000000011984 | CD3d molecule delta (CD3-TCR complex) | ENSG00000160654 |
| ENSGALP000000013480 | V-set and immunoglobulin domain containing 1 | ENSG00000101842 |
| ENSGALP000000015326 | serine/arginine-rich splicing factor 5 | ENSG00000100650 |
| ENSGALP000000034612 | NADH-ubiquinone oxidoreductase chain 1 | ENSG00000198888 |
| ENSGALP000000037469 | acyl-CoA synthetase family member 2 | ENSG00000167107 |
| ENSGALP000000041979 | protein kinase cAMP-dependent catalytic beta | ENSG00000142875 |
| ENSGALP000000002186 | WD repeat domain 77 | ENSG00000116455 |
| ENSGALP000000005126 | SUB1 homolog (<i>S. cerevisiae</i>) | ENSG00000113387 |

| | | |
|--------------------|---|-----------------|
| ENSGALP00000005619 | polyamine oxidase (exo-N4-amino) | ENSG00000148832 |
| ENSGALP00000017339 | tyrosyl-DNA phosphodiesterase 1 | ENSG00000042088 |
| ENSGALP00000041061 | threonyl-tRNA synthetase 2 mitochondrial (putative) | ENSG00000143374 |

B cell specific proteins

| Accession | Protein name | H. sap. Gene ID |
|--------------------|--|-----------------|
| ENSGALP00000020534 | heterogeneous nuclear ribonucleoprotein K-like | ENSG00000165119 |
| ENSGALP00000029288 | v-yes-1 Yamaguchi sarcoma viral related oncogene homolog | ENSG00000254087 |
| ENSGALP00000043066 | guanosine monophosphate reductase | ENSG00000137198 |
| ENSGALP00000007995 | catechol-O-methyltransferase domain containing 1 | ENSG00000165644 |
| ENSGALP00000013852 | atlastin GTPase 2 | ENSG00000119787 |
| ENSGALP00000012199 | glutaminase | ENSG00000135423 |
| ENSGALP00000019372 | transglutaminase 4 (prostate) | ENSG00000163810 |
| ENSGALP00000007936 | Bruton agammaglobulinemia tyrosine kinase | ENSG00000010671 |
| ENSGALP00000023753 | peptidylprolyl isomerase domain and WD repeat containing 1 | ENSG00000113593 |
| ENSGALP00000032879 | no description available | N/A |
| ENSGALP00000004444 | vesicle amine transport 1 | ENSG00000108828 |
| ENSGALP00000007528 | mitogen-activated protein kinase 3 | ENSG00000034152 |
| ENSGALP00000042563 | RNA binding motif protein 24 | ENSG00000112183 |
| ENSGALP00000016918 | eukaryotic translation initiation factor 2A | ENSG00000144895 |
| ENSGALP00000005291 | pleckstrin homology domain containing A2 | ENSG00000169499 |
| ENSGALP00000028428 | early B cell factor 1 | ENSG00000164330 |
| ENSGALP00000019357 | transcription factor 20 (AR1) | ENSG00000100207 |
| ENSGALP00000040628 | NADH:ubiquinone oxidoreductase core subunit V1 | ENSG00000167792 |
| ENSGALP00000042265 | cathelicidin-B1-like | N/A |
| ENSGALP00000013350 | cancer susceptibility candidate 4 | ENSG00000166734 |
| ENSGALP00000016414 | ADP-ribosylation factor interacting protein 1 | ENSG00000164144 |
| ENSGALP00000022849 | LIM and senescent cell antigen-like domains 1 | ENSG00000256671 |
| ENSGALP00000000975 | NIN1/PSMD8 binding protein 1 homolog | ENSG00000141101 |
| ENSGALP00000006364 | La ribonucleoprotein domain family member 1 | ENSG00000155506 |
| ENSGALP00000007621 | N(alpha)-acetyltransferase 25 NatB auxiliary subunit | ENSG00000111300 |
| ENSGALP00000015204 | hematological and neurological expressed 1-like | ENSG00000206053 |
| ENSGALP00000025797 | chromatin assembly factor 1 subunit B | ENSG00000159259 |
| ENSGALP00000037252 | polymerase (DNA) eta | ENSG00000170734 |

The *Gallus gallus* ENSEMBL gene IDs of the T cell and B cell specific proteins were then converted into ENSEMBL gene IDs of their human orthologs. The list of human ortholog genes were used as input for GO analysis with g:profiler and g:cacao [127] and for the network analysis with STRING [111] to determine biological processes and pathways associated with the identified proteins. First, the T cell or B cell lists were compared to an unbiased background list to determine enriched GO terms in the category biological process (significance threshold with an experimental wide threshold of $p : 0.05$,

calculated with the g:SCS method implemented in g:profiler, was used). T cell specific proteins were enriched in biological processes including 'T-cell receptor signaling pathway' (GO:0050852), 'T-cell activation' (GO:0042110), 'Th1 and Th2 cell differentiation' (Kegg:04658) and 'immune response-activating cell surface receptor signaling pathway' (GO:0002429) (original output table can be found as Supptbl 16 on the accompanying CD).

Using protein lists that had been constructed under less restrictive conditions (inclusion of all proteins identified exclusively in one cell type in only one of the independent replicates), the GO-term enrichment and KEGG analysis resulted in the identification of more general biological processes like 'RNA processing' (GO:0006396), 'cellular component organization or biogenesis' (GO:0071840) and 'mitotic cell cycle' (GO:0000278), but also 'B-cell receptor signaling pathways' (KEGG:04662) and 'Fc epsilon RI signaling pathway' (KEGG:04664) as summarized in Supptbl 17 (on the accompanying CD).

The comparison of B cell and T cell specific proteins with the g:cacao software confirmed these results (Supppdf 18 on the accompanying CD). The B cell specific proteins were again assigned to 'B-cell receptor signaling pathways' (KEGG:04662) and 'Fc epsilon RI signaling pathway' (KEGG:04664), whereas the T cell specific proteins were assigned to 'Th1 and Th2 cell differentiation' (Kegg:04658) and 'T-cell receptor signaling pathway' (Kegg:04660). In addition, the B cell specific proteins were associated with 'organelle organization' (GO:0006996) and the T cell specific proteins to 'immune response-regulating cell surface receptor signaling pathway' (GO:0002768).

For determination of quantitative differences between B and T cells, the peptide tables (with variable dimethyl modifications set for the Mascot search) were compiled for the 12 fractions per experiment and the compiled lists were exported from ProteinScape (Supptbl 19 and 20 on the accompanying CD). The intensity ratios of heavy and light peptide peaks were calculated to result in SoC ratios (sample (heavy-labeled) over control (light-labeled)) given in the text and figures. The peptide lists as retrieved from PS software were corrected for proteins in which peptides with mixed label had been assigned, shared peptides were present or relative standard deviations exceeded 1.0 using an in-house R script

in order to reduce the number of proteins that would have to undergo manual inspection. The thus modified mean isotope ratio of the peptides calculated for every protein are shown as red circles in **Figure 12** in comparison to the untreated data (black dots). The vast majority of proteins are not regulated and lie within the 2-fold range. This indicates that only few proteins differed relevantly in abundance between the two cell types. The quantile plots for the raw and the modified medians are shown in **Figure 13**. With 10 % and 90 % percentiles calculated to SoC values of -0.63 and 0.68 (for the modified SoC values) only 20 % of all proteins range beyond this interval.

Proteins that were at least 2-fold up- or downregulated and with a standard deviation of less than 1 for the isotope ratio of the corresponding peptides were used as basis for the GO-enrichment analysis.

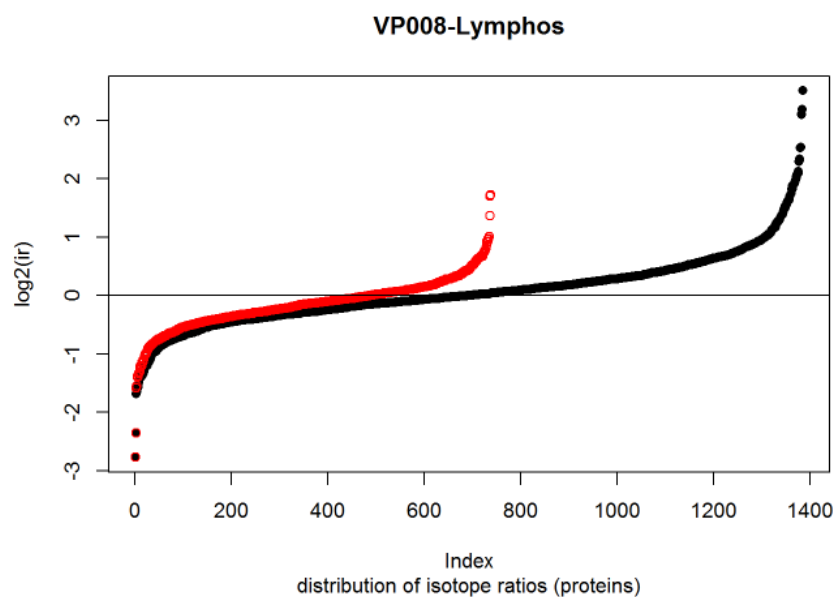


Figure 12 Mean isotope ratio of the proteins identified in the mass spectrometric analysis as determined by the ProteinScape software for the compiled list of all twelve fractions of first comparison of B cell- and T cell proteins. The black dots show the raw mean isotope ratios for the different proteins, whereas the red circles show the mean isotope ratio after the removal of mislabeled peptides. Binary logarithms of the SoC values are given on the y-axis. Peptides from B cells were light labeled with CH_2O (are equivalent to control C), while peptides from T cells were heavy labeled with CD_2O (are equivalent to sample S). Proteins shared between both lymphocyte populations with an isotope ratio of one are found around zero in this logarithmic scale on the y-axis, proteins with higher abundance in T cell samples are found in the positive range while proteins with high abundance in B cells are found in the negative range.

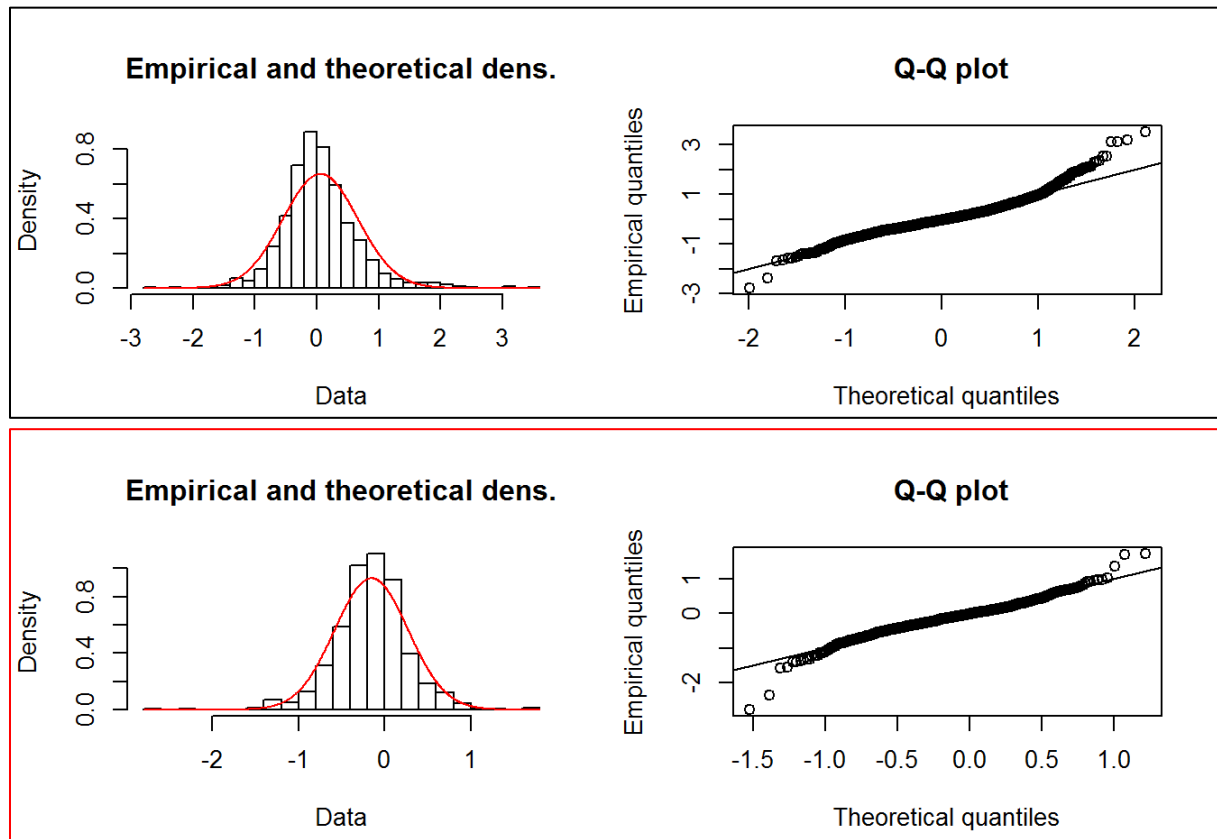


Figure 13 Quantile plots of raw SoC values (black frames) and corrected SoC values (red frames). A Gauss-Poisson distribution was obtained for both data sets. The empirical 10 and 90 % quantiles of -0.81 and 0.89, or -0.63 and 0.68 were determined for raw data and corrected data, respectively.

Using these cutoffs and comparing the results of two replicates, only twenty proteins were differently expressed in B and T cells in both experiments (**Table 5**). No significantly enriched biological processes were associated with the differentially expressed proteins.

Table 5 Differentially expressed proteins in B cells compared to T cells. Proteins with fold change < 0.5 were seen upregulated in B cells and proteins with fold change (FC) < 2 were seen upregulated in T cells.

| Protein ID | Gene ID | Protein description | FC |
|----------------------|---------------------|---|------|
| ENSGALP00000036655 | ENSGALG00000002930 | syntaxin 7 | 0.15 |
| ENSGALP00000005662 | ENSGALG00000003584 | karyopherin alpha 2 (RAG cohort 1 importin alpha 1) | 0.33 |
| ENSGALP00000003263 | ENSGALG00000002095 | charged multivesicular body protein 4B | 0.34 |
| ENSGALP000000041817 | ENSGALG000000025926 | marginal zone B and B1 cell specific protein | 0.36 |
| ENSGALP000000007299 | ENSGALG000000004594 | CD74 molecule | 0.40 |
| ENSGALP000000000423 | ENSGALG000000000318 | cysteine and glycine-rich protein 1 | 0.43 |
| ENSGALP0000000042929 | ENSGALG000000028470 | glutathione reductase | 0.44 |

Results

| | | | |
|--------------------|--------------------|---|------|
| ENSGALP00000014379 | ENSGALG00000008862 | DnaJ heat shock protein family (Hsp40) member C10 | 0.47 |
| ENSGALP00000041444 | ENSGALG00000010641 | saccharopine dehydrogenase (putative) | 0.49 |
| ENSGALP00000027982 | ENSGALG00000017351 | stromal interaction molecule 1 | 2.00 |
| ENSGALP00000014599 | ENSGALG00000008985 | sorcin | 2.03 |
| ENSGALP00000004366 | ENSGALG00000002771 | Cysteine-rich protein 1 | 2.17 |
| ENSGALP00000033741 | ENSGALG00000001428 | EF-hand domain family member D1 | 2.23 |
| ENSGALP00000010935 | ENSGALG00000029077 | Cbl proto-oncogene E3 ubiquitin protein ligase | 3.26 |
| ENSGALP00000041423 | ENSGALG00000028204 | glutathione peroxidase 1 | 3.29 |
| ENSGALP00000013480 | ENSGALG00000008290 | V-set and immunoglobulin domain containing | 3.85 |
| ENSGALP00000002442 | ENSGALG00000001607 | chromosome 17 open reading frame 62 | 4.90 |
| ENSGALP00000010210 | ENSGALG00000006323 | leukocyte cell derived chemotaxin 2 | 8.60 |
| ENSGALP00000040190 | ENSGALG00000024273 | pyroglutamyl-peptidase I | 8.63 |
| ENSGALP00000017495 | ENSGALG00000010770 | scinderin | 9.09 |

The results of the experiments with isotope labeling were compared to those of the label-free quantitation based on the emPAI. Twenty proteins were found to be differentially expressed using both methods. However, many of the differentially expressed proteins are expressed below 0.1 % according to determined mole-% so that evaluation of quantitative differences based on emPAI have to be considered with caution for these proteins.

Table 6 Mole-percentages (mole-%) of B and T cell specific proteins as measured in the mass-spectrometric analysis of unlabeled samples. '-' indicates the protein was not identified.

| Accession | Protein description | mole-% in B cells | mole-% in T cells |
|--------------------|---|-------------------|-------------------|
| ENSGALP00000036655 | syntaxin 7 | 0.16 | - |
| ENSGALP00000005662 | karyopherin alpha 2 (RAG cohort 1 importin alpha 1) | 0.05 | - |
| ENSGALP00000003263 | charged multivesicular body protein 4B | 0.15 | 0.02 |
| ENSGALP00000041817 | marginal zone B and B1 cell specific protein | 0.35 | - |
| ENSGALP00000007299 | CD74 molecule | 0.06 | - |
| ENSGALP00000000423 | cysteine and glycine-rich protein 1 | 0.03 | - |
| ENSGALP00000042929 | glutathione reductase | 0.02 | 0.01 |
| ENSGALP00000014379 | DnaJ heat shock protein family (Hsp40) member C10 | 0.01 | 0.005 |
| ENSGALP00000041444 | saccharopine dehydrogenase (putative) | 0.12 | 0.01 |
| ENSGALP00000027982 | stromal interaction molecule 1 | 0.01 | 0.02 |
| ENSGALP00000014599 | sorcin | 0.02 | 0.09 |
| ENSGALP00000004366 | Cysteine-rich protein 1 | 0.17 | 0.17 |
| ENSGALP00000033741 | EF-hand domain family member D1 | - | 0.07 |
| ENSGALP00000010935 | Cbl proto-oncogene E3 ubiquitin protein ligase | - | 0.01 |

Results

| | | | |
|--------------------|--|------|------|
| ENSGALP00000041423 | glutathione peroxidase 1 | 0.11 | 0.07 |
| ENSGALP00000013480 | V-set and immunoglobulin domain containing | - | 0.05 |
| ENSGALP00000002442 | chromosome 17 open reading frame 62 | - | 0.05 |
| ENSGALP00000010210 | leukocyte cell derived chemotaxin 2 | - | 0.15 |
| ENSGALP00000040190 | pyroglutamyl-peptidase I | 0.02 | 0.05 |
| ENSGALP00000017495 | scinderin | - | 0.02 |

The differences in abundance of the identified proteins were confirmed in the mass-spectrometric analyses as can be seen exemplary in the original spectra of representative peptides for the ‘marginal B and B1 cell specific protein’ and for ‘stromal interaction molecule’ in **Figure 14** and **Figure 15**, respectively.

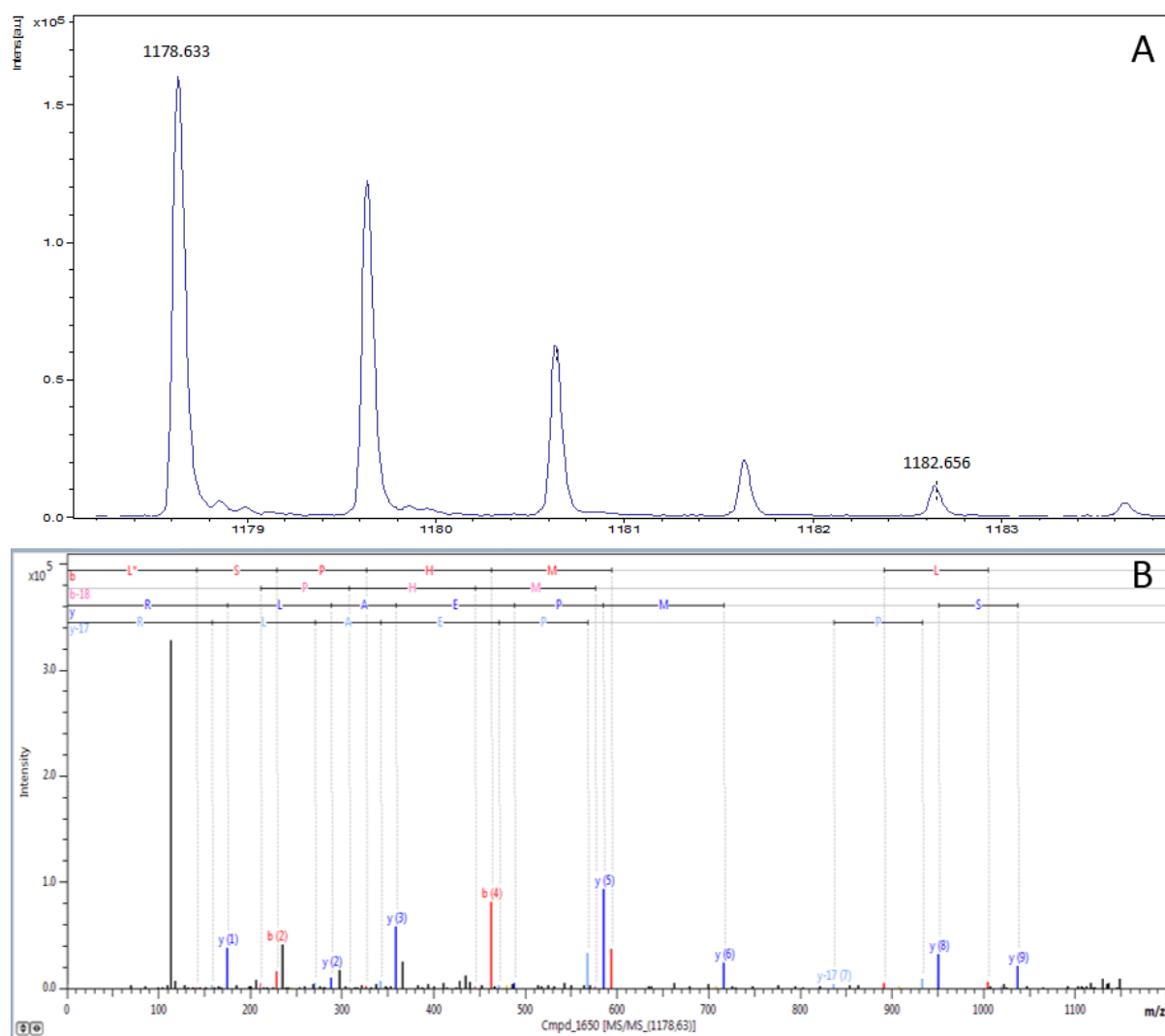


Figure 14 Exemplary spectra of one tryptic peptide of ,marginal zone B and B1 cell specific protein’. A) The mass spectrum of the peptide, showing the light-labeled (1178.633 Da) peak with higher intensity and the heavy-labeled (1182.656 Da) peak

Results

with lower intensity, originating from B- and T cell samples, respectively. **B)** The MS/MS fragment spectrum of the light labeled peptide with the sequence 'LSPHMPEALR' confirmed the identity of the peptide with complete annotation of the peptide sequence as b- and y-series.

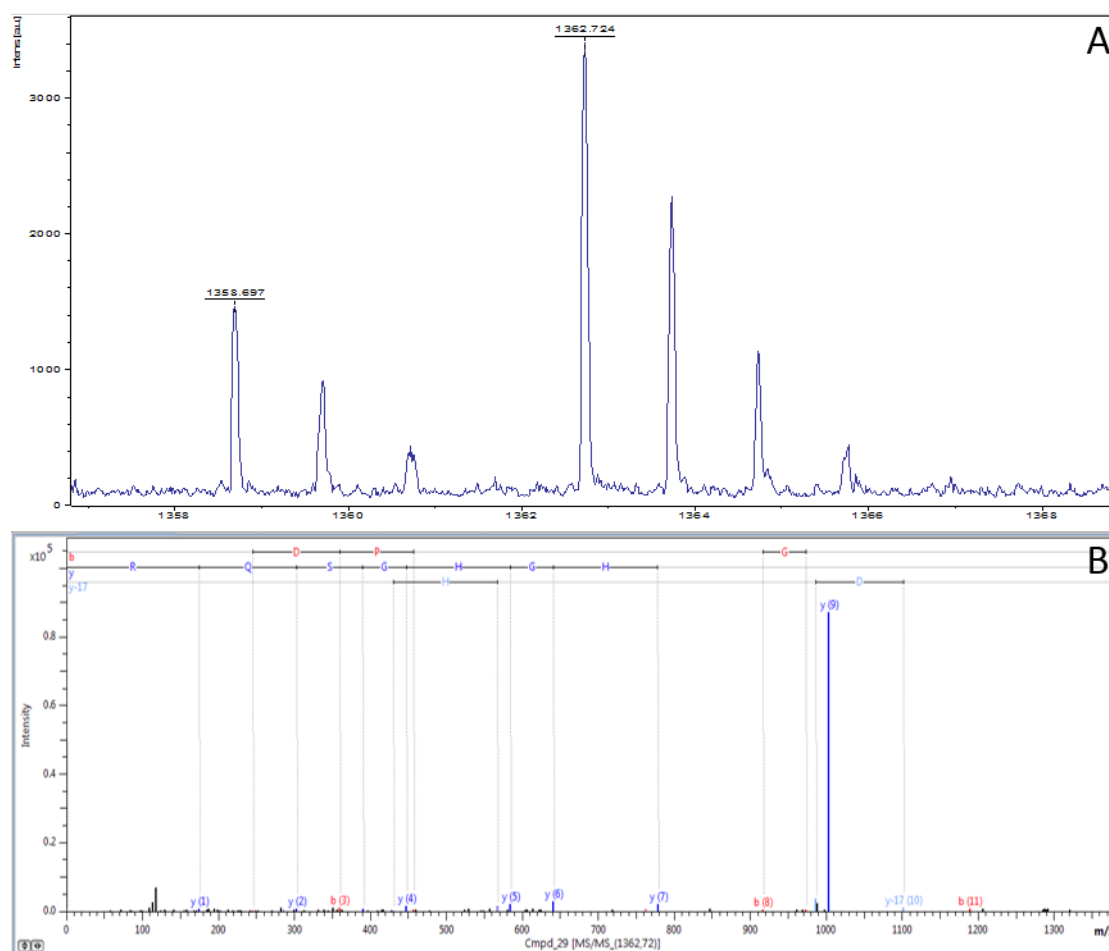


Figure 15 Exemplary spectra of one tryptic peptide of ,stromal interaction molecule. A) The MS spectrum of the peptides, showing the light-labeled (1358.697 Da) peak with lower intensity and the heavy-labeled (1362.726 Da) peak with higher intensity, originating from B- and T-cell samples, respectively. **B)** The MS/MS fragment spectrum of the light labeled peptide with the sequence 'LVDPQHGHSQR' confirmed the identity of the peptide with complete annotation of the peptide sequence as b- and y-series.

5.2. Proteomic analysis of infected chicken B cells in the cytolytic phase

The characterization of primary lymphocytes served as baseline for the quantitative proteome analysis of MDV infected primary lymphocytes. The workflow that had been established for naïve lymphocytes was now applied to infected B cells.

5.2.1. *In vitro* infection of primary B cells

Due to the varying infection rates from 15-50 % with MDV *in vitro* it was necessary to isolate infected cells from the inoculated cell batch prior to the proteome analysis. This was achieved by FACS as recombinant MDV strains vRB-1B and vCVI988 were used for the infection which expressed GFP under the control of the early HSV-1 TK promoter. Primary B cells were isolated from the bursa of Fabricius, inoculated with MDV recombinants and the infected cells were sorted based on GFP signal after inoculation (**Figure 16**).

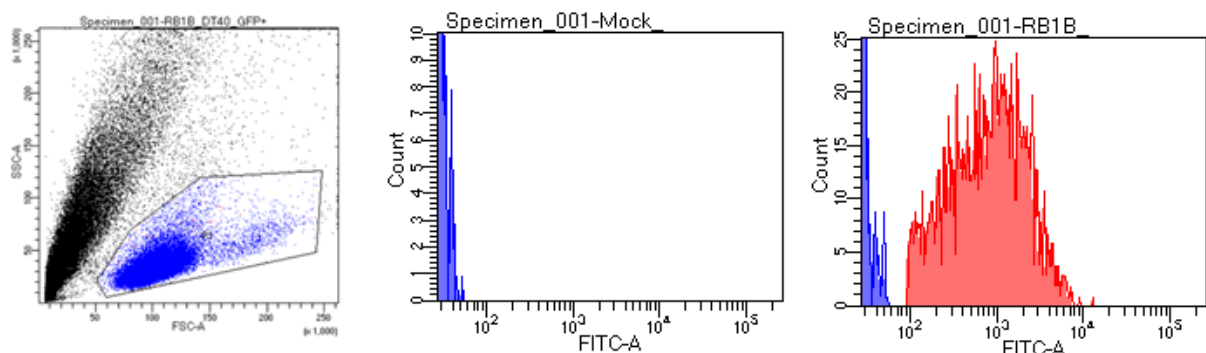


Figure 16 FACS analysis of mock infected and RB-1B infected B cells. The panel on the left side shows the sideward scatter over forward scatter. The dead cells (black) can clearly be distinguished from the viable lymphocytes (blue) based on small size and high granularity. A gate was set across the viable cells. The middle panel shows the mock infected B cells detecting possible GFP signal, which was detected by the FITC-A channel, while the right panel depicts the RB-1B infected B lymphocytes. The GFP + RB-1B infected cells can be clearly differentiated (red) from non-infected cells (blue).

5.2.2. Determination of protein content of primary B cells.

Prior to mass spectrometric analyses, the protein content of infected and mock infected B cells was determined in order to adjust the workflow. Aliquots of 10^6 sorted mock- or RB-1B infected B cells

were lysed and the protein extracted. The extracted proteins were evaluated by SDS-PAGE to estimate the protein content (**Figure 17**). The 10^6 primary mock or RB-1B infected B lymphocytes contained 23 and 18 μg of proteins, respectively. The limited infection rate of primary lymphocytes in cell culture posed difficulties to obtain the required 150 μg of protein for additional fractionation and thus, the workflow for the proteomic analysis was adjusted to avoid sample loss as far as possible.

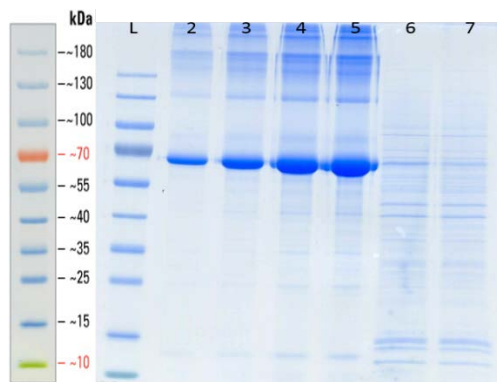


Figure 17 SDS-PAGE of RB-1B infected B cells compared to mock infected B cells and different concentrations of BSA separated on gradient gel (7.5-15 %). Proteins were stained with Coomassie brilliant blue and the protein content was determined by densitometry. L: PageRuler prestained Protein Ladder, 2: 2 μg BSA, 3: 4 μg BSA, 4: 8 μg BSA, 5: 10 μg BSA, 6: 2.3 μg mock infected B cells and 7: 1.8 μg RB-1B- infected (GFP+) B cells.

5.2.3. Identification of changes in protein expression profiles of MDV infected B cells

10^6 infected and mock-infected cells each were analyzed in a bottom-up proteomic approach to identify differentially regulated proteins. 20 μg peptides were isotope-coded with differential dimethyl labeling after FASP digest and equally mixed prior to LC-MALDI TOF/TOF MS analysis. 8 μg of peptides were introduced to the nanoLC and analyzed by MALDI-TOF/TOF MS. An additional OG IEF fractionation was not performed due to the low protein content of sorted cells as determined by SDS-PAGE. The proteins were identified by matching the acquired spectra to the EMBL database containing the *Gallus gallus* proteome. For each comparison two biological replicates were analyzed with inverted labels. The assigned protein and peptide tables were retrieved from the ProteinScape software after the identification query with Mascot (the complete tables can be found in Supptbl 21-28 on the accompanying CD). After elimination of peptides which were associated with several proteins or

contained incorrect number of dimethyl labeled amino acids and intermediate variants, the relative expression level of each protein was calculated as the mean of the isotope ratios of its identified peptides (**Figure 18**). The 10 and 90 % quantile was determined to -0.37 and 0.35 for the corrected SoC values. Using this cutoff and the quantiles determined for the other experiment, only twelve host proteins were differently expressed in RB-1B infected B cells compared to mock infected B cells, which were identified in both replicates.

MDV proteins identified in RB-1B or CVI988 infected B cells are listed in **Table 7**. The description of the identified viral proteins was determined with the UniProt database [132]. As expected, all viral proteins are associated with lytic infection. Thus, the proteins are associated with DNA synthesis and replication [11, 133, 134], cell-to-cell spread [135] and several proteins, such as ICP4, are immediate-early gene products [136].

Table 7 MDV proteins identified in the RB-1B infected B cells. The same proteins were also identified in CVI988 infected B cells, but with less associated peptides.

| Gene Symbol | Gene Name | Protein Name/Description |
|-------------------|-----------|--|
| MDV014 | UL2 | Uracil-DNA glycosylase |
| MDV031 | UL19 | Major capsid protein |
| MDV036 | UL23 | Thymidine kinase |
| MDV038 | UL26 | Capsid scaffolding protein |
| MDV042 | UL29 | Major DNA binding protein |
| MDV047 | UL34 | Nuclear egress protein 2 |
| MDV052 | UL39 | Ribonucleoside-diphosphate reductase large subunit |
| MDV053 | UL40 | Ribonucleoside-diphosphate reductase small subunit |
| MDV055 | UL42 | DNA polymerase cofactor |
| MDV062 | UL49 | Tegument protein VP22 |
| MDV063 | UL50 | Deoxyuridine 5'-triphosphate nucleotidohydrolase (DUT) |
| MDV073 | R-LORF14a | Phosphoprotein 38 |
| MDV084/ MDV100 | ICP4 | transcriptional regulator ICP4 |

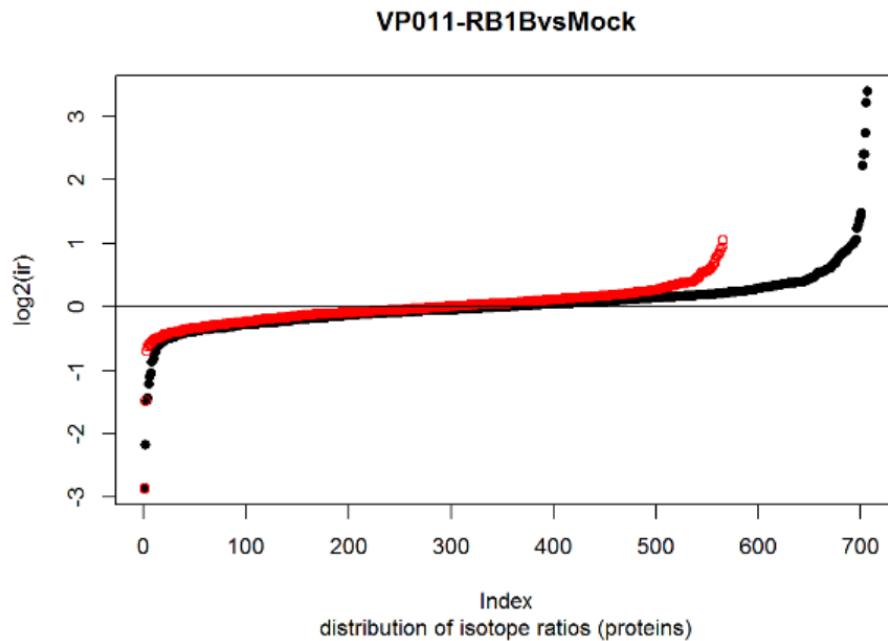


Figure 18 Relative expression levels of cellular proteins after infection of B cells with RB-1B in comparison to mock-infection. Proteins with an isotope ratio of one are found around zero in this logarithmic scale on the y-axis, upregulated proteins are found in the positive range while down-regulated proteins after infection are found in the negative range.

The majority of identified host proteins were found within the two-fold change range (equivalent to between -1 and 1 in logarithmic scale, **Figure 18**), which was set as cut-off for regulated proteins. However, only twelve proteins, which seem to be affected by RB-1B infection and which were at least two fold up or down regulated, could be identified (**Table 8**). Only six differentially expressed proteins were identified in the CVI988-infected B cells compared to mock infected B cells, after elimination of irregularly labeled and shared peptides. These included the avian beta defensin 2 (avBD2, ENSGALG00000016669), interleukin 18 (IL-18, ENSGALG00000007874) and the major histocompatibility complex class II beta chain BLB1 (ENSGALG00000000141). These proteins were down-regulated after CVI988 infection. Only one protein, namely avBD2, was detected directly in both lists of quantitatively differentially expressed protein after RB-1B- and CVI988-infection. However, six potential infection markers could be detected in the original spectra of all experiments, with similar trend in isotope ratios (SoC, in this case sample is consistent with MDV-infection and control is equivalent to mock-infection), namely, avian beta defensin 2 (SoC after RB-1B infection: 0.18, SoC after CVI988-infection: 0.23), interleukin 18 (SoC after RB-1B infection: 0.60, SoC after CVI988-infection: 0.23),

0.33), BLB1 (SoC after RB-1B infection: 0.81, SoC after CVI988-infection: 0.43), CD74 (SoC after RB-1B infection: 0.48, SoC after CVI988-infection: 0.74), ribosomal protein S10 (SoC after RB-1B infection: 0.47, SoC after CVI988-infection: 0.83) and lactate dehydrogenase A (SoC after RB-1B infection: 2.36, SoC after CVI988-infection: 1.48).

Table 8 Differentially expressed proteins after infection with RB-1B. Shown are the proteins that are at least two-fold up (>2) or down (<0.5) regulated after infection of primary B cells with the very virulent RB-1B strain. FC: fold change.

| Protein ID | Gene ID | Protein | FC |
|--------------------|--------------------|---|------|
| ENSGALP00000023926 | ENSGALG00000014852 | myosin light chain 12B | 2.99 |
| ENSGALP00000035593 | ENSGALG00000028273 | Hemoglobin subunit beta | 2.57 |
| ENSGALP00000026127 | ENSGALG00000016233 | Thyroglobulin | 2.50 |
| ENSGALP00000038904 | ENSGALG00000007468 | hemoglobin alpha 1 (HBAA) mRNA | 2.38 |
| ENSGALP00000006415 | ENSGALG00000004034 | capping actin protein of muscle Z-line beta subunit | 2.38 |
| ENSGALP00000038626 | ENSGALG00000006300 | lactate dehydrogenase A | 2.36 |
| ENSGALP00000007705 | ENSGALG00000004831 | ribosomal protein S4 X-linked | 2.15 |
| ENSGALP00000038463 | ENSGALG00000003197 | ribosomal protein L7a | 2.03 |
| ENSGALP00000022269 | ENSGALG00000013726 | phosphoribosylaminoimidazole carboxylase phosphoribosylaminoimidazolesuccinocarbox amide synthase (PAICS) | 0.49 |
| ENSGALP00000007299 | ENSGALG00000004594 | CD74 molecule | 0.48 |
| ENSGALP00000004437 | ENSGALG00000002813 | ribosomal protein S10 | 0.47 |
| ENSGALP00000030904 | ENSGALG00000016669 | avian beta-defensin 2 | 0.18 |

For the GO analysis of proteins differentially expressed after RB-1B and CVI988 infection, the protein IDs were converted into their associated Gene ID's and cross-referenced to the *Homo sapiens* homolog Gene IDs using the ENSEMBL biomaRt [126]. Using the QuickGO platform [110], the differentially expressed proteins were associated with 70 different biological processes, including oxygen transport (GO:0015671, 9.09 %), oxidation-reduction process (GO:0055114, 5.45 %), immune response (GO:0006955, 3.64 %), translation (GO:0006412, 3.64 %) and inflammatory response (GO:0006954, 2.73 %) (Supptbl 29 on the accompanying CD).

Hemoglobin subunit beta, thyroglobulin and hemoglobin alpha1 (HBAA) were most likely the result of contamination by leukocytes and erythrocytes during isolation of primary B cells from the bursa of Fabricius.

The expression of three ribosomal proteins, S10, L71 and S4 X-linked, was affected in MDV infected B cells, which were associated with the biological process 'translation'. In addition, the protein expression of Immune response associated proteins, including the MHC II beta chain, interleukin 18, CD74 molecule and avian beta-defensin 2, were detected to be regulated by MDV infection. All of these proteins were down regulated in infected B lymphocytes compared to mock-infected cells. Especially, the avian beta-defensin 2 protein was down-regulated 5-fold and 5.6-fold after infection with CVI988 or the very virulent RB-1B strain, respectively. Exemplary MS spectra of the isotopomers of the peptide 'GGSCHFGGCPSHLIK' with 1669.81 Da and 1677.87 Da, respectively, are shown in **Figure 19A**. The peak for CH₂O-labeled peptide in this spectrum originated from mock-infected B-cells and the CD₂O-labeled peak from RB-1B infected cells. The annotated fragment spectrum of the peptide is given in **Figure 19B**.

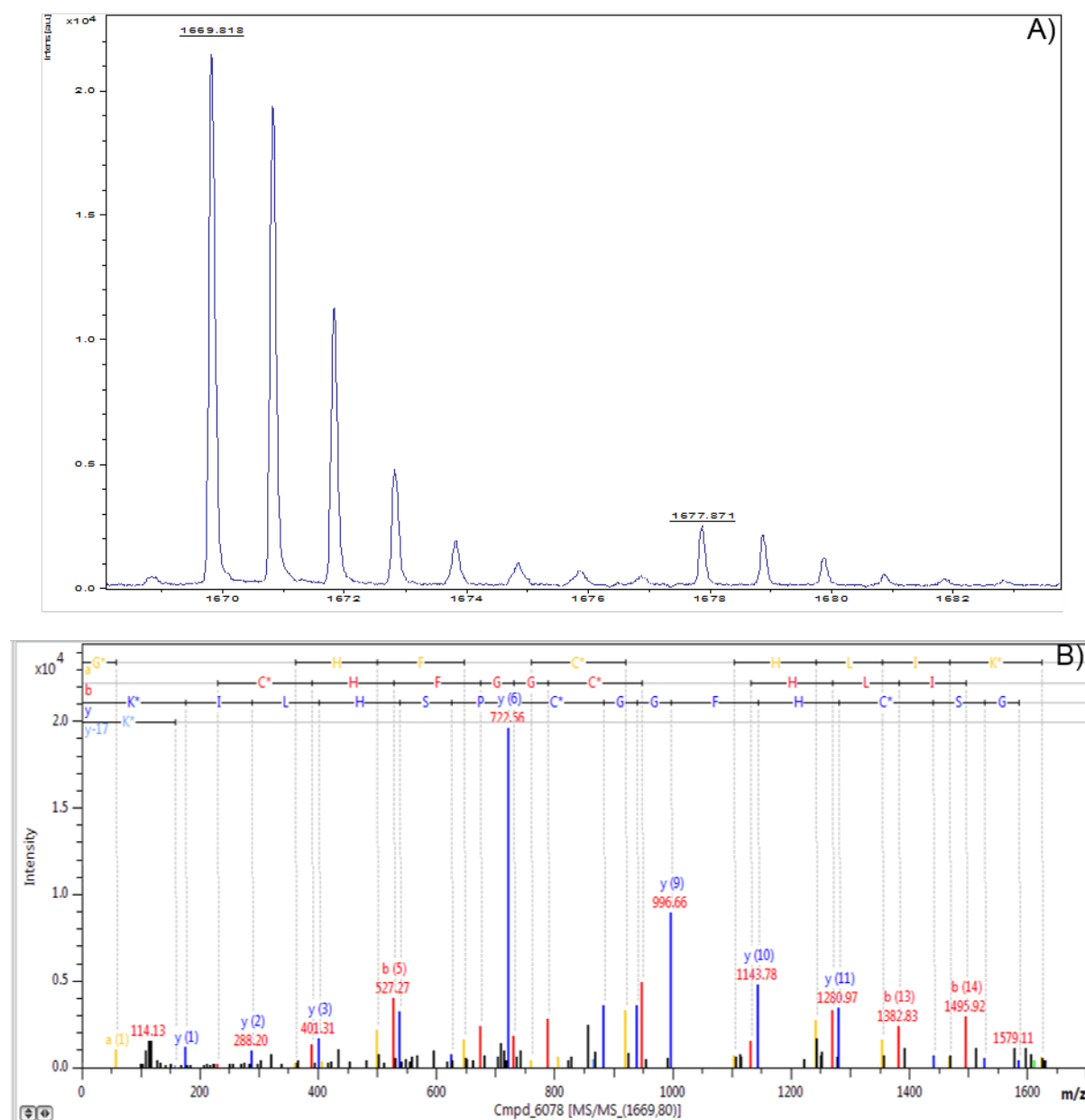


Figure 19 MS spectrum (A) and fragment spectrum (B) of avBD2 peptide 'GGSCHFGGCPSHLIK' from the comparison of RB-1B infected B cells to mock infected B cells. The peak for CH₂O labeled peptide (L) at 1669.81 Da has a 5.0 times higher intensity than the peak for CD₂O labeled peptide (H) at 1677.87 Da. The fragment spectrum in panel B shows the light-labeled (CH₂O) form. The almost complete sequence was identified in the y-series.

The IL-18 protein was identified as in the original MS spectrum depicting the CH₂O and CD₂O labeled forms of the peptide 'DIPGESNIIFFK' at 1435.78 Da and 1443.83 Da, respectively (**Figure 20A**). The CH₂O-labeled peptide originated in this case from mock-infected B-cells and the CD₂O-labeled peptide

from CVI988 infected cells. The peptide was identified by fragmentation and detection of the almost complete amino acid sequence in the y-series (**Figure 20B**).

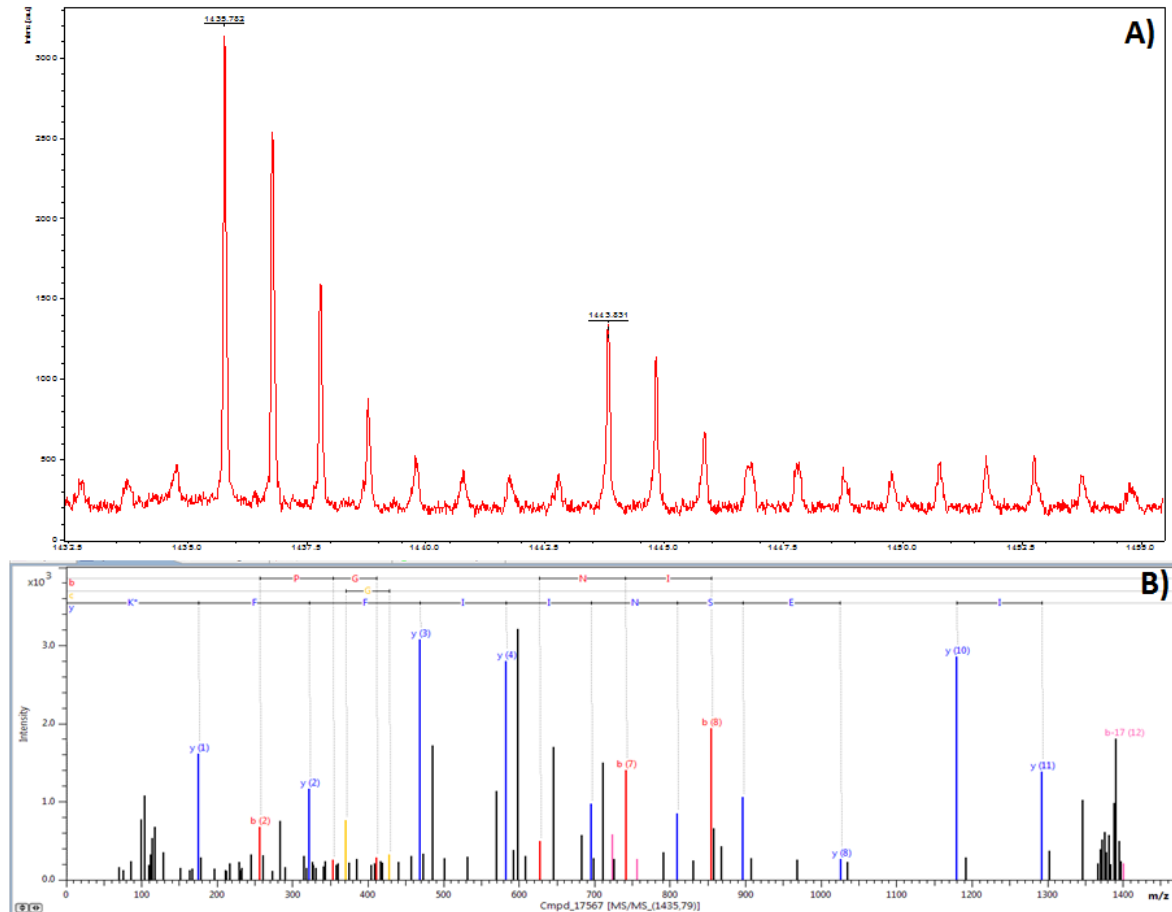


Figure 20 MS spectrum (A) and fragment spectrum (B) of IL-18 peptide ‘DIPGESNIIFFK’ from the comparison of CVI988 infected B cells with mock infected B cells. The CH₂O labeled peptide (L) at 1435.78 Da has a 3.0 times higher intensity than the CD₂O labeled peptide (H) at 1443.83 Da. The fragment spectrum in panel B shows the light-labeled (CH₂O) form. The almost complete sequence was confirmed in the y-series.

5.2.4. Sequence analysis of mRNA isolated from MDV-infected B lymphocytes

To confirm the potential infection markers and investigate the corresponding gene expression levels, three biological replicates each of mRNA isolated from RB-1B-, CVI988- or mock-infected B cells were sequenced. After preparation of the cDNA libraries, the quality and mean fragment length was evaluated on a DNA 7500 chip. All samples except RB-1B 1 and RB-1B 2 showed libraries of high quality

and sufficient concentration with expected mean fragment lengths of 200 bp (**Figure 21**). However, all libraries were sequenced.

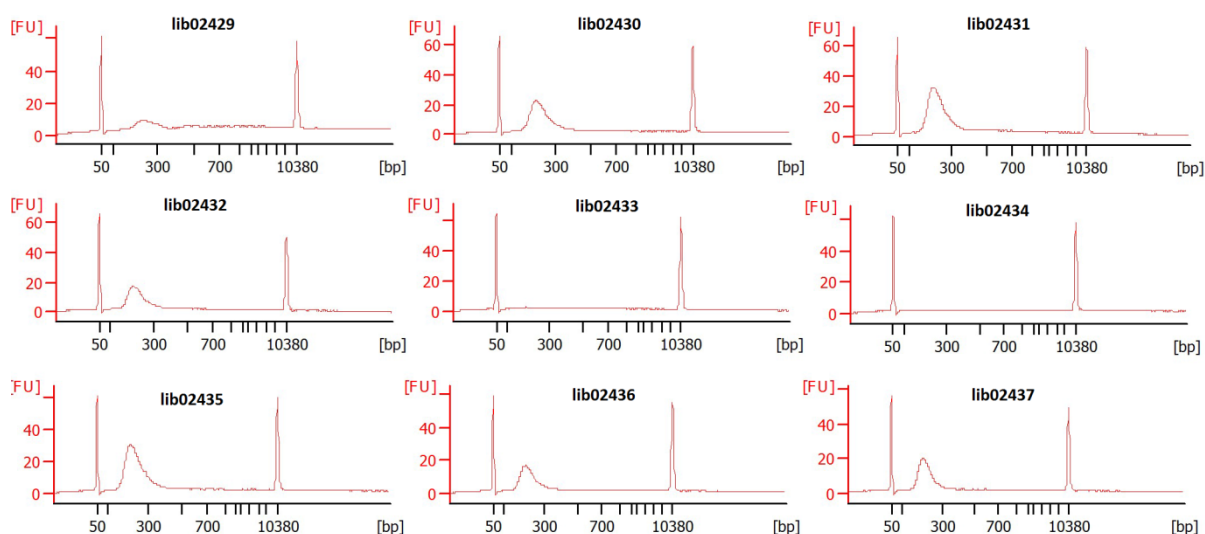


Figure 21 Quality control of generated cDNA libraries. For each sample library, fragments with a mean length of 200 bp were expected and were detected for all libraries, except lib02433 and lib02434.

The two sequencing runs resulted in detection of 13 million to almost 18 million sample reads per analyzed library, except for the RB-1B 3 sample, for which only about 500,000 reads were obtained (**Table 9**).

Table 9 Summary and evaluation of sequencing runs, of number of reads that were sequenced. *Due to low number of sequenced reads in first run, the sample RB-1B 3 was not sequenced in a second run. ERCC: internal controls.

| Sample | Library | Reads 1. run | Reads 2. run | Total Reads | Amount ERCC [%] | Sample Reads |
|----------|----------|--------------|--------------|-------------|-----------------|--------------|
| Mock 1 | lib02429 | 3,395,241 | 15,498,198 | 18,893,439 | 5.02 | 17,944,988 |
| Mock 2 | lib02430 | 10,387,697 | 7,778,933 | 18,166,630 | 19.75 | 14,578,721 |
| Mock 3 | lib02431 | 6,731,533 | 10,503,506 | 17,235,039 | 7.30 | 15,976,881 |
| RB1B 1 | lib02432 | 10,101,304 | 8,281,020 | 18,382,324 | 25.23 | 13,744,464 |
| RB1B 2 | lib02433 | 11,741,374 | 5,400,315 | 17,141,689 | 10.39 | 15,360,668 |
| RB1B 3 | lib02434 | 601,281 | 0* | 601,281 | 14.25 | 515,598 |
| CVI988 1 | lib02435 | 9,217,190 | 7,088,954 | 16,306,144 | 13.80 | 14,055,896 |
| CVI988 2 | lib02436 | 10,565,041 | 5,631,143 | 16,196,184 | 9.02 | 14,735,288 |
| CVI988 3 | lib02437 | 12,835,575 | 4,670,089 | 17,505,664 | 15.37 | 14,815,043 |

Results

The amount of ERCC controls varied between 5 and 25 %, but all showed a high correlation with coefficients (R^2) between 0.83 - 0.94, which indicated a good correlation between read numbers and transcript concentration as shown in **Figure 22**.

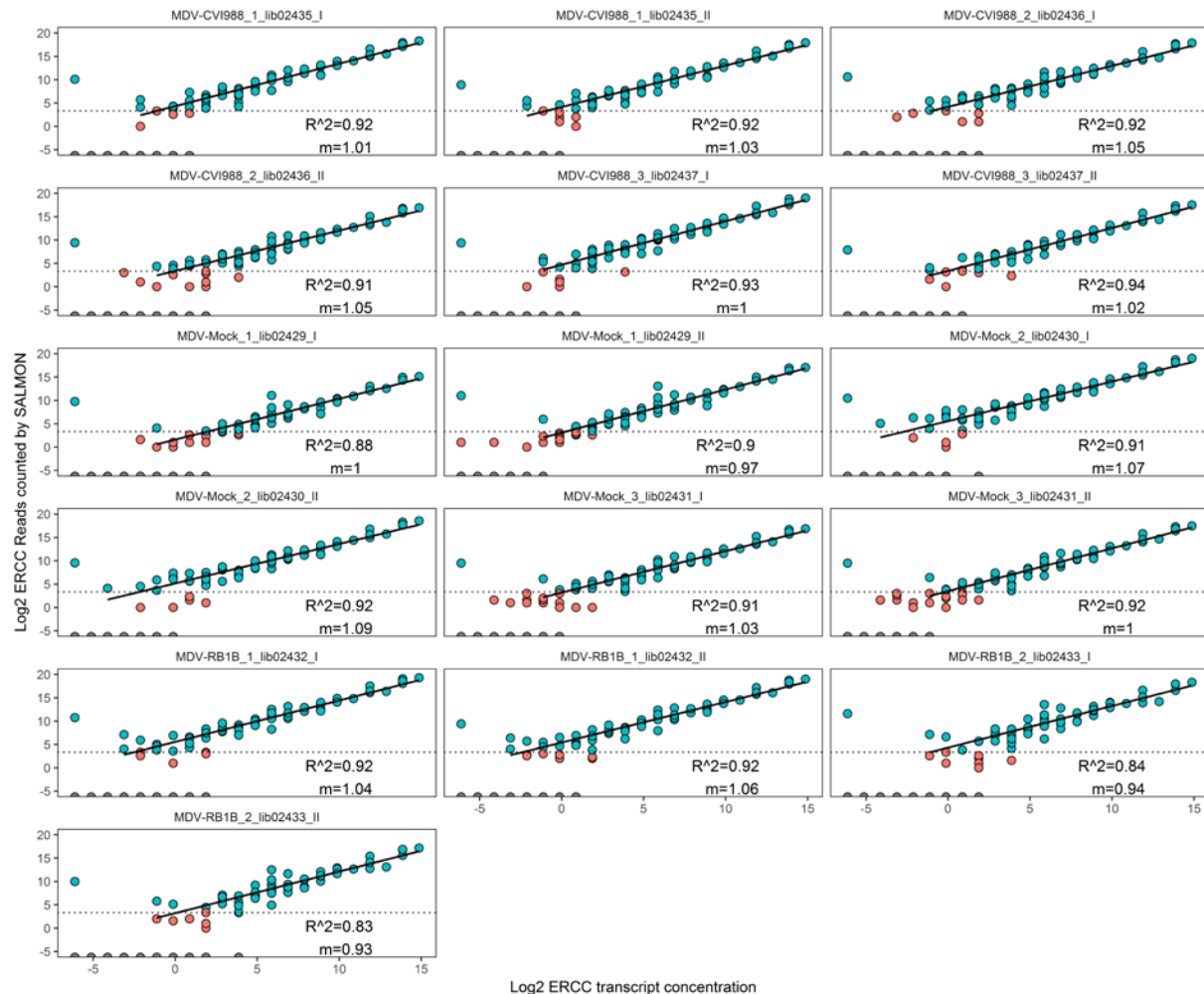
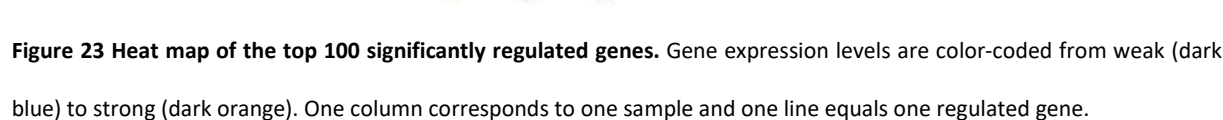


Figure 22 ERCC analysis as internal control for sequencing runs. A linear correlation of the number of sequenced reads and the transcript concentration was observed for all samples. As the transcript concentration increases, also the number of reads per transcript increased. The correlation coefficient shows values close to 1, as it was expected for data with a narrow variation range and tight correlation phase. m: slope, R^2 : correlation coefficient.

In order to assign the reads to the transcripts of the database and quantify the expression of transcripts, the RNA sequencing data was evaluated with the tool ‘Salmon’ [137]. After normalization, a statistical analysis based on Benjamini and Hochberg algorithm [138] was performed and a list of regulated genes was obtained for each possible comparison (Supptbl 30-32 on the accompanying CD). A gene was considered as regulated when a minimum binary logarithmic fold change of ± 2 was

obtained and the adjusted p-value, which is used to account for multiple testing, was less than 0.01. The top 100 significantly regulated genes are shown in **Figure 23**. The underlying cluster analysis resulted in two distinct clusters of CVI988 1-3 and mock 1-3. However, the RB-1B samples do not cluster with each other, as variation of sequenced reads was too high. All infected samples could be clearly differentiated from mock-infected samples based on gene expression pattern.



In order to identify differences in the gene expression profiles, the fold changes (FC) of the comparisons between all analyzed groups were calculated and thus, three different comparisons were possible: CVI988 vs. mock, RB-1B vs. mock and CVI988 vs. RB-1B.

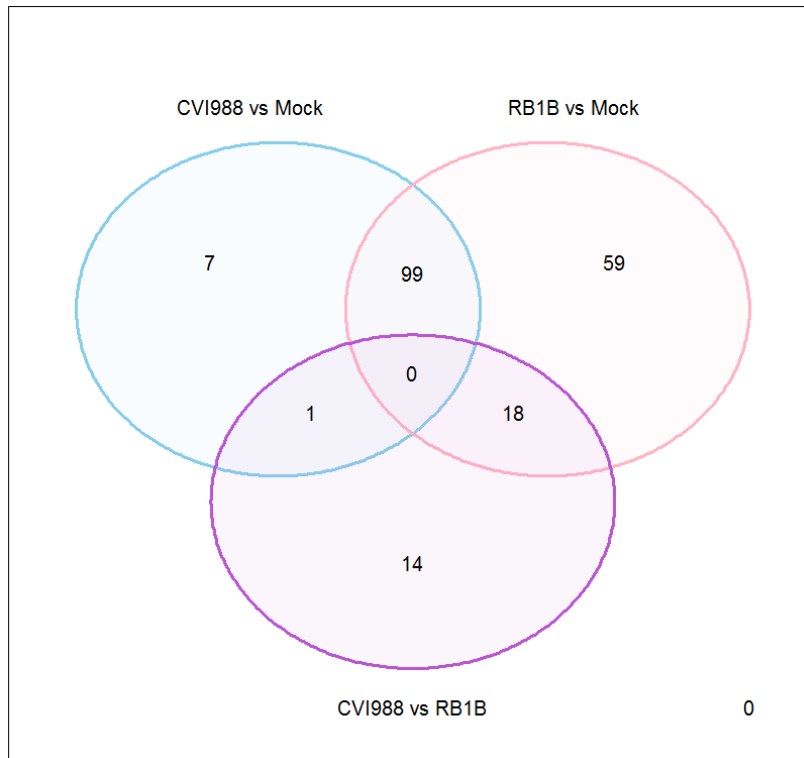


Figure 24 Venn-diagram of all regulated genes in the three different comparisons. In the comparison CVI988 vs Mock – infected B cells in total 107 genes were differentially expressed, from which 99 were also seen differentially expressed in the comparison RB-1B vs. mock infected B cells (in total 176 differentially expressed genes). Only 33 differentially expressed genes were observed in the comparison between RB-1B vs CVI988 infected B cells.

In total, in the comparison CVI988 - versus mock-infected B cells 107 genes were significantly regulated and comparing RB-1B - with mock-infected B cells 176 genes were significantly regulated. The two comparisons share 99 differentially expressed genes, 80 genes were identified as MDV genes (**Figure 24**). No qualitative or quantitative differences in the expression of viral genes were observed in the comparison CVI988 and RB-1B infected B cells. The identified MDV genes are summarized in **Table 10**. For the 13 MDV proteins, which were identified in the proteomic analysis of RB-1B and CVI988 infected B cells, expression of the corresponding mRNA was confirmed as well.

Table 10 Identified MDV transcripts in the RNA sequencing experiments in both RB-1B and CV1 infected B cells.

| Gene Symbol | Gene Name | Protein Name |
|--------------------|------------------|---|
| MDV003 | RLORF2 | vIL-8 |
| MDV005 | Meq | oncoprotein |
| MDV008 | pp24 | phosphoprotein 24 |
| MDV010 | MDV010 | virulence factor |
| MDV012 | LORF2 | uncharacterized protein |
| MDV013 | UL1 | envelope glycoprotein L |
| MDV014 | UL2 | uracil-DNA glycosylase |
| MDV015 | UL3 | nuclear phosphoprotein |
| MDV015.5 | UL3.5 | HSV-1 UL3.5-like protein |
| MDV016 | UL4 | nuclear protein |
| MDV017 | UL5 | DNA replication helicase |
| MDV018 | MDV018 | portal protein |
| MDV019 | UL7 | cytoplasmic envelopment protein 1 |
| MDV020 | MDV020 | DNA helicase/primase complex-associated protein |
| MDV021 | UL9 | replication origin-binding protein |
| MDV022 | UL10 | envelope glycoprotein M |
| MDV023 | UL11 | cytoplasmic envelopment protein 3 |
| MDV024 | UL12 | alkaline nuclease |
| MDV025 | UL13 | serine/ threonine-protein kinase |
| MDV026 | UL14 | tegument protein |
| MDV027 | UL15 | tripartite terminase subunit 3 |
| MDV028 | UL16 | cytoplasmic envelopment protein 2 |
| MDV029 | UL17 | capsid vertex component 1 |
| MDV030 | UL18 | triplex capsid protein 2 |
| MDV031 | UL19 | major capsid protein |
| MDV032 | UL20 | HSV-1 UL20-like protein |
| MDV033 | UL21 | tegument protein |
| MDV034 | UL22 | envelope glycoprotein H |
| MDV035 | UL24 | HSV-1 UL24-like protein |
| MDV036 | UL23 | thymidine kinase |
| MDV037 | UL25 | capsid vertex component 2 |
| MDV038 | UL26 | capsid scaffolding protein |
| MDV039 | UL26.5 | LORF5 |
| MDV040 | UL27 | envelope glycoprotein B |
| MDV041 | UL28 | tripartite terminase subunit 1 |
| MDV042 | UL29 | major DNA-binding protein |
| MDV043 | MDV043 | DNA polymerase catalytic subunit |
| MDV044 | UL31 | nuclear egress protein 1 |
| MDV045 | UL32 | tripartite terminase subunit 2 |
| MDV046 | MDV046 | packaging protein UL32 homolog |
| MDV047 | UL34 | nuclear egress protein 2 |

| | | |
|----------|-----------|--|
| MDV048 | UL35 | small capsomere-interacting protein |
| MDV049 | MDV049 | large tegument protein deneddylase |
| MDV050 | UL37 | inner tegument protein |
| MDV051 | UL38 | triplex capsid protein 1 |
| MDV052 | UL39 | ribonucleoside-diphosphate reductase large subunit |
| MDV053 | UL40 | ribonucleoside-diphosphate reductase small subunit |
| MDV054 | UL41 | virion host shutoff protein |
| MDV055 | UL42 | DNA polymerase processivity factor |
| MDV056 | UL43 | membrane protein UL43 homolog |
| MDV057 | UL44 | glycoprotein 57-65 |
| MDV058 | UL45 | cell fusion protein |
| MDV059 | UL46 | tegument protein |
| MDV060 | UL47 | tegument protein |
| MDV061 | UL48 | tegument protein VP16 homolog |
| MDV062 | UL49 | tegument protein VP22 homolog |
| MDV063 | UL50 | deoxyuridine 5'-triphosphate nucleotidohydrolase (DUT) |
| MDV064 | UL49.5 | envelope glycoprotein N |
| MDV065 | UL51 | tegument protein |
| MDV066 | UL52 | DNA primase |
| MDV067 | UL54 | envelope glycoprotein K |
| MDV068 | MDV068 | mRNA export factor ICP27 homolog |
| MDV069 | MDV069 | uncharacterized gene 69 protein |
| MDV070 | UL55 | tegument protein |
| MDV071 | MDV071 | uncharacterized gene 71 protein |
| MDV072 | MDV072 | uncharacterized gene 72 protein |
| MDV072.5 | MDV072.5 | type 2 membrane protein |
| MDV073 | R-LORF14a | phosphoprotein pp38 |
| MDV084 | ICP4 | major viral transcription factor ICP4 |
| MDV087 | MDV087 | uncharacterized gene 87 protein |
| MDV088 | US1 | transcriptional regulator ICP22 |
| MDV089 | US10 | virion protein US10 homolog |
| MDV090 | MDV090 | uncharacterized gene 90 protein |
| MDV091 | US2 | protein US2 homolog |
| MDV092 | US3 | protein kinase US3 homolog |
| MDV093 | MDV093 | uncharacterized gene 93 protein |
| MDV094 | US6 | envelope glycoprotein D |
| MDV095 | US7 | envelope glycoprotein I |
| MDV096 | US8 | envelope glycoprotein E |
| MDV097 | MDV097 | uncharacterized gene 97 protein |

In total, 5 % of the total identified reads could be mapped to the MDV transcriptome. All of the identified MDV genes are actively expressed during lytic infection of B cells. However, we were primarily interested in differentially expressed host genes and conducted RNA sequencing experiments to confirm the potential infection markers identified by LC-MALDI TOF/TOF MS. Expression of candidate infection markers identified by proteome analysis could be detected in the transcriptome. However, gene expression, apart from LADH, was not significantly altered after MDV infection (**Table 11**). However, a log₂FC of -1.6 or -1.9 for mRNA expression of LADH was seen after CVI988 or RB-1B infection, respectively. But these fold changes were only observed with an adjusted p-value of 0.13 and hence, were not considered as significant. The mRNA for avBD2 was not identified in any of the samples by RNA sequencing analysis.

Table 11 Gene expression of infection marker candidates identified in proteome analysis. The log₂FC of protein or mRNA expression is shown. A log₂FC between -2 and 2 or log₂FC between -1 and 1 was set as range of no relevant changes in mRNA expression or protein expression, respectively. MDV is equivalent to either RB-1B or CVI988.

| Potential infection marker | log ₂ FC in proteome analysis in compare MDV vs mock | Log ₂ FC in RNA-seq in compare CVI988 vs mock | Log ₂ FC in RNA-seq in compare RB-1B vs mock |
|----------------------------|---|--|---|
| avBD2 | -2.47 | - | - |
| IL-18 | -1.00 | -0.8 | -0.3 |
| PAICS | -1.02 | -0.19 | -0.74 |
| CD74 | -1.06 | -0.76 | -0.02 |
| RPS10 | -1.09 | 0.005 | 0.25 |
| RPL7A | 1.02 | -0.09 | 0.09 |
| RPS4X | 1.10 | -0.1 | 0.37 |
| LDHA | 1.24 | -1.59 | -1.9 |
| CAPZB | 1.26 | -0.37 | -0.4 |
| BLB1 | -1.0 | 1.5 | -0.78 |

In total, 26 and 95 differentially expressed host genes were identified in the compares CVI988 vs. mock (**Table 12**) and RB-1B vs. mock (**Table 13**), respectively.

Results

Table 12 Differentially expressed host genes in the comparison CVI988 vs mock-infected B cells. Galgal: *Gallus gallus*, Hsap:

Homo sapiens, FC: fold change, padj: adjusted p-value.

| GalGal_GeneID | Hsap_GeneID | log2FC | padj | Gene Name |
|--------------------|-----------------|--------|-------------|---|
| ENSGALG00000030005 | ENSG00000186431 | 6.034 | 2.70609E-12 | Fc fragment of IgA receptor |
| ENSGALG00000023818 | N/A | 5.841 | 2.73398E-29 | heat shock protein family B (small) member 9 |
| ENSGALG00000009433 | ENSG00000151929 | 5.198 | 2.42968E-12 | BCL2 associated athanogene 3 |
| ENSGALG00000038019 | N/A | 4.876 | 1.04363E-09 | Uncharacterized |
| ENSGALG00000004184 | ENSG00000113140 | 4.059 | 2.71706E-08 | secreted protein acidic and cysteine rich |
| ENSGALG00000032687 | ENSG00000181649 | 4.053 | 1.11822E-07 | pleckstrin homology like domain family A member 2 |
| ENSGALG00000041683 | N/A | 4.007 | 1.44688E-06 | Uncharacterized |
| ENSGALG00000011715 | ENSG00000126803 | 3.572 | 6.07777E-14 | heat shock protein family A (Hsp70) member 2 |
| ENSGALG00000045632 | N/A | 3.548 | 1.84333E-05 | Uncharacterized |
| ENSGALG00000045085 | ENSG00000185745 | 3.135 | 0.00044254 | interferon induced protein with tetratricopeptide repeats 1 |
| ENSGALG00000039895 | ENSG00000142627 | 3.092 | 0.001670239 | EPH receptor A2 |
| ENSGALG00000039786 | ENSG00000077782 | 3.040 | 0.000882476 | fibroblast growth factor receptor 1 |
| ENSGALG00000009400 | ENSG00000100678 | 2.991 | 8.51256E-08 | solute carrier family 8 member A3 |
| ENSGALG00000013723 | ENSG00000135114 | 2.958 | 7.16543E-05 | 2'-5'-oligoadenylate synthetase like |
| ENSGALG00000003932 | ENSG00000124145 | 2.909 | 0.006569892 | syndecan 4 |
| ENSGALG00000003261 | ENSG00000177469 | 2.766 | 0.002868509 | caveolae associated protein 1 |
| ENSGALG00000046283 | ENSG00000131711 | 2.132 | 0.00988534 | microtubule associated protein 1B |
| ENSGALG00000045371 | ENSG00000262664 | 1.939 | 0.001224911 | OVCA2, serine hydrolase domain containing |
| ENSGALG00000040463 | ENSG00000100314 | -1.709 | 0.004991038 | calcium binding protein 7 |
| ENSGALG00000041240 | N/A | -2.271 | 0.006743279 | Uncharacterized |
| ENSGALG00000030602 | ENSG00000149451 | -2.296 | 0.000307467 | ADAM metalloproteinase domain 33 |
| ENSGALG00000008970 | ENSG00000123572 | -2.605 | 0.000984854 | Nik related kinase |
| ENSGALG00000030233 | N/A | -2.750 | 0.000665792 | Uncharacterized |
| ENSGALG00000040221 | N/A | -2.799 | 0.001510286 | Uncharacterized |
| ENSGALG00000013371 | ENSG00000125910 | -3.094 | 0.005790505 | sphingosine-1-phosphate receptor 4 |
| ENSGALG00000011149 | ENSG00000153246 | -3.479 | 5.74075E-05 | phospholipase A2 receptor 1 |

Table 13 Differentially expressed host genes in the compare RB-1B vs mock-infected B cells. Galgal: *Gallus gallus*, Hsap:

Homo sapiens, FC: fold change, padj: adjusted p-value.

| GalGal_GeneID | Hsap_GeneID | log2FC | padj | Gene Name |
|--------------------|-----------------|--------|------------|--|
| ENSGALG00000023818 | N/A | 6,651 | 6,5185E-33 | heat shock protein family B (small) member 9 |
| ENSGALG00000038019 | N/A | 5,553 | 1,3468E-11 | Uncharacterized |
| ENSGALG00000030005 | ENSG00000186431 | 5,469 | 1,9881E-10 | Fc fragment of IgA receptor |

Results

| | | | | |
|---------------------|-----------------|--------|------------|---|
| ENSGALG00000009433 | ENSG00000151929 | 5,285 | 9,8536E-12 | BCL2 associated athanogene 3 |
| ENSGALG00000004184 | ENSG00000113140 | 5,198 | 2,1724E-12 | secreted protein acidic and cysteine rich |
| ENSGALG000000041683 | N/A | 4,405 | 2,9634E-07 | Uncharacterized |
| ENSGALG000000032997 | ENSG00000132205 | 4,194 | 0,00020954 | elastin microfibril interfacier 2 |
| ENSGALG000000011715 | ENSG00000126803 | 3,976 | 2,4542E-15 | heat shock protein family A (Hsp70) member 2 |
| ENSGALG000000032687 | ENSG00000181649 | 3,955 | 2,4339E-06 | pleckstrin homology like domain family A member 2 |
| ENSGALG000000012367 | ENSG00000100505 | 3,868 | 2,6814E-05 | tripartite motif containing 9 |
| ENSGALG000000045632 | N/A | 3,723 | 2,5833E-05 | Uncharacterized |
| ENSGALG000000039786 | ENSG00000077782 | 3,697 | 3,7799E-05 | fibroblast growth factor receptor 1 |
| ENSGALG000000003932 | ENSG00000124145 | 3,687 | 8,5217E-05 | syndecan 4 |
| ENSGALG000000000362 | ENSG00000134369 | 3,629 | 0,00013952 | neuron navigator 1 |
| ENSGALG000000013723 | ENSG00000135114 | 3,589 | 2,9634E-07 | 2'-5'-oligoadenylate synthetase like |
| ENSGALG000000045085 | ENSG00000185745 | 3,527 | 0,00010758 | interferon induced protein with tetratricopeptide repeats 1 |
| ENSGALG000000023364 | ENSG00000179604 | 3,503 | 0,00024291 | CDC42 effector protein 4 |
| ENSGALG000000028568 | ENSG00000119661 | 3,467 | 0,00063477 | dynein axonemal light chain 1 |
| ENSGALG000000006751 | ENSG00000154096 | 3,413 | 0,00171869 | Thy-1 cell surface antigen |
| ENSGALG000000001926 | ENSG00000106211 | 3,388 | 0,00031136 | heat shock protein family B (small) member 1 |
| ENSGALG000000011885 | ENSG00000164111 | 3,197 | 0,00201083 | annexin A5 |
| ENSGALG000000046283 | ENSG00000131711 | 3,161 | 0,00016568 | microtubule associated protein 1B |
| ENSGALG000000028318 | ENSG00000124762 | 3,125 | 0,00130899 | cyclin dependent kinase inhibitor 1A |
| ENSGALG000000032933 | ENSG00000158406 | 3,097 | 0,00528632 | histone cluster 1 H4 family member h |
| ENSGALG000000043513 | ENSG00000007866 | 3,085 | 0,00891051 | TEA domain transcription factor 3 |
| ENSGALG000000012277 | ENSG00000185022 | 3,024 | 0,00074124 | MAF bZIP transcription factor F |
| ENSGALG000000039028 | ENSG00000143369 | 3,001 | 0,0099065 | extracellular matrix protein 1 |
| ENSGALG000000026970 | ENSG00000142089 | 2,958 | 1,6192E-05 | interferon induced transmembrane protein 3 |
| ENSGALG000000009400 | ENSG00000100678 | 2,912 | 1,8409E-06 | solute carrier family 8 member A3 |
| ENSGALG000000007000 | ENSG00000185551 | 2,755 | 0,00424585 | nuclear receptor subfamily 2 group F member 2 |
| ENSGALG000000028567 | N/A | 2,707 | 0,00621225 | myosin, light chain 9, regulatory |
| ENSGALG000000040995 | N/A | 2,666 | 0,00020768 | Uncharacterized |
| ENSGALG000000012414 | ENSG00000100522 | 2,647 | 0,00407285 | glucosamine-phosphate N-acetyltransferase 1 |
| ENSGALG000000009507 | ENSG00000054690 | 2,540 | 0,00296253 | pleckstrin homology, MyTH4 and FERM domain containing H1 |
| ENSGALG000000036616 | ENSG00000163545 | 2,442 | 0,00594179 | NUAK family kinase 2 |
| ENSGALG000000015977 | ENSG00000088826 | 2,298 | 0,00738419 | spermine oxidase |
| ENSGALG000000036738 | ENSG00000143061 | 2,195 | 0,00995778 | immunoglobulin superfamily member 3 |
| ENSGALG000000005584 | ENSG00000110328 | 2,031 | 0,00621225 | polypeptide N-acetylgalactosaminyltransferase 18 |
| ENSGALG000000045371 | ENSG00000262664 | 1,863 | 0,00241807 | OVCA2, serine hydrolase domain containing |
| ENSGALG000000045136 | N/A | -1,308 | 0,00875381 | Uncharacterized |
| ENSGALG000000031980 | ENSG00000176533 | -1,567 | 0,00311155 | G protein subunit gamma 7 |

Results

| | | | | |
|---------------------|------------------|--------|------------|---|
| ENSGALG00000001618 | ENSG00000181396 | -1,762 | 0,00837742 | 2-oxoglutarate and iron dependent oxygenase domain containing 3 |
| ENSGALG00000000466 | ENSG00000182866 | -1,769 | 0,00973848 | LCK proto-oncogene, Src family tyrosine kinase |
| ENSGALG000000027067 | ENSG00000133466 | -1,824 | 0,00280033 | C1q and TNF related 6 |
| ENSGALG000000008401 | ENSG00000196372 | -1,938 | 0,00681746 | ankyrin repeat and SOCS box containing 13 |
| ENSGALG000000012761 | ENSG00000136048 | -1,957 | 0,00629632 | DNA damage regulated autophagy modulator 1 |
| ENSGALG000000027397 | ENSG00000112679 | -1,999 | 0,00194074 | dual specificity phosphatase 22 |
| ENSGALG000000005208 | ENSG00000170989 | -2,032 | 0,00924908 | sphingosine-1-phosphate receptor 1 |
| ENSGALG000000008491 | ENSG00000101966 | -2,066 | 0,00328231 | X-linked inhibitor of apoptosis |
| ENSGALG000000008054 | ENSG00000139223 | -2,158 | 0,00314592 | acidic nuclear phosphoprotein 32 family member D |
| ENSGALG000000007526 | N/A | -2,175 | 0,00560406 | ES1 protein homolog, mitochondrial-like 2 |
| ENSGALG000000035973 | ENSG00000181704 | -2,181 | 0,0034014 | Yip1 domain family member 6 |
| ENSGALG000000016449 | ENSG00000162976 | -2,186 | 0,00389604 | PQ loop repeat containing 3 |
| ENSGALG000000030602 | ENSG00000149451 | -2,198 | 0,00496634 | ADAM metalloproteinase domain 33 |
| ENSGALG000000017241 | ENSG00000166575 | -2,248 | 0,00069083 | transmembrane protein 135 |
| ENSGALG000000026838 | ENSG00000135272 | -2,266 | 0,00372048 | MyoD family inhibitor domain containing |
| ENSGALG000000037791 | ENSG00000114541 | -2,287 | 0,00057787 | FERM domain containing 4B |
| ENSGALG000000014721 | ENSG00000155545 | -2,291 | 0,00142671 | MIER family member 3 |
| ENSGALG000000015398 | N/A | -2,309 | 0,00765404 | B and T lymphocyte associated |
| ENSGALG000000030643 | ENSG00000162738 | -2,372 | 0,00201083 | VANGL planar cell polarity protein 2 |
| ENSGALG000000011203 | ENSG00000173083 | -2,506 | 0,00029709 | heparanase |
| ENSGALG000000033338 | ENSG00000166123 | -2,508 | 0,00108786 | glutamic--pyruvic transaminase 2 |
| ENSGALG000000001595 | ENSG00000119403 | -2,561 | 0,00998165 | PHD finger protein 19 |
| ENSGALG000000011121 | ENSG00000116704 | -2,580 | 0,00560406 | solute carrier family 35 member D1 |
| ENSGALG000000027420 | ENSG00000132429 | -2,589 | 0,00069256 | popeye domain containing 3 |
| ENSGALG000000012227 | ENSG00000168785 | -2,625 | 0,00062992 | tetraspanin 5 |
| ENSGALG000000008604 | ENSG00000125355 | -2,636 | 0,00842269 | transmembrane protein 255A |
| ENSGALG000000006708 | ENSG00000050767 | -2,639 | 0,00021595 | collagen type XXIII alpha 1 chain |
| ENSGALG000000011320 | ENSG00000057704 | -2,647 | 0,00311155 | transmembrane and coiled-coil domain family 3 |
| ENSGALG000000014978 | N/A | -2,659 | 0,00356587 | IQ motif containing GTPase activating protein 2 |
| ENSGALG000000016518 | ENSG00000044446 | -2,673 | 0,00371666 | phosphorylase kinase regulatory subunit alpha 2 |
| ENSGALG000000004604 | ENSG00000171097 | -2,717 | 0,00346954 | kynurenine aminotransferase 1 |
| ENSGALG000000012199 | ENSG00000198554 | -2,769 | 0,00492715 | WD repeat and HMG-box DNA binding protein 1 |
| ENSGALG000000016758 | ENSG00000144182 | -2,831 | 0,00122162 | lipoyltransferase 1 |
| ENSGALG000000001845 | ENSG00000116793 | -2,841 | 0,00018427 | putative homeodomain transcription factor 1 |
| ENSGALG000000013210 | ENSG00000111731 | -2,885 | 0,00407285 | C2 calcium dependent domain containing 5 |
| ENSGALG000000038096 | ENSG000000007171 | -2,921 | 0,00395973 | nitric oxide synthase 2 |
| ENSGALG000000011426 | ENSG000000026297 | -2,922 | 0,00108786 | ribonuclease T2 |

Results

| | | | | |
|--------------------|-----------------|--------|------------|--|
| ENSGALG00000011404 | ENSG00000171476 | -3,028 | 0,00123217 | HOP homeobox |
| ENSGALG00000025851 | ENSG00000185477 | -3,123 | 0,00037285 | GPRIN family member 3 |
| ENSGALG00000005678 | ENSG00000136068 | -3,159 | 0,00018664 | filamin B |
| ENSGALG00000023691 | ENSG00000198018 | -3,199 | 0,00028877 | ectonucleoside triphosphate diphosphohydrolase 7 |
| ENSGALG00000012877 | ENSG00000182158 | -3,209 | 0,00034806 | cAMP responsive element binding protein 3 like 2 |
| ENSGALG00000002639 | ENSG00000144935 | -3,338 | 0,00072886 | transient receptor potential cation channel subfamily C member 1 |
| ENSGALG00000011392 | ENSG00000057468 | -3,380 | 0,00011405 | mutS homolog 4 |
| ENSGALG00000015026 | ENSG00000056972 | -3,426 | 3,7668E-05 | TRAF3 interacting protein 2 |
| ENSGALG00000033379 | ENSG00000144597 | -3,459 | 5,5397E-05 | ELL associated factor 1 |
| ENSGALG00000009823 | ENSG00000132334 | -3,497 | 0,00110148 | protein tyrosine phosphatase, receptor type E |
| ENSGALG00000013232 | ENSG00000132677 | -3,727 | 0,00074124 | Rh family B glycoprotein (gene/pseudogene) |
| ENSGALG00000021136 | ENSG00000128218 | -3,874 | 1,4021E-05 | V-set pre-B cell surrogate light chain 3 |
| ENSGALG00000038875 | ENSG00000141524 | -4,187 | 1,3475E-07 | transmembrane channel like 6 |
| ENSGALG00000021658 | ENSG00000158006 | -4,222 | 7,8047E-06 | platelet activating factor acetylhydrolase 2 |
| ENSGALG00000007070 | ENSG00000155719 | -4,267 | 2,037E-06 | otoancorin |
| ENSGALG00000015059 | N/A | -4,298 | 5,8693E-09 | fatty acid amide hydrolase-like |
| ENSGALG00000013371 | ENSG00000125910 | -5,294 | 4,5705E-08 | sphingosine-1-phosphate receptor 4 |

To identify associated biological processes, the list of differentially expressed genes was used as input for the g:profiler website and STRING protein-protein interaction analysis. However, no significantly enriched processes could be identified for neither the *Gallus gallus* genes nor for the corresponding *H. sapiens* genes. However, when using associated UniProt identifiers of the human genes as input for the GO analysis with QuickGO website, these terms were associated with several biological processes (**Table 14** and **Table 15**, as well as Supptbl 33 and 34 on the accompanying CD). The differentially expressed proteins were associated with e.g. signal transduction, immune response, apoptotic processes, cell migration and angiogenesis, transcription and response to virus infection.

Table 14 Shows the 25 GO terms most frequently associated with differentially expressed genes after CVI988 infection.

| GO term | Description | Percentage |
|------------|-------------------------------|------------|
| GO:0006898 | receptor-mediated endocytosis | 19.05 |
| GO:0007165 | signal transduction | 19.05 |
| GO:0006955 | immune response | 14.29 |
| GO:0016310 | Phosphorylation | 14.29 |
| GO:0016477 | cell migration | 14.29 |
| GO:0009615 | response to virus | 9.52 |

| | | |
|------------|---|------|
| GO:0018108 | peptidyl-tyrosine phosphorylation | 9.52 |
| GO:0006468 | protein phosphorylation | 9.52 |
| GO:0045071 | negative regulation of viral genome replication | 9.52 |
| GO:0051607 | defense response to virus | 9.52 |
| GO:0001525 | Angiogenesis | 9.52 |
| GO:0001657 | ureteric bud development | 9.52 |
| GO:0002376 | immune system process | 9.52 |
| GO:0006351 | transcription, DNA-templated | 9.52 |
| GO:0006355 | regulation of transcription, DNA-templated | 9.52 |
| GO:0006915 | apoptotic process | 9.52 |
| GO:0007420 | brain development | 9.52 |
| GO:0010468 | regulation of gene expression | 9.52 |
| GO:0016032 | viral process | 9.52 |
| GO:0030154 | cell differentiation | 9.52 |
| GO:0030324 | lung development | 9.52 |
| GO:0042060 | wound healing | 9.52 |
| GO:0042127 | regulation of cell proliferation | 9.52 |
| GO:0045087 | innate immune response | 9.52 |
| GO:0060337 | type I interferon signaling pathway | 9.52 |

Table 15 Shows the 25 GO terms most frequently associated with differentially expressed genes after RB-1B infection.

| GO term | Description | Percentage |
|----------------|---|-------------------|
| GO:0006355 | regulation of transcription, DNA-templated | 13.10 |
| GO:0006351 | transcription, DNA-templated | 13.10 |
| GO:0007165 | signal transduction | 10.71 |
| GO:0043066 | negative regulation of apoptotic process | 8.33 |
| GO:0055114 | oxidation-reduction process | 7.14 |
| GO:0007275 | multicellular organism development | 7.14 |
| GO:0042127 | regulation of cell proliferation | 7.14 |
| GO:0006915 | apoptotic process | 7.14 |
| GO:0006357 | regulation of transcription by RNA polymerase II | 5.95 |
| GO:0006955 | immune response | 5.95 |
| GO:0006468 | protein phosphorylation | 4.76 |
| GO:0009615 | response to virus | 4.76 |
| GO:0045944 | positive regulation of transcription by RNA polymerase II | 4.76 |
| GO:0046208 | spermine catabolic process | 4.76 |
| GO:0001525 | Angiogenesis | 4.76 |
| GO:0007155 | cell adhesion | 4.76 |
| GO:0016477 | cell migration | 4.76 |
| GO:0042060 | wound healing | 4.76 |
| GO:0035556 | intracellular signal transduction | 4.76 |
| GO:0043312 | neutrophil degranulation | 4.76 |
| GO:0045087 | innate immune response | 4.76 |
| GO:0071346 | cellular response to interferon-gamma | 4.76 |
| GO:0007186 | G-protein coupled receptor signaling pathway | 3.57 |
| GO:0051607 | defense response to virus | 3.57 |
| GO:0045071 | negative regulation of viral genome replication | 3.57 |

Eighteen differentially expressed genes were shared between RB-1B and CVI988 infected B cells in comparison to mock-infected B cells (**Table 16**). The results of the GO analysis with QuickGO are available in the Supptbl 35 (on the accompanying CD). The gene products were associated with receptor-mediated endocytosis (25 %, GO:0006898), signal transduction (18.75 %, GO:0007165), cell migration (18.75 %, GO:0016477), angiogenesis (12.5 %, GO:0001525), apoptotic process (12.5 %, GO:0006915), immune response (12.5 %, GO:0006955) and cell differentiation (12.5 %, GO:0030154). Particularly, the MAPK signaling cascade (GO:0000165) was associated with the identified infection markers.

Table 16 Differentially expressed host genes identified in both RB-1B and CVI988 infected B cells compared to mock infected B cells.

| GalGal_GeneID | Hsap_GeneID | GeneName |
|--------------------|-----------------|---|
| ENSGALG00000030005 | ENSG00000186431 | Fc fragment of IgA receptor |
| ENSGALG00000023818 | N/A | heat shock protein family B (small) member 9 |
| ENSGALG00000009433 | ENSG00000151929 | BCL2 associated athanogene 3 |
| ENSGALG00000038019 | N/A | Uncharacterized |
| ENSGALG00000004184 | ENSG00000113140 | secreted protein acidic and cysteine rich |
| ENSGALG00000032687 | ENSG00000181649 | pleckstrin homology like domain family A member 2 |
| ENSGALG00000041683 | N/A | Uncharacterized |
| ENSGALG00000011715 | ENSG00000126803 | heat shock protein family A (Hsp70) member 2 |
| ENSGALG00000045632 | N/A | Uncharacterized |
| ENSGALG00000045085 | ENSG00000185745 | interferon induced protein with tetratricopeptide repeats 1 |
| ENSGALG00000039786 | ENSG00000077782 | fibroblast growth factor receptor 1 |
| ENSGALG00000009400 | ENSG00000100678 | solute carrier family 8 member A3 |
| ENSGALG00000013723 | ENSG00000135114 | 2'-5'-oligoadenylate synthetase like |
| ENSGALG00000003932 | ENSG00000124145 | syndecan 4 |
| ENSGALG00000046283 | ENSG00000131711 | microtubule associated protein 1B |
| ENSGALG00000045371 | ENSG00000262664 | OVCA2, serine hydrolase domain containing |
| ENSGALG00000030602 | ENSG00000149451 | ADAM metalloproteinase domain 33 |
| ENSGALG00000013371 | ENSG00000125910 | sphingosine-1-phosphate receptor 4 |

No overlapping candidates were identified through proteome and transcriptome analyses. However, the identified proteins and expressed genes in the proteomic and transcriptome analysis of MDV infected B cells, respectively, affected related biological processes, especially immune response and oxidation-reduction process.

5.3. Proteomic analyses of Marek's Disease lymphomas

In order to elucidate the MDV transformation process we used laser capture microdissection to excise the tumor regions with as little as possible contamination from surrounding tissue. The tumor sections were processed in comparison to healthy organ tissue and naïve T cells in the proteomic workflow described and evaluated in section **5.1. *Proteomic characterization of naive chicken B- and T lymphocytes.***

5.3.1. Evaluation of MD tumor morphology

Differences in tumor morphology and composition were determined by evaluating histological sections of WT and Δ vTR tumors stained for CD3+ lymphocytes with the HALO™ imaging software (**Figure 25**). Especially helper (CD4+) and cytotoxic (CD8+) T cells carry CD3 co-receptor, which are main targets for MDV infection and transformation.

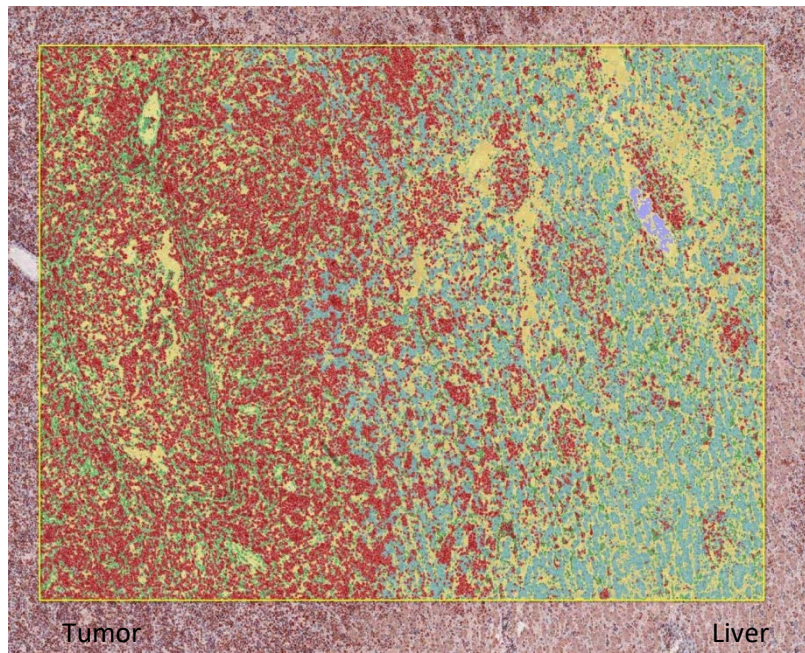


Figure 25 Evaluation of morphology and composition of a MD tumor with HALO software induced after infection with ΔvTR RB-1B in liver. Red: CD3 + T cells, green: CD3 – T cells, Cyan blue: hepatocytes, yellow: connective tissue, purple: blank space. CD3 + T cells (red) dominate the tumor area while hepatocytes (cyan) characterized the naïve liver tissue.

The determined percentages are provided in Supptbl 36 (on the accompanying CD). CD3+ and CD3- lymphocytes, connective tissue and hepatocytes were quantified in distinct areas and the percentage of each cell type was calculated (**Figure 26**). Differences in the percentage of the same cell types were already detected between different tumors of the same type. The proportion of hepatocytes varied from 8-21 % for ΔvTR tumors and 17-54 % for WT tumors. In addition, between 48-73 % and 36-63 % CD3+ lymphocytes were detected in ΔvTR tumors or in WT tumors, respectively. In healthy liver tissue, up to 66 % hepatocytes and about 15 % CD3+ lymphocytes were found. This indicates that MD tumor morphology greatly varies already between same tumor types in different animals. However, the ΔvTR tumors contained lower portions of hepatocytes and higher portions of CD3+ lymphocytes compared to WT tumors in all tested tumor samples. Thus, for determination of differences in protein expression profile of tumors and naïve T cells, we chose to use ΔvTR tumors.

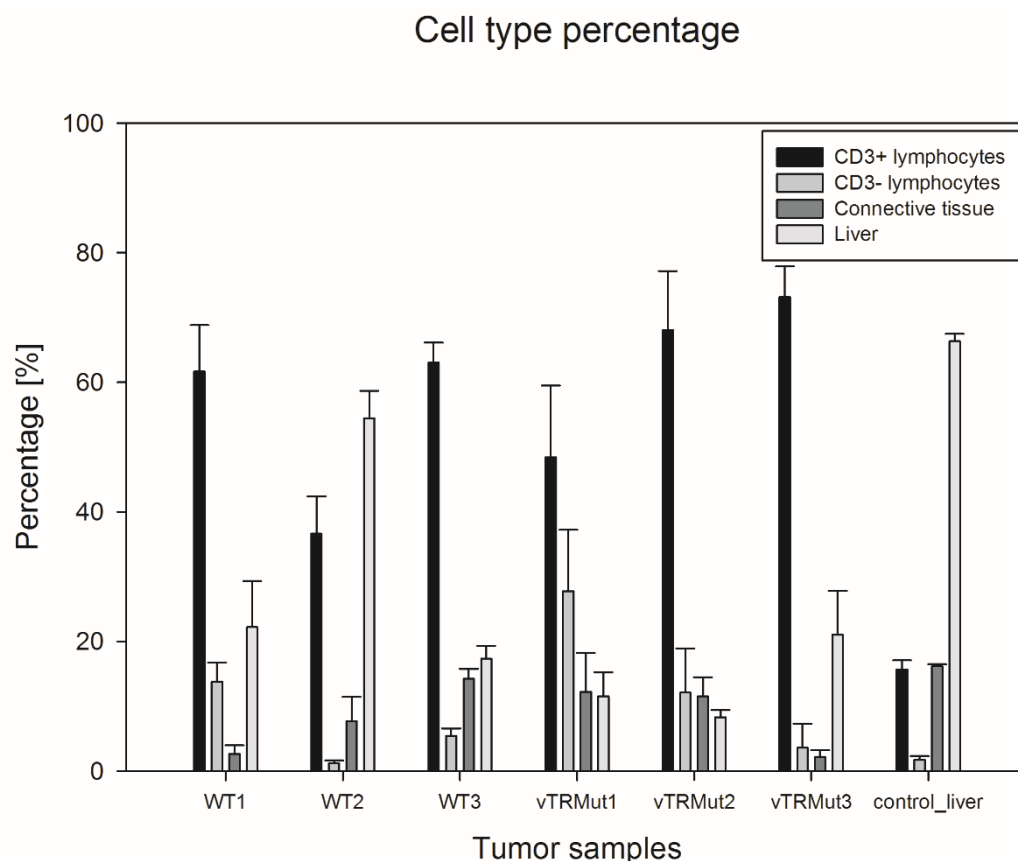


Figure 26 Quantitation of cell types in different tumor samples with the HALO software. Six distinct areas of three different tumors per tumor type and in healthy liver tissue were analyzed and the percentage of CD3+, CD3- lymphocytes, connective tissue and liver tissue was calculated.

For proteome analysis 0.075 mm³ tissue was lysed and proteins were extracted. The protein amounts were determined densitometrically after SDS-PAGE. In total, 0.075 mm³ of tumor or liver sample corresponded to 10-15 µg of protein. This is equivalent to 3-4 µg/mm² for 20 µm sections and similar to values that have been published for other tissues [139]. Hence, laser capture microdissection yielded sufficient amounts of proteins. MDV transformed tumors in unstained liver were readily visible with the naked eye as white-pink proliferates within the dark red liver tissue and could be differentiated through the light microscope from surrounding non-transformed liver tissue. The tumor displayed a compact structure different from the loose structure of healthy liver lobules (**Figure 27**). The differentiation of tumor from liver tissue for LCM was based on this observation only. Unstained material was processed to avoid any incompatibilities with mass spectrometric analysis.

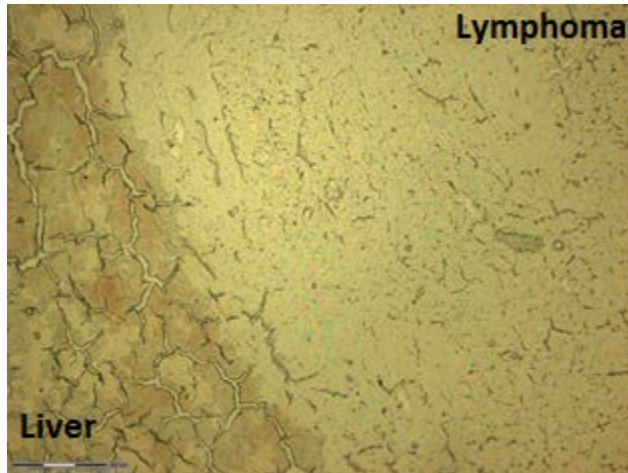


Figure 27 MDV- induced tumor in liver after infection with the ΔvTR mutant as seen through the light microscope for LCM with 10x magnification. The tumor region can be differentiated from the darker hepatocytes.

For the investigation of the transformation process, ΔvTR tumors were compared to T cells in a LC-MALDI TOF/TOF MS analysis of differentially dimethyl labeled peptides subsequent to OG-IEF separation. In order to confirm differences in protein expression profiles, WT tumors were also analyzed in comparison to naïve T cells. Two independent replicates with inverse labeling were studied and between 100 and 150 μg of proteins were digested in each experiment. In total 1314 and 919 proteins were identified, for the two replicate experiments (Supptbl 37 and 38 on the accompanying CD). Similarly, 959 and 841 proteins were identified for the two experiments comparing WT tumor with T cells, respectively (Supptbl 39 and 40 on the accompanying CD). Viral proteins could not be identified in the tumor samples.

For each mixed sample, the protein and peptide lists of the separately analyzed twelve OFFGEL fractions were compiled into joint lists by ProteinScape. These peptide lists (Supptbl 41-44 on the accompanying CD) were then used as input for an R script, which removed shared peptides and irregularly labeled peptides. Subsequently, the mean isotope ratio with its standard deviation for each single protein was calculated based on the cleared peptide lists. Promising candidates were confirmed by inspection of the spectra from both tumor types. In this way, 19 promising potential transformation

markers could be identified (**Table 17**). The markers could also be detected in the experiments comparing tumor vs. unsuspecting liver tissue with the same regulation of protein expression.

Table 17 Potential transformation markers. Proteins with fold change < 0.5 were interpreted as upregulated in T cells compared to both WT and ΔvTR tumors and proteins with fold changes > 2 as upregulated in both tumor types compared to T cells and liver. FC: fold change, corresponds to the fold change in one exemplary analysis.

| Protein ID | Gene ID | Protein description | FC |
|---------------------|---------------------|---|------|
| ENSGALP00000005345 | ENSGALG00000003389 | interferon gamma-inducible protein 30 | 3.83 |
| ENSGALP000000041758 | ENSGALG000000026269 | transporter 1 ATP-binding cassette sub-family B | 3.26 |
| ENSGALP000000010210 | ENSGALG000000006323 | leukocyte cell derived chemotaxin 2 | 2.82 |
| ENSGALP000000016536 | ENSGALG000000010185 | heat shock 70kDa protein 4-like | 2.53 |
| ENSGALP000000028664 | ENSGALG000000013723 | 2'-5'-oligoadenylate synthetase-like | 2.49 |
| ENSGALP000000039235 | ENSGALG000000002139 | cold shock domain containing E1 | 2.39 |
| ENSGALP000000013029 | ENSGALG000000008038 | splicing factor 3b subunit 1 | 2.29 |
| ENSGALP000000042479 | ENSGALG000000026546 | stress induced phosphoprotein 1 | 2.23 |
| ENSGALP000000011961 | ENSGALG000000007403 | phosphatidylethanolamine binding protein 1 | 0.47 |
| ENSGALP000000016363 | ENSGALG000000010079 | heterochromatin protein 1 binding protein 3 | 0.47 |
| ENSGALP000000015128 | ENSGALG000000009305 | lamin B receptor | 0.42 |
| ENSGALP000000010358 | ENSGALG000000006426 | p21 protein (Cdc42/Rac)-activated kinase 2 | 0.41 |
| ENSGALP000000033650 | ENSGALG000000003792 | FYN binding protein | 0.39 |
| ENSGALP000000003584 | ENSGALG000000002286 | H3 histone family 3B | 0.35 |
| ENSGALP000000039872 | ENSGALG000000000468 | regulator of chromosome condensation 2 | 0.35 |
| ENSGALP000000041526 | ENSGALG000000025786 | histone cluster 1 H4-VI germinal H4 | 0.34 |
| ENSGALP000000008341 | ENSGALG000000005204 | glutathione S-transferase theta 1-like | 0.27 |
| ENSGALP000000040653 | ENSGALG000000028417 | H2A histone family member J (H2AFJ) | 0.26 |
| ENSGALP000000027541 | ENSGALG000000017082 | high mobility group box 1 | 0.25 |

Eight proteins were detected as upregulated in MDV tumors in comparison to T cells and healthy liver, whereas eleven proteins were seen downregulated in both tumor types compared to naïve T cells.

GO analysis with g:profiler or STRING did not produce any significantly enriched biological processes for the identified potential markers. However, the GO analysis with QuickGO [110] assigned the potential transformation markers to biological processes such as nucleosome assembly ((GO:0006334, 21.4 % of candidates were associated with this GO term), regulation of transcription (GO:0006355, 14.3 %), inflammatory response (GO:0006954, 7.1 %), immune response (GO:0006955, 14.3 %) and oxidation-reduction process (GO:0055114, 14.3 %) (Supptbl 45 on the accompanying CD). Especially, the proteins identified as downregulated in MD tumors were associated with nucleosome assembly (GO:0006334, 33.3 %), inflammatory response (GO:0071103, 11.1 %) and chromatin silencing (GO:0006325, 11.1 %).

To confirm the potential transformation markers identified by the proteomic analysis, the gene expression levels in the different tumor samples, naïve T cells and healthy non-transformed liver were investigated by quantitative real-time PCR. The RNA was isolated from laser-dissected material or naïve cells, and equal amounts were used in the one-step RT-qPCR. Several of the tested potential transformation markers could be verified by RT-qPCR (**Table 18**).

Table 18 differential expression of genes in tumor samples compared to naïve T cells determined by one-step RT-qPCR.

Fold changes of <0.5 and > 2 were interpreted as significant regulations and are highlighted in grey. FC values were calculated as $2^{\Delta CT}$; FC values lower than 0.5 represent downregulation in tumor samples (dark grey background), FC values higher than 2 define upregulation in tumor samples (light background). FC: fold change, GAPDH: Glyceraldehyde-3-phosphate dehydrogenase, IFI30: interferon inducible protein 30, HSPA4L: heat shock 70kDa protein 4-like, OASL: 2'-5'-oligoadenylate synthetase-like, TAP1: transporter 1 ATP-binding cassette sub-family B, LBR: lamin B receptor, GSTT1L: glutathione S-transferase theta 1-like, RCC2: regulator of chromosome condensation 2, FYB: FYN binding protein, H2AFJ: H2A histone family member J.

| Gene | T cells-WT1 | | T cells-WT 752 | | T cells-WT 754 | | T cells- Δ vTR 1113 | | T cells- Δ vTR 1173 | |
|----------------|-------------|------|----------------|------|----------------|------|----------------------------|------|----------------------------|------|
| | Δ CT | FC | Δ CT | FC | Δ CT | FC | Δ CT | FC | Δ CT | FC |
| GAPDH | -0.05 | 0.97 | -0.43 | 0.74 | -0.24 | 0.85 | -0.61 | 0.66 | 0.58 | 1.49 |
| 28SrRNA | -0,48 | 0,72 | -0,50 | 0,71 | -0,48 | 0,72 | -1,18 | 0,44 | -0,59 | 0,66 |
| Actin | 0.56 | 1.47 | 0.77 | 1.71 | 1.13 | 2.19 | -0.06 | 0.96 | 1.27 | 2.41 |

| | | | | | | | | | | |
|----------------------|-------|------|-------|--------|-------|--------|-------|--------|-------|--------|
| <i>IFI30</i> | -0.08 | 0.95 | 1.23 | 2.35 | 2.29 | 4.89 | 1.74 | 3.34 | 2.65 | 6.28 |
| <i>HSPA4L</i> | -0.59 | 0.66 | -0.46 | 0.73 | -0.51 | 0.70 | -0.59 | 0.66 | 0.51 | 1.42 |
| <i>OASL</i> | -2.17 | 0.22 | -0.69 | 0.62 | -0.46 | 0.73 | -0.30 | 0.81 | 1.07 | 2.10 |
| <i>TAP1</i> | -1.49 | 0.36 | -0.56 | 0.68 | -0.25 | 0.84 | -0.26 | 0.84 | 0.23 | 1.17 |
| <i>LBR</i> | -3.15 | 0.11 | -2.17 | 0.22 | -2.38 | 0.19 | -2.20 | 0.22 | -1.91 | 0.27 |
| <i>GSTT1L</i> | -1.58 | 0.33 | -2.73 | 0.15 | -2.40 | 0.19 | -3.39 | 0.10 | -2.63 | 0.16 |
| <i>RCC2</i> | -2.52 | 0.17 | -1.62 | 0.33 | -1.69 | 0.31 | -0.54 | 0.69 | -1.54 | 0.34 |
| <i>FYB</i> | -5.47 | 0.02 | 0.71 | 1.64 | -3.65 | 0.08 | -4.08 | 0.06 | -1.27 | 0.41 |
| <i>H2AFJ</i> | -1.01 | 0.50 | -1.61 | 0.33 | -1.12 | 0.46 | -1.22 | 0.43 | -1.06 | 0.48 |
| <i>ICP4</i> | 11.0 | 1992 | 11.80 | 3565.8 | 12.08 | 4329.6 | 11.58 | 3061.5 | 11.58 | 3061.5 |

As expected, the MDV *ICP4* transcript could not be detected in naïve T cells or liver. Unexpectedly, also actin transcripts were regulated 2-fold in two of the tumors. Similar to the result of the proteome analysis, the transcripts of *IFI30* were upregulated in four of the five tested tumor samples compared to T cells. *OASL* was only detected as upregulated in one tumor compared to T cells, namely ΔvTR tumor sample 1173, and downregulated in one WT virus induced tumor (WT1). Similarly, *TAP1* did not show significant regulation on transcript level in four out of five tumor samples and was even inversely regulated in WT1 with respect to the results of the proteome analysis. Similar to the protein expression, also the mRNA levels of *LBR*, *GSTT2L*, *RCC2*, *FYB* and *H2AFJ* were downregulated in at least 4 of the 5 tested tumors compared to T cells.

6. Discussion

Due to the highly contagious nature of MDV infection and potential economic loss, MD in Germany has to be reported to the authorities so that these can get an overview about the incidence, course and occurrence of the disease [38]. Although MD is well controlled nowadays by vaccination with the CVI988/Rispens strain at day 18 of embryonation *in ovo* or of one-day old chicks combined with good hygiene management [19], the use of suboptimal vaccines may favor the emergence of strains with increased virulence. In addition to being a threat to the poultry industry, MDV is a model for virus-induced lymphoma formation similar to EBV-induced Hodgkin's disease [140]. Despite the importance of MDV as an animal pathogen and a transformation model, the pathogenesis of MD is not fully understood and virus-host interactions need further study.

Previous proteome analyses after MDV infection relied on chicken embryo fibroblasts, stable cell lines or primary organ cells, such as kidney epithelial cells. However, these cells do not reflect a natural infection as B and T lymphocytes are preferentially infected by MDV *in vivo* and thus, studies of infected fibroblasts may have only limited significance for the elucidation of MDV pathogenesis.

6.1. Characterization of naïve chicken lymphocytes

Lymphocytes are central players of the host immune system during infections [63, 64]. Like many human viruses, including Epstein-Barr virus and Human immunodeficiency virus [141, 142], MDV also targets lymphocytes in the course of the infection cycle [11]. Infection of B cells and T cells with MDV leads to completely different outcomes with respect to manifestation of infection (lytic infection versus latent infection), which could be due to different functions and protein profiles of the two lymphocyte populations. Hence, the proteome of naïve chicken lymphocytes was investigated first. In addition, in order to test compatibility of FASP digest, dimethyl labeling and OG IEF we analyzed naïve chicken lymphocytes in our workflow. Similar, comparative studies of the proteomes of chicken B- and T lymphocytes have not been conducted yet. In order to fill this knowledge gap, a straightforward shotgun proteomic approach was established to identify the proteins of chicken T- and B cells. To

improve the yields of identified proteins, T cell and B cell lysates were also analyzed in a workflow consisting of a filter-aided digest, dimethyl labeling of the peptides and fractionation of the peptides by OG IEF. With this approach, approximately 1400 proteins could be identified. However, the number of B cell or T cell specific proteins that were consistently identified in the two independent experiments was surprisingly low indicating a high variance of the samples which may in part be caused by the MALDI TOF/TOF platform that was used. There are several factors that influence the quality of proteome analysis, but most differences are observed due to stochastic variations during fragmentation process [143]. In addition, chromatographic separation techniques are prone to degradation and column contaminations over time and also the mass spectrometric detection will decrease with increasing contaminations [144].

Previously, the protein composition of naïve or activated murine B- and / or T cells has been studied [145, 146]. Also, the gene expression profiles of human [147-150] and murine immune cells [151] have been determined by transcriptomic techniques. First insights into the proteome of chicken B-lymphocytes were obtained in a recent analysis of the bursa of Fabricius as whole organ [68]. McCarthy *et al.* [68] identified 5198 proteins, of which 1753 were B cell specific, while 1972 were specific for the surrounding stroma, and 1473 were shared between both compartments. These B cell specific proteins were mostly assigned to signaling, cell migration, proliferation, and apoptosis but also to protein modification, chromatin assembly and disassembly, and regulation of transcription. A comparison of the gene expression of human peripheral CD4+ T cells, CD8+ T cells and B cells also revealed cell-type specific processes, such as signal transduction, T cell receptor signaling pathway or antigen processing and presentation, respectively [147]. The results of these GO analyses of mouse or human lymphocytes are consistent with our findings for the T- and B cell specific proteins. The KEGG terms 'mitotic cell cycle' and 'RNA processing', but also 'B cell receptor signaling pathway' were enriched in the KEGG analysis for the B cell specific proteins that we have identified. Similarly, T lymphocyte specific KEGG terms, such as 'T cell activation', were enriched for the proteins identified specifically in T cells. Since identifiers of the homologous human genes were used as basis for the GO and KEGG analyses, the

results must be regarded with caution as homologous human genes were not available for approximately 5 % of the identified chicken genes, and also, gene function might vary between species. Therefore, some information may have been lost and the results of the GO-term enrichment analysis may be somewhat incomplete. However, our results provide a good basis for the evaluation of differences in protein composition between chicken B- and T lymphocytes.

Using samples of naïve lymphocytes, a convenient workflow for the following quantitative analysis of MDV-infected B cells and MD tumors was established which combined dimethyl labeling with the FASP digest in a one-pot reaction and peptide fractionation by OG IEF. The dimethylated peptides were efficiently fractionated by OG IEF compared to unlabeled material. Dimethylation did result neither in any loss of separation power (**Figure 11**) nor in systematic iP shifts during focusing. An increase in identification score, sequence coverage and number of identified proteins was obtained.

6.2. MDV Infection of primary B cells

The recently developed *in vitro* MDV infection system of primary lymphocytes [61] provided a basis for the quantitative proteome analysis of primary B cells after infection with two different strains of MDV, the very virulent RB-1B strain and the attenuated live vaccine strain CVI988/Rispens. We aimed at a detailed investigation of virus-host interaction and influence of MDV infection on the protein expression profile of primary B lymphocytes, which are the first natural target of a lytic MDV infection.

6.2.1. MDV induced changes in expression levels of host proteins

Although the new cultivation system extended their life span, primary B cells could not be labeled by stable isotope labeling by amino acids in cell culture (SILAC) due to incompatibility with the labeling medium. We assume that although essential amino acids are substituted the lack of smaller molecules in the dialyzed serum (e.g. some dialyzable hormones, growth factors and cytokines) resulted in reduced growth of the cells. Although the infection rate could be improved to 20-30 % in standard cultivation medium, the number of infected cells was still too low for an additional fractionation step prior to LC-MALDI TOF/TOF MS analysis, as the 10^6 sorted B cells contain only about 20 µg of protein.

In order to meet these limitations, we used a sample preparation workflow consisting of a FASP digest of cell lysates, followed by differential dimethyl labeling of peptides, which were subjected to LC-MALDI TOF/TOF MS without further fractionation. Quantitative differences were determined by calculating the ratio of isotope-labeled peak intensities for protein-specific peptides in the sample and reference. The cut-off values for the SoC that defined the detection of regulation could be set approximately between 0.8 and 1.2, due to isotope impurities of reagents and low intensive peaks that influences precision of the mass spectrometric quantitation.

In general, we detected only few alterations of the protein expression levels of B cells proteins after MDV infection while the levels of the majority of the cellular proteins remained unaffected (e.g. **Figure 12**). This observations matches the situation after infection of bovine kidney cells with another alphaherpesvirus, PrV, where the cellular proteome also remained very stable [152]. Thus, infections with both alphaherpesviruses left the steady-state level of the cellular protein pool mainly unaltered [152], which is surprising. The described shut-off by herpesviruses involves degradation of mostly host mRNA and suppresses synthesis of host proteins [76, 153], which conflicts with the mild alterations in the protein expression profile. Berard *et al.* identified 148, 87 and 122 differentially expressed proteins after 4, 10 and 24 h post-infection, respectively, with HSV-1 of SILAC-labeled HEK293 cells [154]. Similar, Stahl *et al.* observed regulation of 86 % of detectable phosphopeptides and identified in total 405 proteins that were only detected after infection or in the control after lytic infection of Swiss-albino 3T3 fibroblasts with murine gammaherpesvirus 68 (MHV68) [155]. However, it has been shown before, that the vhs-protein of HSV-1 degrades specific host mRNAs, while stabilizing and delaying degradation of other host mRNAs [156]. A similar mechanism of MDV vhs could explain the only minor alterations in the protein expression profile early after MDV infection. Indeed, the transcript of UL41 was identified in the RNA-sequencing analysis of MDV infected B cells.

Twelve and six differentially expressed host proteins were identified after RB1B and CVI988 infection, respectively, which met the requirements that we had set (at least two-fold regulation, a standard

deviation <1, confirmation of most abundant peptides in one replicate experiment). Slight differences between the infections with the two different MDV strains were observed with regard to the number of differentially expressed proteins. Six proteins were also identified with the same direction of regulation, e.g. downregulated after infection, for at least one associated peptide in the MS spectra after the other viral infection. In order to increase confidence, the differentially expressed proteins after RB-1B and CVI988 infection were used together as input for GO analysis. The identified candidates were analyzed by GO term enrichment analysis with the QuickGO website, which performs only a descriptive statistical analysis and no enrichment analysis. The differentially expressed proteins were assigned to GO terms in the category biological processes, such as immune response (GO:0006955), translation (GO:0006412) and inflammatory response (GO:0006954). Similarly, also Skiba *et al.* observed an influence on the translation process after infection by PrV [152]. Although identically regulated proteins were not identified after PrV [152], HSV-1 [154] and MDV infection, the similar outcomes of GO-term enrichment analyses point towards similarities in the induced changes in proteome after alphaherpesvirus infections. The different identified regulated proteins could be the result of the different time points after infection, different cell types and viruses. However, it could also be a result of the different ways the cells sense the viruses and a sign of different evolutionary paths of the related viruses for interaction with the cells in order to secure replication [157].

6.2.2. Alterations in expression levels of immune system associated proteins after MDV infection

The expression of three immune system-associated proteins was affected by MDV infection. CD74 is associated with MHC class II molecules and acts as chaperone, also regulating antigen processing. Previous studies have shown a down regulation of CD74 in EBV infected B cells [158]. In addition, down regulation of different MHC II molecules, such as mSUG1 and B-LA [159] and B-LB [160, 161] by MDV in spleen tissue has already been reported. Interleukin 18, member of the interleukin 1 (IL-1) family, assists in production of IFN- γ , promoting inflammation and immune response [162]. The IFN- γ signaling pathway in turn induces transcription of MHC II molecules [161, 163]. Hence, reduction of IL-18 protein

expression could also indirectly influence expression of MHC II molecules. Previous studies have revealed that expression of IL-18 did not vary between MDV-susceptible and -resistant chicken lines [164, 165] but IL-18 expression was upregulated in MDV infected CD8+ T cells compared to uninfected cells [165]. In contrast, Heidari *et al.* showed a downregulation of IL-18 gene expression during the latent stage of MDV infection in spleen tissue [166]. Recent studies could also demonstrate the degradation of IL-18 by several MDV microRNAs as restriction mechanism for the host innate immune response [167]. IL-18, MHC II beta chain and CD74 were all identified with approximately two-fold downregulation in infected B cells. MHC I and II molecules are important for the production of antiviral molecules, such as 2'-5'-oligoadenylate synthetase, as they present antigens to effector cells, which produce antiviral effectors. Hence, these molecules are often targeted by viruses to evade the antiviral immune response [168, 169]. The downregulation of these proteins suggests that this is also the case for MDV.

6.2.3. MDV infection downregulates avBD2

Of the listed differentially expressed proteins, the avian beta defensin 2 was regulated most intensively by MDV infection. An approximately fivefold downregulation of the protein was detected after infection with the two strains of different virulence. The avBD2, also designated as Gal-2, is a small protein (64 AA) with known antimicrobial activity against several gram negative and gram positive bacteria, including *Listeria monocytogenes* [170], which persist mainly intracellularly in phagocytic cells, similar to MDV. Next to their direct role in first defense against microbial infections, it has been shown that defensins also possess chemotactic activities and the ability to activate dendritic cells and lymphocytes, to link the innate immune system with adaptive immune response [171, 172]. Human defensins have been associated with antiviral activity against both enveloped and non-enveloped viruses. Defensins can inhibit viral membrane fusion by interacting with viral envelopes and glycoproteins, masking host cell receptors and interfering with intracellular signaling cascades [173]. However, the precise mechanism of activity against intracellular pathogens by beta defensins is not

fully understood yet. The downregulation of avBD2 also indicates an evasion strategy of MDV which has not been reported before.

6.2.4. Correlation of changes in transcriptome and proteome of MDV infected B cells

In order to confirm the potential infection markers, a RNA sequencing analysis of three biological replicates of each RB-1B -, CVI988- and mock infected B cells was performed. Transcripts for all identified MDV proteins were confirmed and several additional MDV transcripts could be identified, which were associated with lytic infection. These transcripts were assigned to 80 out of 103 predicted functional MDV genes [21]. Similarly, Heidari *et al.* found 79 upregulated MDV transcripts during lytic infection compared to latent infection of chickens after microarray analysis of spleen tissue and 11 transcripts with similar expression between the two phases, including the oncogene meq [174]. In my RNA-seq analysis, the same MDV proteins were identified after infection with RB-1B or CVI988, and thus, both virus strains of different virulence showed no differences in their mRNA expression profiles during lytic infection. This was unexpected, as also for suggested virulence factors such vIL8, pp38, US3, UL49.5 and meq [174] no differences in mRNA expression was observed.

The potential infection markers identified in the proteome analysis were not confirmed by mRNA sequencing. Expression of the identified host proteins was not notably affected by MDV infection, which suggests the cellular response to MDV is rather based on post-transcriptional modifications and regulation steps than on regulation of transcription.

Transcripts for the avBD2 were not detected in any of the analyzed samples. This could be explained by the weak correlation of transcript and protein abundance. As Nagaraj *et al.* [120] have shown, there is no strict quantitative correlation between transcriptome and proteome of HeLa cells. Thus, although sensitivity of mRNA sequencing by far exceeds that of MALDI-TOF MS, high protein abundances may in some cases allow mass spectrometric identification although a transcript cannot be identified. Also, the response time to stimuli and the turnover of mRNA and proteins has to be taken into account. It is possible that while the transcriptome has fully adapted to a certain condition, the proteome has not

fully responded yet [175]. Similarly, weak correlation between changes in transcriptome and proteome after PrV infection have also been reported previously [176].

Discrepancies between induced changes in the host proteome and transcriptome can be explained by the dynamic imbalance due to delayed protein synthesis and degradation compared to transcriptional induction. Hence, the delay between transcription and translation has to be considered [177]. A fast and short term response of cells to an infection or altered condition in general, mostly requires post-transcriptional processes. The lag between transcription, translation and protein turnover limits the speed at which a proteome can adapt to new environmental conditions solely based on transcription induction. However, translation of existing transcripts, also known as ‘translation on demand’, represents a fast way of synthesizing required proteins and similar, degradation of existing proteins accelerates removal of unnecessary proteins [177].

6.2.5. MDV induced changes in expression levels of host mRNA

Interesting infection marker candidates showing altered expression levels after MDV infection were also identified by RNA sequencing. Similar to the proteome data, only few transcripts were significantly altered upon MDV infection, although in total 14-18 million reads were obtained and mapped to 11952 transcripts in the RNA-seq analyses. The 26 and 95 differentially expressed genes that were identified after CVI988 or RB-1B infection, respectively, were used as input for GO analyses. Especially biological processes, such as immune response (GO:0006955), apoptotic process (GO:0006915), signal transduction (GO:0007165), cell migration (GO:0016477) and response to virus (GO:0009615) were relevantly enriched after MDV infection. These enriched GO terms are in agreement with the findings after proteome analysis of MDV-infected B cells and confirm the above mentioned observation of minor alterations by MDV in the cellular proteome during lytic infection.

Eighteen potential infection markers, for which altered transcript levels were observed after both infection with the very virulent RB-1B and the vaccine strain CVI988 were identified (**Table 16**).

6.2.6. Alterations in expression levels of immune system associated transcripts

FCAR, also known as CD89, is usually expressed on the surface of blood myeloid cells, such as macrophages, neutrophils, dendritic cells and also B cells, and ligation leads to engulfment and killing of infected cells [62]. IgA can act against intracellular pathogens, including both bacteria and viruses, as it interferes with virus antigens during transcytosis, preventing viral synthesis and assembly [178]. IFIT1 belongs to the interferon-stimulated genes (ISGs) and is induced after viral infection [179]. IFIT1 recognizes mRNA that lacks 2'-O methylation on the 5' cap and inhibits translation of viral RNA as has been shown after infection of mouse embryonic fibroblasts and macrophages with different members of *Flaviviridae* and *Coronaviridae* [179] families. However, also DNA viruses such as HSV-1 activate special sensors, which trigger signaling cascades that induce expression of type I interferon. As response, interferon regulatory factor 3 (IRF3) is induced, which finally activates the IFIT genes and interfere with translation of viral proteins [179, 180]. The upregulation of the IFIT1 gene in MDV infected cells indicates an anti-viral immune response. Several interferon-response factors and interferon-inducible proteins have been associated with MDV infection before. Morgan *et al.* [58] investigated the host response in chicken embryo fibroblasts after infection with RB-1B with custom-made microarrays and observed 13 regulated genes including interferon-response factor 1 and interferon-inducible protein. Several IFNs, especially IFN- γ , are routinely found upregulated after MDV infection as reviewed by Haq *et al.* [181]. The here identified OASL is also an IFN- γ -induced gene and regulates the early phase of viral infection by degrading viral RNA, but also pro-viral functions are associated with members of the OAS family [182]. For example, the murine OASL1 protein suppresses type I interferon production and hence, inhibits T cell response and enhances viral persistence [182]. Different OAS members are upregulated in various autoimmune and chronic diseases [182]. Previous experiments have shown that the interferon gamma induced pathway is altered in MDV-transformed chicken CD4+ T cell lymphoma cell line, resembling activation of T cells [183]. Experiments in mice have also shown that IFN- γ coordinates activation of immune processes that lead to elimination of developing tumors [184]. Although not exactly the same transcripts were identified, similarities were

observed in the identified pathways. Upregulated immune system associated genes in MDV infected B cells indicates an anti-viral immune response. IFN- γ also plays an important role in host immune defense against VZV infection [185].

6.2.7. Alterations in expression levels of stress response transcripts

Transcripts of two heat shock proteins were upregulated after MDV infection, which is consistent with previous RNA-seq of spleen from MDV-infected chickens, which identified HSP70, HSP90 and HSP110 as upregulated in MDV infected spleen tissue [186]. HSP70 has been reported to be upregulated after MDV infection in proteome and transcriptome studies [181]. BAG3 is a co-chaperone that is suggested to link HSP70 to small heat shock proteins [187] and to introduce chaperone-bound substrates to macroautophagy [188]. It was previously shown that BAG3 regulates gene expression of HSV-1 immediate early genes [189] and is required for efficient replication of VZV [190]. However, BAG3 has not been identified in connection with MDV infection before.

6.2.8. Alterations in expression levels of transcripts associated with signaling cascades

FGFR1 belongs to the family of fibroblast growth factor receptors. It activates a cascade of downstream signals influencing mitogenesis and differentiation after interaction with fibroblast growth factor [191]. Fibroblast growth factor receptors in general are expressed mostly on endothelial cells and play an important role for angiogenesis in a variety of different tumors [192]. SDC4 is one of many heparan sulfate proteoglycans on mature cells that is involved in intracellular signaling. It acts as co-receptor for FGFR1-4 and induces the mitogen-activated protein kinase (MAPK) signaling pathway [193]. Previously, it was shown that *meq* activates several signaling cascades by acting as transcription factor for major kinases involved in the ERK/MAPK pathway [181, 194]. Stahl *et al.* described a similar upregulation of the MAPK signaling cascade after infection with MHV68 and suggested an important role for the kinases in viral replication [155]. The solute carrier family 8 member A3 belongs to the sodium/calcium exchanger integral membrane protein family and maintains the intracellular Ca^{2+} homeostasis. Calcium ions are important messengers in eukaryotic cells and are involved in many

cellular processes. Ca^{2+} is essential for B cell survival and activation and it is known that EBV remodels ER calcium homeostasis during immortalization of B cells [195, 196]. Many viruses, including HSV-1, change intracellular calcium levels as Ca^{2+} plays important roles in virion formation, virus entry, gene expression and virus replication, as well as posttranslational processing of viral proteins and virus release [197]. SPARC, another calcium binding protein, was upregulated in MDV infected B cells. SPARC is a matricellular glycoprotein essential for the assembly and molding of extracellular matrix (ECM) [198]. In addition, it is expressed in cell populations that undergo migration and differentiation [199] and has been identified in a number of cancers and as part of fibroblast-specific inflammation [200-202].

6.2.9. Alterations in expression levels of transcripts associated with autophagy

One interesting candidate can be linked to autophagy. MAP1B belongs to the microtubule associated proteins, which are important for the formation of the cytoskeleton of mostly axons and dendrites [203]. However, the light chain 3B of microtubule associated proteins 1A/1B, also known as LC3B, is a known marker for autophagy [204, 205]. Autophagy mediates stress-induced adaptation and damage control of the cell by forming double-membrane vesicles engulfing organelles, protein or cytoplasm contents for transport to lysosomal degradation [206]. Autophagy plays a role in innate immunity as it helps defending the cell against infections, inflammation and neoplastic diseases [206]. However, certain viruses can use autophagy for their advantage, such as Newcastle disease virus (NDV). NDV induces autophagy to enhance viral replication [207]. Contradicting roles of autophagy have been observed previously for herpesvirus infections. HSV-1 protein ICP34.5 for example triggers accumulation of autophagosomes but interferes with fusion with lysosomes and hence, inhibits degradation of proteins [208]. During early infection with PrV, autophagy is first induced probably by viral DNA or proteins as host response, but during the course of infection it is reduced to enhance viral replication [209]. However, a role for autophagy in MDV infection has not been described so far.

6.2.10. Transcripts downregulated after MDV infection

The two downregulated genes, ADAM13 and S1PR4 are associated with cell-cell/ cell-matrix interactions and cell signaling, respectively. S1PR4 is expressed by immune cells and interaction with the receptor leads to modulation of immune cell migration and secreted cytokine profile and hence, affects innate and adaptive immunity [210]. For example, signaling by S1PR4 activates ERK1/2 pathway [210]. The downregulation of this receptor indicates an interference mechanism of MDV with the immune response.

6.2.11. Conclusion and Outlook

Several transcriptome analyses of MDV infected cultured embryo and organ cells have been conducted before [18, 57, 181, 186]. The observed lack of correlation between the results of our RNA sequencing experiment and published transcriptome analyses after MDV infection can be explained by the use of different virus strains, different sampling time points, different cell types and different experimental approaches. Although there were differences between the panels of transcripts that were identified in the different studies, there was more conformity with regard to the biological processes that were identified as being influenced, such as immune response, apoptotic process and signal transduction.

In total, the effects of MDV infection on the proteome and transcriptome of B cells seem to be restricted. As mentioned previously, these findings are consistent with minimal changes induced in the proteome of PrV infected bovine kidney cells [152]. MDV is a highly cell-associated virus and is dependent on the host cell machinery for its replication cycle. However, our results suggest that MDV even reinforces this immune response by upregulating certain innate immune response associated proteins to attract more immune cells for sufficient spread of the virus in the infected animal. However, certain cell signaling and immune response associated proteins and genes were also downregulated in MDV infected B cells which could indicate a viral mechanism of immune evasion. It seems that MDV induced differences in gene and protein expression profiles, which promote an efficient virus replication and transmission of the virus from B cell to T cells.

This proteome analysis focused on the lytic infection of MDV in B cells. However, to unravel the full pathogenesis of MDV, also the proteome of primary T cells needs to be investigated. In order to determine differences in protein expression profiles during lytic and latent infection, the analysis of infected T cells is required. To distinguish lytic and latent infection, the infection could be performed with double labeled virus strains, e.g. with UL49-RFP and Meq-GFP. An alternative could be the use of a latently MDV infected T cell line that can be reactivated upon a stimulus.

6.3. Proteome analysis of MD tumors

6.3.1. Evaluation of MD tumor morphology

The most prominent characteristic of MDV is the ability to transform CD4⁺ T cells. Although the major viral genes associated with transformation have been identified, the response of the cell during virus-induced transformation is not fully understood. Changes in the expression level of cellular proteins during the transformation process have been investigated previously by analysis of macroscopically isolated tumors. However, the present study shows that MD tumors appear disseminated in the liver. The results of the HALO quantitation indicated varying portions of hepatocytes, connective tissue and CD3⁺ lymphocytes in tumors induced with the same virus strain in different animals. This emphasizes the need to specifically excise tumor regions with LCM, to examine transformation and tumor formation at the molecular level. Lesser variation and higher proportions of T cells were observed unexpectedly in the Δ vTR-induced tumors, since deletion of vTR is usually associated with the decrease of tumor formation and incidence [16]. MD lymphoma mainly consist of transformed CD4⁺ T cells and manifest in different visceral organs. The disseminated morphology of the tumors in the organs makes the selection of an appropriate reference tissue for the proteome analysis difficult. The most suitable controls for the investigations re naïve T cells. However, they do not reflect the unavoidable contamination of the tumor sample by surrounding organ tissue. Pure organ tissue (liver, in our case) as control will not represent the T cell background and may not even be a good control for the interspersed organ tissue within the tumor, as the tumor itself may influence the protein expression

of neighboring organ cells. Thus, a perfect control for the proteome analysis of MDV induced tumors is difficult to find unless an additional level of purification is introduced e.g. by enzymatic dissociation of the LCM samples followed by FACS [211]. The proteomes of spleens from chickens infected with the very virulent RB-1B strain have been analyzed before, comparing homogenized tumorous spleen to spleen from uninfected animals in a 1D LC-ESI MS approach [159]. Similarly, the proteome of MDV transformed thymus was analyzed in comparison to healthy thymus [112]. In these studies 119 differentially expressed proteins were identified in the affected thymus [112] and 48 in the affected spleens [159], respectively. Hu *et al.* suggested the high number of differentially expressed proteins in transformed thymus to be also a result of increased size of the organ and changes in cellular composition as observed during thymic atrophy, which causes immune suppression of the animal [112]. A microarray study comparing MD lymphoid tumor and liver from control animals identified 269 differentially expressed genes [59]. However, the high number of identified potentially regulated proteins could be a result of the natural differences between liver or spleen and T cells.

The analysis of pure target cells within their native environment is an important challenge of proteomic studies performed with tissue samples. Tissues are highly complex and heterogeneous structures containing different cell types and extracellular matrix, which all may influence the protein and gene expression of the cells of interest, which constitutes only a specific fraction of the sample. If the target cells have to be enriched or purified, a preparation method must be chosen that preserves the native state of the cells during the extraction process to allow further analysis [212]. Our workflow for proteome analyses consists of laser capture microdissection of MD tumors and reference material, lysis of the sections and filter aided digest of proteins. The resulting peptides of the different samples were differentially dimethyl labeled. In order to reduce complexity of mixture and improve resolution of proteomic analysis, the samples were fractionated by OG IEF prior to LC-MALDI TOF/TOF MS.

6.3.2. MDV induced changes in expression levels of host proteins during transformation

Proteome analysis of LCM dissected Δ vTR-induced tumors compared to naïve T cells, the main targets of transformation, identified nineteen potential transformation markers (**Table 17**). These interesting candidates could be confirmed in WT tumors. The results show only minor differences in the protein expression profiles between naïve T cells and MDV-transformed T cells. In addition, only minor differences between WT virus induced tumors and Δ vTR-induced tumors could be detected in the protein expression profiles. Several of the identified markers that were differentially expressed in both tumor types could also be verified by RT-qPCR on transcript level. Five different tumor samples were tested for gene expression of nine selected transformation markers. In the proteome analysis of MD tumors, the immune response associated proteins interferon gamma-inducible protein 30 (*IFI30*), heat shock 70kDa protein- 4like (*HSPA4L*), 2'-5'-oligoadenylate synthetase-like (*OASL*) and transporter 1 ATP-binding cassette sub-family B (*TAP1*) were upregulated. In contrast, lamin B receptor (*LBR*), glutathione S-transferase theta 1-like (*GSTT1L*), regulator of chromosome condensation 2 (*RCC2*), FYN binding protein (*FYB*), H2A histone family member J (*H2AFJ*) were downregulated in both tumor types compared to naïve T cells. Differences in the expression level in different tumor samples induced by the WT and mutant MDV strains from different animals were observed. These variations may rather be due to differences in cell composition as detected with the HALO quantitation software. Especially the tumor from one chicken infected with WT virus, (**Figure 26**), contained a higher percentage of liver cells within the transformed region compared to all other tested tumors. In addition, three of the four markers which were identified as upregulated in the proteomic analysis of tumor samples compared to T cells, were not found regulated at the transcript level in the RT-qPCR. As mentioned in chapter **6.2.4 Correlation of changes in transcriptome and proteome of MDV infected B cells** the protein expression levels generally are not strictly correlated with the transcript levels.

6.3.3. Proteins upregulated in MD lymphomas

IFI30 was upregulated in both the proteome and transcript analyses in four of five tested tumor samples compared to T cells. This protein, also known as gamma-interferon-inducible lysosomal thiol

reductase (GILT), is constitutively expressed by many antigen-presenting cells, but also in low levels in T cells and fibroblasts [213]. The expression is upregulated by IFN- γ , which activates the JAK and STAT1 pathway, and STAT1 in turn induces production of GILT [213]. GILT has diverse cellular functions. It maintains the redox state of the cell and influences autophagy, cellular activation and proliferation. Deletion of GILT in T cells led to increased phosphorylation of the extracellular signal-regulated kinase 1/2 ERK1/2 kinases, activation of the ERK1/2 pathway, and resulted in increased cell proliferation [213]. GILT enhances MHC II-restricted presentation of endocytosed antigens by catalyzing disulfide bond reduction in endosomes and lysosomes, thus activating CD4⁺ T cell response [214-216]. Viral glycoproteins, for example gB from HSV-1, contain epitopes that are cleaved by GILT and hence, GILT plays a role in eliciting an immune response against HSV-1 infection [216]. Also, cancer-infiltrating antigen-presenting cells elicit MHC II antigen processing and presentation by GILT, representing an anti-tumor T cell strategy. GILT may also influence tumorigenesis as deletion of GILT leads to increased levels of reactive oxygen species and decreased proliferation [213]. These features of GILT suggest that the upregulation of GILT in MD tumors might be a sign of the host anti-tumor response. Similarly, the proteins 2'-5'-oligoadenylate synthetase-like (*OASL*) and transporter 1 ATP-binding cassette sub-family B (*TAP1*) were upregulated in MD tumors compared to T cells and liver. However, the expression was not regulated at the transcript level as demonstrated by the RT-qPCR. *OASL* was also increased in MDV infected B cells as discussed in section 6.2.6. Similar to our results, several cytokines promoting anti-tumor immune response, such as IFN- γ , IFN- β , IFN- α , TNFR and IL-12 have been previously identified as upregulated in a MDV transformed CD4⁺ T cell line [183]. Many anti-cancer therapies make use of the anti-tumor activity of IFNs and IFN- α is used for the treatment of several different types of cancer, including B- and T cell lymphomas [184]. The transporter associated with antigen presentation (TAP) is associated with MHC class I antigen presentation and required for the transport of the antigen from the cytoplasm to the lumen of the endoplasmic reticulum (ER), where it is then loaded onto the MHC class I molecules [217]. A slight upregulation of TAP2 in feather tips of MDV infected chickens was reported previously [218]. The upregulation of several immune response associated proteins indicates

activation of T cells and possible anti-tumor strategy. In contrast to our study, Thanthrige-Don *et al.* [161], observed down-regulation of several IFN- γ -inducible MHC class II associated molecules in chickens infected with MDV. Contradicting effects of MDV infection on expression of MHC class I and II molecules have been described before [218]. These diverse results may be due to the differing time points after infection and tumor formation that were chosen. However, analysis of different tumor stages and time points in tumor development is difficult for MD lymphomas as kinetics of infection and tumor formation can hardly be synchronized and depend on several factors [58].

6.3.4. Proteins downregulated in MD lymphomas

Whereas several immune response associated proteins were upregulated in MD lymphomas compared to T cells, eleven proteins were downregulated in both tumor types. Two and three proteins were associated with regulation of transcription and nucleosome assembly, respectively. Transcription related processes were also detected as regulated in microarray studies of MDV transformation in chicken spleens [186]. Similarly, a MudPIT proteomic analysis of MDV infected CEFs detected an increase of phosphoproteins in the nucleus indicating an effect of infection on transcription regulation [219]. Two of the downregulated proteins of the present study were associated with signaling pathways that regulate the cytoskeleton, namely the FYN-binding protein (FYB) [220] and the p21-activated kinase 2 (PAK2) [221].

6.3.5. Conclusion and Outlook

We successfully applied LC-MALDI TOF/TOF MS to analyze dimethyl labeled, OG IEF fractionated peptides isolated from MD lymphoma tissue compared to naïve T cells and healthy liver tissue. Changes in host protein expression during transformation process were analyzed. The identified potential transformation markers were associated with nucleosome assembly, regulation of transcription, inflammatory response, immune response and oxidation-reduction process. However, further functional analyses are necessary to confirm a role of the identified markers during transformation.

To further decrease contamination from healthy organ cells, transformed T cells can be specifically isolated via FACS from isolated MDV lymphoma. In addition, to identify protein expression profiles of different stages of transformation and to determine the optimal time-point for tumor cell analysis, *in vivo* infection kinetic experiments are necessary. In order to investigate spatial differences in protein expression profiles in tumors and correlate expression with histological data MALDI imaging mass spectrometry can be used [222] and can be multiplexed for analysis of a wide range of analytes [223].

7. List of Abbreviations

| | |
|-------------|---|
| Δ | delta |
| AA | amino acid |
| AB | Antibody |
| ADAM13 | ADAM metallopeptidase domain 13 |
| APC | antigen-presenting cell |
| APS | ammonium peroxodisulfate |
| ATP | adenosintriphosphate |
| avBD2 | avian beta defensin 2 |
| BAC | bacterial artificial chromosome |
| BHV | Bovine herpesvirus |
| BSA | bovine serum albumin |
| bZIP | basic leucine zipper |
| C'-terminus | carboxy terminus |
| CAPZB | capping actin protein of muscle Z-line beta subunit |
| CBB | Coomassie brilliant blue |
| CD | cluster of differentiation |
| CEF | chicken embryonic fibroblasts |
| CHCA | α -cyano-4-hydroxycinnamic acid |
| chTR | chicken telomerase RNA |
| D | dimensional |
| Da | Dalton |
| DNA | deoxyribonucleic acid |
| DHB | 2,5-dihydroxybenzoic acid |
| DTT | dithiothreitol |
| EBV | Epstein-Barr-virus |
| e.g. | for example (<i>Exempli gratia</i>) |
| ECM | extracellular matrix |
| emPAI | exponentially modified protein abundance index |
| ER | endoplasmic reticulum |
| ERK | extracellular-signal regulated kinase |
| ESI | electrospray ionization |
| FASP | filter aided sample preparation |

| | |
|-----------|---|
| FC | fold change |
| FCAR/CD89 | Fc fragment of IgA receptor |
| FGFR | fibroblast growth factor receptor |
| Fig. | Figure |
| FPKM | fragments per kilobase of exon per million fragments mapped |
| FTICR | Fourier transform ion cyclotron resonance |
| FYB | FYN binding protein |
| g | Glycoprotein |
| GAPDH | glyceraldehyde-3-phosphate dehydrogenase |
| GILT | Gamma-interferon-inducible lysosomal thiol reductase |
| GO | Gene Ontology |
| GSTT1L | glutathione S-transferase theta 1-like |
| H&E stain | hematoxylin and eosin stain |
| H2AFJ | H2A histone family member J |
| HHV8 | Human herpesvirus 8 |
| HIV | Human immunodeficiency virus |
| HSP | heat shock protein |
| HSV | Herpes simplex virus |
| HVT | Herpesvirus of turkeys |
| IAA | iodoacetamide |
| iBAQ | intensity-based absolute quantification |
| IEF | isoelectric focusing |
| IFI30 | interferon-inducible protein 30 |
| IFN | interferon |
| IFIT | interferon-induced protein |
| Ig | immunoglobulin |
| IL | interleukin |
| IRL | internal repeat long |
| IRS | internal repeat short |
| ISG | interferon-stimulated gene |
| IT | ion trap |
| JAK | Janus kinase |
| KEGG | Kyoto Encyclopedia of Genes and Genomes |
| KSHV | Kaposi sarcoma-associated herpesvirus |

| | |
|-------------|---|
| LBR | lamin B receptor |
| LC | liquid chromatography |
| LCM | laser-capture microdissection |
| LDHA | lactate dehydrogenase A |
| m/z | mass-to-charge ratio |
| MALDI | matrix-assisted laser desorption ionization |
| MAP1B | microtubule associated protein 1 |
| MAPK | mitogen-activated protein kinase |
| Meq | MDV EcoRI-Q |
| MD | Marek's disease |
| MDV | Marek's disease virus |
| MHC | major histocompatibility complex |
| MHV | Murine gammaherpesvirus |
| min | minutes |
| mRNA | messenger RNA |
| MS | mass spectrometry |
| MudPIT | multidimensional protein identification technology |
| N'-terminus | amino terminus |
| NDV | Newcastle disease virus |
| nLC | nano liquid chromatography |
| OASL | 2'-5'-oligoadenylate synthetase-like |
| OG | OFFGEL |
| ON | overnight |
| PAI | protein abundance index |
| PAICS | phosphoribosylaminoimidazole carboxylase |
| | phosphoribosylaminoimidazolesuccinocarboxamide synthase |
| PCR | polymerase chain reaction |
| PET | polyethylene tetraphthalate |
| pH | <i>Potentia hydrogenii</i> |
| pI | isoelectric point |
| pp | phosphoprotein |
| PrV | Pseudorabies virus |
| PTM | post transcriptional modifications |
| q | quantitative |

| | |
|----------|---|
| RCC2 | regulator of chromosome condensation 2 |
| RNA | ribonucleic acid |
| RP | reversed phase |
| RPL7A | ribosomal protein L7A |
| RPS10 | ribosomal protein S10 |
| RPS4X | ribosomal protein S4X |
| RT | reverse transcriptase |
| rt | room temperature |
| S1PR4 | sphingosine-1-phosphate receptor 4 |
| SA | 3,5-dimethoxy-4-hydroxycinnamic acid/ Sinapinic acid |
| SDC4 | syndecan-4 |
| SDS PAGE | sodium dodecyl sulfate polyacrylamide gel electrophoresis |
| sec | seconds |
| Seq | sequencing |
| SILAC | stable isotope labeling by amino acids in cell culture |
| SoC | sample over control (isotope ratio) |
| SPARC | secreted protein acidic and cysteine rich |
| STAT1 | signal transducer and activator of transcription 1 |
| STRING | search tool for the retrieval of interacting genes/proteins |
| TAP1 | transporter 1 ATP-binding cassette sub-family B |
| TBE | Tris-borate-EDTA buffer |
| TCEP | Tris(2-carboxyethyl)phosphine hydrochloride |
| TCR | T cell receptor |
| TEAB | triethyl ammonium bicarbonate |
| TEMED | tetramethylethylenediamine |
| TFA | trifluoroacetic acid |
| TOF | time of flight |
| TRL | terminal repeat long |
| TRS | terminal repeat short |
| UB | urea buffer |
| US | unique short |
| UL | unique long |
| UV | ultraviolet radiation |
| v/v | volume per volume |

| | |
|------|------------------------|
| vhs | viral host shut-off |
| vIL | viral interleukin |
| vLIP | viral lipase |
| vTR | viral telomerase RNA |
| VZV | Varicella Zoster virus |
| WT | wild type |

Amino acid one-letter code

| | |
|---|---------------|
| A | Alanine |
| C | Cysteine |
| D | Aspartic acid |
| E | Glutamic acid |
| F | Phenylalanine |
| G | Glycine |
| H | Histidine |
| I | Isoleucine |
| K | Lysine |
| L | Leucine |
| M | Methionine |
| N | Asparagine |
| P | Proline |
| Q | Glutamine |
| R | Arginine |
| S | Serine |
| T | Threonine |
| V | Valine |
| W | Tryptophan |
| Y | Tyrosine |

8. List of Figures

| | |
|---|-----|
| Figure 1 Genome organization of Marek's disease virus | 10 |
| Figure 2 Pathogenesis of Marek's disease virus infection adapted from [2] | 13 |
| Figure 3 Different applications and fields of proteomics [69]. | 19 |
| Figure 4 Schematic principle of matrix-assisted laser desorption ionization | 23 |
| Figure 5 Schematic representation of ESI ionization | 24 |
| Figure 6 Dimethyl labeling reaction (taken from Hsu et al. [100]). | 26 |
| Figure 7 Schematic picture of non-contact LCM with Zeiss P.A.L.M. microbeam | 30 |
| Figure 8 Analytical workflow | 50 |
| Figure 9 Overview of the workflow for the proteomic analysis of MDV-infected primary B cells.... | 51 |
| Figure 10 Overview of the workflow for the proteomic analysis of MD tumors. | 61 |
| Figure 11 Comparison of the fractionation efficiency | 70 |
| Figure 12 Mean isotope ratio of the proteins identified | 74 |
| Figure 13 Quantile plots of raw SoC values (black frames) and corrected SoC values (red frames). 75 | |
| Figure 14 Exemplary spectra of one tryptic peptide of ,marginal zone B and B1 cell specific protein' | |
| | 77 |
| Figure 15 Exemplary spectra of one tryptic peptide of ,stromal interaction molecule. | 78 |
| Figure 16 FACS analysis of mock infected and RB-1B infected B cells. | 79 |
| Figure 17 SDS-Page of RB-1B infected B cells compared to mock infected B cells..... | 80 |
| Figure 18 Relative expression levels of cellular proteins after infection of B cells with RB-1B | 82 |
| Figure 19 MS spectrum (A) and fragment spectrum (B) of avBD2 peptide 'GGSCHFGGCPSHLIK' | 85 |
| Figure 20 MS spectrum (A) and fragment spectrum (B) of IL-18 peptide 'DIPGESNIIFFK' | 86 |
| Figure 21 Quality control of generated cDNA libraries.. | 87 |
| Figure 22 ERCC analysis as internal control for sequencing runs..... | 88 |
| Figure 23 Heat map of the top 100 significantly regulated genes | 90 |
| Figure 24 Venn-diagram of all regulated genes in the three different comparisons. | 91 |
| Figure 25 Evaluation of morphology and composition of a MD tumor | 102 |
| Figure 26 Quantitation of cell types in different tumor samples with the HALO software | 103 |
| Figure 27 MDV- induced tumor in liver after infection with the Δ vTR mutant..... | 104 |

9. List of Tables

| | |
|--|------------|
| Table 1 Advantages and disadvantages of MALDI and ESI..... | 24 |
| Table 2 Pooling scheme for first sequencing run of the libraries | 58 |
| Table 3 Pooling scheme for second sequencing run of the libraries. | 58 |
| Table 4 Summary of T cell and B cell specific proteins..... | 71 |
| Table 5 Differentially expressed proteins in B cells compared to T cells..... | 75 |
| Table 6 Mole-percentages (mole-%) of B and T cell specific proteins | 76 |
| Table 7 MDV proteins identified in the RB-1B infected B cells | 81 |
| Table 8 Differentially expressed proteins after infection with RB-1B | 83 |
| Table 9 Summary and evaluation of sequencing runs | 87 |
| Table 10 Identified MDV transcripts in the RNA sequencing experiments in both RB-1B and CVI infected B cells. | 92 |
| Table 11 Gene expression of infection marker candidates identified in proteome analysis..... | 94 |
| Table 12 Differentially expressed host genes in the comparison CVI988 vs mock-infected B cells .. | 95 |
| Table 13 Differentially expressed host genes in the compare RB-1B vs mock-infected B cells..... | 95 |
| Table 14 Shows the 25 GO terms most frequently associated with differentially expressed genes after CVI988 infection..... | 98 |
| Table 15 Shows the 25 GO terms most frequently associated with differentially expressed genes after RB-1B infection. | 99 |
| Table 16 Differentially expressed host genes identified in both RB-1B and CVI988 infected B cells compared to mock infected B cells. | 100 |
| Table 17 Potential transformation markers | 105 |
| Table 18 differential expression of genes in tumor samples compared to naïve T cells determined by one-step RT-qPCR. | 106 |

10. Summary

‘Proteome analysis of chicken lymphocytes after infection and transformation by the oncogenic Marek’s disease virus’

The highly oncogenic alphaherpesvirus Marek’s disease virus (MDV) causes immense economic losses in the poultry industry. The main targets of *in vivo* MDV infection are primary B and T lymphocytes. The cytolytic infection of B cells leads to depletion of lymphoid cells results in severe immunosuppression. Infected B cells recruit and activate T cells. The close interaction between B cells and T cells enables efficient intercellular transfer of MDV. During infection of T cells, the virus enters a latent state. Infection of T cells can lead to transformation of these cells and formation of lymphoma, which manifest in various visceral organs. This study aimed at the characterization of the proteomes of MDV-infected lymphocytes during the lytic and latent phases of infection.

Previous *in vitro* studies concerning the MDV pathogenesis and host-virus interactions have been mainly conducted with primary fibroblasts or kidney cells, due to the short lifespan of primary lymphocytes in cell culture. Recently, a cultivation system has been established that extends the lifespan of primary lymphocytes through the addition of cytokines to the growth medium. This allowed the infection of B cells *in vitro* and to conduct quantitative proteomic analysis of primary lymphocytes. Infection with GFP labelled virus recombinants allowed the isolation of infected cells by FACS for the proteome analysis of MDV infected B lymphocytes. An efficient quantitative proteomic workflow was developed, which consisted of a filter-aided (FASP) digest of the extracted proteins, followed by differential dimethyl chemical labeling of the peptides for quantitative evaluation prior to LC-MALDI TOF/TOF mass spectrometry. Only few alterations of the protein and transcript expression profiles were observed after infection of primary B cells with the very virulent RB-1B and the live-attenuated vaccine strain CVI988/Rispens. Relevant changes in relative protein levels were found for only twelve and six interesting host proteins after RB1B and CVI988 infection, respectively. However, the

regulations were confirmed by inspection of the spectra from all experiments. The identified candidates play a role in immune response, translation and inflammatory response.

To confirm the potential infection markers, RNA-seq analysis of three biological replicates of each RB-1B -, CVI988- and mock-infected B cells was performed. Eighty expressed MDV transcripts could be identified, which were associated with lytic infection. The same MDV proteins were identified after infection with RB-1B or CVI988. However, transcriptome and proteome analysis of MDV-infected primary B cells showed only poor correlation. This indicates that the changes in protein expression profiles are mostly due to posttranscriptional events. Infection marker candidates were identified by the RNA-seq analysis, for which the gene expression was altered by MDV infection. Although almost 12,000 transcripts were identified, only few transcript levels changed markedly after MDV infection. The biological processes immune response, apoptotic process, signal transduction, cell migration and response to virus were enriched after MDV infection. The RNA-seq results confirm the observation that alterations of protein levels early after MDV infection are rare.

Most notably, MDV induces transformation of lymphocytes leading to malignant T-cell lymphomas in visceral organs with mortalities of up to 100 %. While several factors involved in MDV tumorigenesis have been identified, the transformation process is not fully understood. Therefore, we set out to fill this knowledge gap using proteome analysis of transformed T-cells *ex vivo*. In addition, the role of the viral telomerase RNA during transformation was assessed by comparison of tumors that had formed after infection with WT-virus or a telomerase RNA negative mutant. A major obstacle for tumor proteome analyses is the preparation of sufficient amounts of homogenous tumor tissue, as tumors appear with a dispersed morphology in the affected organs. The quantitation of cell types within the tumors indicated varying portions of hepatocytes, connective tissue, and CD3+ lymphocytes even with the same virus strain in different animals. However, the Δ vTR-induced tumors contained lower levels of hepatocytes and higher levels of CD3+ lymphocytes compared to WT tumors in all tested tumor samples. Thus, Δ vTR tumors were chosen for determination of differences in protein expression

profiles of tumors and naïve T cells for their lower content of liver cells. We developed a workflow for the proteome analysis of T cell tumors from livers of MDV-infected chickens. Samples included laser capture micro-dissected tissue cuts from tumors and surrounding healthy liver tissue as well as naïve T-cells prepared from thymus. To enable quantitative proteome analysis, samples were digested using the FASP protocol and peptides were isotope-coded by differential dimethyl labeling. To improve proteome analysis peptides were fractionated by preparative isoelectric focusing prior to nano-HPLC MALDI/TOF-TOF mass- spectrometric analysis.

Proteomic analyses of LCM dissected ΔvTR tumor compared to naïve T cells, the main targets of transformation, identified nineteen potential transformation markers but again only minor changes in relative levels were observed. Several of the identified markers could also be verified by RT-qPCR on transcript level. The identified transformation candidates were associated with nucleosome assembly, regulation of transcription, inflammatory response, immune response and oxidation-reduction process.

However, further functional analyses are necessary to fully elucidate the role of the identified markers during MDV infection and transformation.

11. Zusammenfassung

‘Eine Proteomanalyse von Lymphozyten nach Infektion und Transformation mit dem onkogenen Virus der Marek’schen Krankheit’

Das onkogene Alphaherpesvirus der Marek’schen Krankheit (MDV) verursacht erhebliche wirtschaftliche Verluste in der Geflügelindustrie. Die wesentlichen Zielzellen einer natürlichen MDV Infektion sind primäre B- und T Lymphozyten. Die zytolytische Infektion von B Zellen führt zu deren Depletion und damit zu einer schweren Immunsuppression. Die Infektion von B Zellen führt auch zur Rekrutierung und Aktivierung von T Zellen. Die enge Interaktion zwischen B- und T Zellen ermöglicht die Übertragung von MDV zwischen den Lymphozyten. Während der Infektion von T Zellen bildet das Virus Latenz aus. Die Infektion der T Zellen kann zur Transformation und der Bildung von Lymphomen führen, die sich in verschiedenen viszerale Organen manifestieren. Diese Studie zielt auf die Charakterisierung der Proteome von MDV-infizierten primären Lymphozyten während der lytischen und latenten Phase ab.

Frühere *in vitro* Studien bezüglich der MDV-Pathogenese und der Virus-Wirt-Interaktionen wurden aufgrund der kurzen Lebensdauer primärer Lymphozyten in Zellkultur hauptsächlich auf primären Fibroblasten oder Nierenzellen durchgeführt. Vor kurzem wurde ein neues Zellkultursystem etabliert, welches die Lebensdauer der primären Lymphozyten durch die Zugabe von Zytokinen zum Zellkulturmedium verlängert. Dies ermöglichte die *in vitro* Infektion von B Zellen und die Durchführung quantitativer Proteomanalysen von primären Lymphozyten. Die Infektion mit GFP-markierten Virusrekombinanten erlaubte die Isolierung infizierter Zellen durch FACS vor der hier beschriebenen Proteomanalyse von MDV infizierten B Lymphozyten. Es wurde ein effizientes Protokoll zur quantitativen Analyse der Proteinexpression entwickelt. Dieses bestand aus einem Filter-gestützten (FASP) Verdau der extrahierten Proteine, gefolgt von der chemischen Einführung einer Isotopenmarkierung durch reduktive Dimethylierung der Peptide und anschließender LC-MALDI TOF/TOF massenspektrometrischen Analyse. Nach der Infektion der primären B Zellen mit dem sehr

virulenten Stamm RB-1B und dem attenuierten Impfstamm CVI988/Rispens wurden nur wenige Änderungen in den Expressionsprofilen des Proteoms und des Transkriptoms beobachtet. Relevante Veränderungen der relativen Expressionsstärke der Proteine wurden für nur zwölf und sechs Wirtsproteine nach RB-1B- beziehungsweise CVI988-Infektion gefunden. Jedoch wurden die gleichen Proteine auch mit einer gleichsinnigen Regulierung in den Spektren der anderen Virusinfektion identifiziert. Die identifizierten Kandidaten spielen eine Rolle u.a. bei der Immunantwort, Translation und Entzündungsreaktion.

Um die potenziellen Infektionsmarker zu bestätigen, wurde eine RNA-Sequenzierung von je drei biologischen Replikaten der einzelnen RB-1B-, CVI988- und scheininfizierten B Zellen durchgeführt. Achtzig MDV-Transkripte konnten identifiziert werden, die mit lytischen Infektionen assoziiert wurden. Die gleichen MDV-Proteine wurden nach einer Infektion mit RB-1B oder CVI988 identifiziert. Allerdings zeigten die Transkriptom- und Proteomanalysen von MDV-infizierten primären B Zellen eine schlechte Korrelation. Dies deutet darauf hin, dass die Veränderungen in der Proteinmenge vor allem auf posttranskriptionalen Ereignissen beruhen. Interessante Kandidaten wurden durch die RNA-Sequenzanalyse identifiziert, deren Transkriptmenge durch MDV-Infektion verändert waren. Nur wenige Änderungen wurden in dem Transkriptom der B Zellen nach MDV Infektion beobachtet, obwohl insgesamt fast 12.000 Transkripte identifiziert wurden. GO-Terme wie Immunantwort, apoptotische Prozesse, Signaltransduktion, Zellmigration und Antwort auf Virusinfektion wurden nach MDV Infektion angereichert. Die Ergebnisse der RNA-Seq bestätigen die oben genannten Beobachtungen der geringfügigen Änderungen durch MDV in dem zellularen Proteom während lytischer Infektion.

MDV induziert die Transformation von Lymphozyten, was zu bösartigen T Zelllymphomen in viszerale Organen führt und mit einer Mortalität von bis zu 100% einhergehen kann. Während schon mehrere Faktoren identifiziert wurden, die bei der MDV-induzierten Tumorentstehung eine Rolle spielen, ist der Transformationsprozess nicht vollständig verstanden. Diese Wissenslücke sollte mit einer *ex vivo*

Proteomanalyse der transformierten T Zellen gefüllt werden. Darüber hinaus sollte die Rolle der viralen Telomerase RNA während der Transformation durch den Vergleich von Tumoren, die nach der Infektion mit WT-Virus oder einer Telomerase RNA negativen Mutante gebildet wurden, aufgeklärt werden. Ein großes Hindernis für Proteomanalysen von Tumoren ist die Gewinnung ausreichender Mengen an homogenem Tumorgewebe, da die Tumore in den betroffenen Organen disseminiert vorliegen. Die Quantifizierung der Zelltypen ergab schon beim gleichen Tumortyp stark streuende Anteile von Hepatozyten, Bindegewebe und CD3 + Lymphozyten in Proben aus verschiedenen Tieren. Makroskopische Präparate von Tumoren enthalten Kontaminationen von infiltrierendem gesundem Gewebe und die daraus resultierenden Proteomanalysen weisen eine niedrige Sensitivität auf. Da die vTR Tumore, trotz der Streuung den geringeren Leberzellanteil und höheren T-Zell Anteil zu haben schienen, wurde deren Analyse vorangestellt. So wurden Δ vTR Tumore zur Analyse von Proteinexpressionsprofil von Tumoren und naiven T Zellen verwendet. Dazu wurde ein Analysengang für die Proteomanalyse von reinen T Zelltumoren aus der Leber von MDV-infizierten Hühnern entwickelt. Zu den Proben gehörten mikrosezierte Gewebeschnitte von Tumoren und umliegendem gesunden Lebergewebe, sowie naive T Zellen, die aus Hühnerblut isoliert wurden. Um eine quantitative Proteomanalyse zu ermöglichen, wurden Proben mit dem FASP-Protokoll verdaut und die Peptide durch differentieller Dimethylmarkierung Isotopen-kodiert. Zur Verbesserung der Proteomanalyse wurden Peptide durch eine präparative isoelektrischen Fokussierung vor der Analyse durch Nano-HPLC MALDI/TOF-TOF Massenspektrometrie fraktioniert.

Proteinanalysen von LCM-sezierten Δ vTR Tumoren im Vergleich zu naiven T Zellen, den Zielzellen der Transformation, identifizierten neunzehn potenzielle Transformationsmarker. Generell wurden wieder nur wenige Änderungen in der relativen Expressionsstärke der Proteine beobachtet. Mehrere der identifizierten Marker konnten auch durch eine RT-qPCR auf Transkriptebene verifiziert werden. Die identifizierten Transformationskandidaten werden laut Gene Ontology Datenbank mit dem Aufbau des Nukleosoms, der Regulation der Transkription, entzündlicher Reaktion, Immunantwort und Oxidations-Reduktions-Reaktion assoziiert.

Allerdings müssen weitere funktionelle Analysen durchgeführt werden, um die Rolle der identifizierten Marker während der MDV-Infektion und-Transformation vollständig zu klären.

12. References

1. Marek, J., *Multiple Nervenentzündung (Polyneuritis) bei Hühnern*. Deutsche Tierärztliche Wochenschrift, 1907. **15**: p. 417-421.
2. Schat, K.A. and V. Nair, *Marek's Disease*, in *Diseases of Poultry*, Y.M. Saif, Editor. 2008, Blackwell Publishing Professional: Iowa, USA. p. 452-514.
3. Kaupp, B.F., B. S. M. S., and D.V. M., *Paralysis of the Domestic Fowl*. Poultry Science, 1921. **s2-7(4)**: p. 25-31.
4. Van der Walle, N. and E. Winkler-Junius, Tijdschr. Vergelijk. Geenesk. Gezondhlee, 1924. **10**: p. 34-50.
5. Pappenheimer, A.M., L.C. Dunn, and V. Cone, *Studies on Fowl Paralysis (Neurolymphomatosis Gallinarum) : I. Clinical Features and Pathology*. J Exp Med, 1929. **49(1)**: p. 63-86.
6. Biggs, P.M., *The History and Biology of Marek's Disease Virus*, in *Marek's Disease*, K. Hirai, Editor. 2012, Springer Science & Business Media: New York. p. 1-24.
7. Campbell, J.G. and P.M. Biggs, *A proposed classification of the leucosis complex and fowl paralysis*. Br Vet J, 1961. **117**: p. 316-34.
8. Pappenheimer, A.M., L.C. Dunn, and S.M. Seidlin, *Studies on Fowl Paralysis (Neurolymphomatosis Gallinarum) : II. Transmission Experiments*. J Exp Med, 1929. **49(1)**: p. 87-102.
9. Sevoian, M. and D. Chamberlain, *Avian lymphomatosis: Experimental reproduction of the ocular form*. Vet Med, 1962. **57**: p. 608-609.
10. Churchill, A.E. and P.M. Biggs, *Agent of Marek's disease in tissue culture*. Nature, 1967. **215(5100)**: p. 528-30.
11. Osterrieder, N., Kamil, J.P., Schumacher, D., Tischer, B.K., and Sascha Trapp, *Marek's Disease Virus: From Miasma to Model*. Nature Reviews: Microbiology, 2006. **4**: p. 283-294.
12. Venugopal, K. and L.N. Payne, *Molecular pathogenesis of Marek's disease-recent developments*. Avian Pathol, 1995. **24(4)**: p. 597-609.
13. Greco, A., et al., *Role of the short telomeric repeat region in Marek's disease virus replication, genomic integration, and lymphomagenesis*. J Virol, 2014. **88(24)**: p. 14138-47.
14. Osterrieder, K. and J.F. Vautherot, *The genome content of Marek's disease-like viruses*, in *Marek's Disease: An Evolving Problem* F. Davison and V. Nair, Editors. 2004, Elsevier Academic Press: Great Britain.
15. Cebrian, J., et al., *Inverted repeat nucleotide sequences in the genomes of Marek disease virus and the herpesvirus of the turkey*. Proc Natl Acad Sci U S A, 1982. **79(2)**: p. 555-8.
16. Nair, V., *Latency and tumorigenesis in Marek's disease*. Avian Dis, 2013. **57(2 Suppl)**: p. 360-5.
17. Buckmaster, A.E., et al., *Gene sequence and mapping data from Marek's disease virus and herpesvirus of turkeys: implications for herpesvirus classification*. J Gen Virol, 1988. **69 (Pt 8)**: p. 2033-42.
18. Levy, A.M., et al., *Marek's disease virus Meq transforms chicken cells via the v-Jun transcriptional cascade: a converging transforming pathway for avian oncoviruses*. Proc Natl Acad Sci U S A, 2005. **102(41)**: p. 14831-6.
19. Jarosinski, K.W., et al., *Marek's disease virus: lytic replication, oncogenesis and control*. Expert Rev Vaccines, 2006. **5(6)**: p. 761-72.
20. Lee, L.F., et al., *The complete unique long sequence and the overall genomic organization of the GA strain of Marek's disease virus*. Proc Natl Acad Sci U S A, 2000. **97(11)**: p. 6091-6.
21. Tulman, E.R., et al., *The genome of a very virulent Marek's disease virus*. J Virol, 2000. **74(17)**: p. 7980-8.
22. Maki, Y., et al., *Avian sarcoma virus 17 carries the jun oncogene*. Proc Natl Acad Sci U S A, 1987. **84(9)**: p. 2848-52.

23. Jones, D., et al., *Marek disease virus encodes a basic-leucine zipper gene resembling the fos/jun oncogenes that is highly expressed in lymphoblastoid tumors*. Proc Natl Acad Sci U S A, 1992. **89**(9): p. 4042-6.
24. Lupiani, B., et al., *Marek's disease virus-encoded Meq gene is involved in transformation of lymphocytes but is dispensable for replication*. Proc Natl Acad Sci U S A, 2004. **101**(32): p. 11815-20.
25. Horikawa, I. and J.C. Barrett, *Transcriptional regulation of the telomerase hTERT gene as a target for cellular and viral oncogenic mechanisms*. Carcinogenesis, 2003. **24**(7): p. 1167-76.
26. Hanahan, D. and R.A. Weinberg, *Hallmarks of cancer: the next generation*. Cell, 2011. **144**(5): p. 646-74.
27. Fragnet, L., et al., *The RNA subunit of telomerase is encoded by Marek's disease virus*. J Virol, 2003. **77**(10): p. 5985-96.
28. Bellon, M. and C. Nicot, *Regulation of telomerase and telomeres: human tumor viruses take control*. J Natl Cancer Inst, 2008. **100**(2): p. 98-108.
29. Chhab, N., et al., *Viral control of vTR expression is critical for efficient formation and dissemination of lymphoma induced by Marek's disease virus (MDV)*. Vet Res, 2010. **41**(5): p. 56.
30. Trapp, S., et al., *A virus-encoded telomerase RNA promotes malignant T cell lymphomagenesis*. J Exp Med, 2006. **203**(5): p. 1307-17.
31. Kaufer, B.B., et al., *Herpesvirus telomerase RNA (vTR) with a mutated template sequence abrogates herpesvirus-induced lymphomagenesis*. PLoS Pathog, 2011. **7**(10): p. e1002333.
32. Baigent, S.J. and F. Davison, *Marek's disease virus: biology and life cycle*, in *Marek's Disease: An Evolving Problem*, F. Davison and V. Nair, Editors. 2004, Elsevier Academic Press: Great Britain. p. 62-77.
33. Calnek, B.W., *Marek's disease--a model for herpesvirus oncology*. Crit Rev Microbiol, 1986. **12**(4): p. 293-320.
34. Addinger, H.K. and B.W. Calnek, *Pathogenesis of Marek's disease: early distribution of virus and viral antigens in infected chickens*. J Natl Cancer Inst, 1973. **50**(5): p. 1287-98.
35. Calnek, B.W., et al., *Further characterization of Marek's disease virus-infected lymphocytes. I. In vivo infection*. Int J Cancer, 1984. **33**(3): p. 389-98.
36. Payne, L.N. and K. Venugopal, *Neoplastic diseases: Marek's disease, avian leukosis and reticuloendotheliosis*. Rev Sci Tech, 2000. **19**(2): p. 544-64.
37. Morrow, C. and F. Fehler, *Marek's Disease: a worldwide Problem*, in *Marek's Disease: An Evolving Problem*, F.D.a.V. Nair, Editor. 2004, Elsevier Ltd: London, Great Britain. p. 49-61.
38. *Bundesgesetzblatt Teil I Nr. 7*, 2011, Editor., Bundesanzeiger Verlag: Bonn. p. 252-254.
39. Davison, F. and V. Nair, *Use of Marek's disease vaccines: could they be driving the virus to increasing virulence?* Expert Rev Vaccines, 2005. **4**(1): p. 77-88.
40. Calnek, B.W., *Lymphomagenesis in Marek's disease*. Avian Pathology, 1998. **27**: p. S54-S64.
41. Read, A.F., et al., *Imperfect Vaccination Can Enhance the Transmission of Highly Virulent Pathogens*. PLoS Biol, 2015. **13**(7): p. e1002198.
42. Bermudez, A.J. and B. Stewart-Brown, *Disease Prevention and Diagnosis*, in *Diseases of Poultry*, Y.M. Saif, Editor. 2008, Blackwell Publishing Professional: Iowa, USA. p. 5-42.
43. von Bülow, V., *Further characterisation of the CVI 988 strain of Marek's disease virus*. Avian Pathol, 1977. **6**(4): p. 395-403.
44. Baigent, S.J., et al., *Vaccinal control of Marek's disease: current challenges, and future strategies to maximize protection*. Vet Immunol Immunopathol, 2006. **112**(1-2): p. 78-86.
45. Bublot, M. and J. Sharma, *Vaccination against Marek's disease*, in *Marek's Disease: An Evolving Problem*, F. Davison and V. Nair, Editors. 2004, Elsevier Academic Press: Great Britain.
46. Buza, J.J. and S.C. Burgess, *Modeling the proteome of a Marek's disease transformed cell line: a natural animal model for CD30 overexpressing lymphomas*. Proteomics, 2007. **7**(8): p. 1316-26.

47. Dunn, J.R., et al., *Evaluation and Identification of Marek's Disease Virus BAC Clones as Standardized Reagents for Research*. Avian Diseases, 2017. **61**(1): p. 107-114.
48. Schat, K.A., B.W. Calnek, and J. Fabricant, *Characterisation of two highly oncogenic strains of Marek's disease virus*. Avian Pathol, 1982. **11**(4): p. 593-605.
49. Schumacher, D., et al., *Reconstitution of Marek's disease virus serotype 1 (MDV-1) from DNA cloned as a bacterial artificial chromosome and characterization of a glycoprotein B-negative MDV-1 mutant*. J Virol, 2000. **74**(23): p. 11088-98.
50. Petherbridge, L., et al., *Oncogenicity of virulent Marek's disease virus cloned as bacterial artificial chromosomes*. J Virol, 2004. **78**(23): p. 13376-80.
51. Jarosinski, K.W., et al., *Fluorescently tagged pUL47 of Marek's disease virus reveals differential tissue expression of the tegument protein in vivo*. J Virol, 2012. **86**(5): p. 2428-36.
52. Bencherit, D., et al., *Induction of DNA damages upon Marek's disease virus infection: implication in viral replication and pathogenesis*. J Virol, 2017.
53. Petherbridge, L., et al., *Replication-competent bacterial artificial chromosomes of Marek's disease virus: novel tools for generation of molecularly defined herpesvirus vaccines*. J Virol, 2003. **77**(16): p. 8712-8.
54. Kheimar, A. and B.B. Kaufer, *Epstein-Barr virus-encoded RNAs (EBERs) complement the loss of Herpesvirus telomerase RNA (vTR) in virus-induced tumor formation*. Sci Rep, 2018. **8**(1): p. 209.
55. Lu, Z., et al., *Proteomic analysis of the host response in the bursa of Fabricius of chickens infected with Marek's disease virus*. Virus Res, 2010. **153**(2): p. 250-7.
56. Chien, K.Y., H.C. Liu, and M.B. Goshe, *Development and application of a phosphoproteomic method using electrostatic repulsion-hydrophilic interaction chromatography (ERLIC), IMAC, and LC-MS/MS analysis to study Marek's Disease Virus infection*. J Proteome Res, 2011. **10**(9): p. 4041-53.
57. Hu, X., et al., *Transcriptional analysis of host responses to Marek's disease virus infection in chicken thymus*. Intervirology, 2015. **58**(2): p. 95-105.
58. Morgan, R.W., et al., *Induction of host gene expression following infection of chicken embryo fibroblasts with oncogenic Marek's disease virus*. J Virol, 2001. **75**(1): p. 533-9.
59. Chen, C., et al., *Transcriptional profiling of host gene expression in chicken liver tissues infected with oncogenic Marek's disease virus*. J Gen Virol, 2011. **92**(Pt 12): p. 2724-33.
60. Thantrige-Don, N., et al., *Proteomic analysis of host responses to Marek's disease virus infection in spleens of genetically resistant and susceptible chickens*. Dev Comp Immunol, 2010. **34**(7): p. 699-704.
61. Schermuly, J., Greco, A., Härtle, S., Osterrieder, N., Kaufer, B.B. and Bernd Kaspers, *In vitro Model for Lytic Replication, Latency, and Transformation of an Oncogenic Alphaherpesvirus*. PNAS, 2015. **112**: p. 7279-7284.
62. Murphy, K., *Janeway's Immunobiology*. 8th ed. 2012, New York: Garland Science, Taylor & Francis Group, LLC.
63. Denman, A.M., *Lymphocyte function and virus infections*. J Clin Pathol Suppl (R Coll Pathol), 1979. **13**: p. 39-47.
64. Klein, T., R.I. Viner, and C.M. Overall, *Quantitative proteomics and terminomics to elucidate the role of ubiquitination and proteolysis in adaptive immunity*. Philos Trans A Math Phys Eng Sci, 2016. **374**(2079).
65. Caldwell, R.B., et al., *Full-length cDNAs from chicken bursal lymphocytes to facilitate gene function analysis*. Genome Biol, 2005. **6**(1): p. R6.
66. Korte, J., et al., *2D DIGE analysis of the bursa of Fabricius reveals characteristic proteome profiles for different stages of chicken B-cell development*. Proteomics, 2013. **13**(1): p. 119-33.
67. Wu, Y., et al., *Optimized sample preparation for two-dimensional gel electrophoresis of soluble proteins from chicken bursa of Fabricius*. Proteome Sci, 2009. **7**: p. 38.
68. McCarthy, F.M., et al., *Modeling a whole organ using proteomics: the avian bursa of Fabricius*. Proteomics, 2006. **6**(9): p. 2759-71.

69. Graves, P.R. and T.A. Haystead, *Molecular biologist's guide to proteomics*. Microbiol Mol Biol Rev, 2002. **66**(1): p. 39-63; table of contents.
70. Wilkins, M.R., et al., *Progress with proteome projects: why all proteins expressed by a genome should be identified and how to do it*. Biotechnol Genet Eng Rev, 1996. **13**: p. 19-50.
71. Domon, B. and R. Aebersold, *Mass spectrometry and protein analysis*. Science, 2006. **312**(5771): p. 212-7.
72. Tsiatsiani, L. and A.J. Heck, *Proteomics beyond trypsin*. FEBS J, 2015. **282**(14): p. 2612-26.
73. Kwong, A.D., J.A. Kruper, and N. Frenkel, *Herpes simplex virus virion host shutoff function*. J Virol, 1988. **62**(3): p. 912-21.
74. Smiley, J.R., *Herpes simplex virus virion host shutoff protein: immune evasion mediated by a viral RNase?* J Virol, 2004. **78**(3): p. 1063-8.
75. Rutkowski, A.J., et al., *Widespread disruption of host transcription termination in HSV-1 infection*. Nat Commun, 2015. **6**: p. 7126.
76. Tombacz, D., J.S. Toth, and Z. Boldogkoi, *Deletion of the virion host shut: off gene of pseudorabies virus results in selective upregulation of the expression of early viral genes in the late stage of infection*. Genomics, 2011. **98**(1): p. 15-25.
77. Schwyzer, M., et al., *Gene contents in a 31-kb segment at the left genome end of bovine herpesvirus-1*. Vet Microbiol, 1996. **53**(1-2): p. 67-77.
78. Gimeno, I. and R.F. Silva, *Deletion of the Marek's disease virus UL41 gene (vhs) has no measurable effect on latency or pathogenesis*. Virus Genes, 2008. **36**(3): p. 499-507.
79. Jean Beltran, P.M., et al., *Proteomics and integrative omic approaches for understanding host-pathogen interactions and infectious diseases*. Mol Syst Biol, 2017. **13**(3): p. 922.
80. Zhang, G., et al., *Overview of peptide and protein analysis by mass spectrometry*. Curr Protoc Mol Biol, 2014. **108**: p. 10 21 1-30.
81. Han, X., A. Aslanian, and J.R. Yates, *Mass Spectrometry for Proteomics*. Curr Opin Chem Biol, 2008. **12**: p. 483-490.
82. Franz, T. and X. Li, *Step-by-step preparation of proteins for mass spectrometric analysis*. Methods Mol Biol, 2015. **1295**: p. 235-47.
83. Rhem, H. and T. Letzel, *Kapitel 7.5 Massenspektrometrie von Proteinen und Peptiden*, in *Der Experimentator: Proteinbiochemie/Proteomics*. 2010, Spektrum Akademischer Verlag: Heidelberg. p. 243-310.
84. Siuzdak, G., *The emergence of mass spectrometry in biochemical research*. Proc Natl Acad Sci U S A, 1994. **91**(24): p. 11290-7.
85. Pitt, A.R., *Mass Spectrometric Methods*, in *Proteins LABFAX*, N.C. Price, Editor. 1996, BIOS Scientific Publishers Limited: Oxford, UK. p. 174-186.
86. Roepstorff, P., *The interplay between different mass spectrometric techniques in protein chemistry*. Biochem Soc Trans, 1994. **22**(2): p. 533-9.
87. Takach, E.J., et al., *Accurate mass measurements using MALDI-TOF with delayed extraction*. J Protein Chem, 1997. **16**(5): p. 363-9.
88. Caprioli, R.M., *Imaging mass spectrometry: Molecular microscopy for the new age of biology and medicine*. Proteomics, 2016. **16**(11-12): p. 1607-12.
89. Steven, R.T., A. Dexter, and J. Bunch, *Investigating MALDI MSI parameters (Part 1) - A systematic survey of the effects of repetition rates up to 20kHz in continuous raster mode*. Methods, 2016. **104**: p. 101-10.
90. El-Aneed, A., A. Cohen, and J. Banoub, *Mass Spectrometry, Review of the Basics: Electrospray, MALDI, and Commonly Used Mass Analyzers*. Applied Spectroscopy Reviews, 2009. **44**(3): p. 210-230.
91. Yang, Y., et al., *A comparison of nLC-ESI-MS/MS and nLC-MALDI-MS/MS for GeLC-based protein identification and iTRAQ-based shotgun quantitative proteomics*. J Biomol Tech, 2007. **18**(4): p. 226-37.
92. Kuljanin, M., et al., *Comparison of sample preparation techniques for large-scale proteomics*. Proteomics, 2017. **17**(1-2).

93. Magdeldin, S., et al., *Complementary Protein and Peptide OFFGEL Fractionation for High-Throughput Proteomic Analysis*. Anal Chem, 2015. **87**(16): p. 8481-8.
94. Chenau, J., et al., *Peptides OFFGEL electrophoresis: a suitable pre-analytical step for complex eukaryotic samples fractionation compatible with quantitative iTRAQ labeling*. Proteome Sci, 2008. **6**: p. 9.
95. Arrey, T.N., et al., *Approaching the complexity of elastase-digested membrane proteomes using off-gel IEF/nLC-MALDI-MS/MS*. Anal Chem, 2010. **82**(5): p. 2145-9.
96. Henning, A.K., et al., *Analysis of the bovine plasma proteome by matrix-assisted laser desorption/ionisation time-of-flight tandem mass spectrometry*. Vet J, 2014. **199**(1): p. 175-80.
97. Ong, S.E., et al., *Stable isotope labeling by amino acids in cell culture, SILAC, as a simple and accurate approach to expression proteomics*. Mol Cell Proteomics, 2002. **1**(5): p. 376-86.
98. Kruger, M., et al., *SILAC mouse for quantitative proteomics uncovers kindlin-3 as an essential factor for red blood cell function*. Cell, 2008. **134**(2): p. 353-64.
99. Zanivan, S., M. Krueger, and M. Mann, *In vivo quantitative proteomics: the SILAC mouse*. Methods Mol Biol, 2012. **757**: p. 435-50.
100. Hsu, J.L., et al., *Stable-isotope dimethyl labeling for quantitative proteomics*. Anal Chem, 2003. **75**(24): p. 6843-52.
101. Boersema, P.J., et al., *Multiplex peptide stable isotope dimethyl labeling for quantitative proteomics*. Nat Protoc, 2009. **4**(4): p. 484-94.
102. Lau, H.T., et al., *Comparing SILAC- and stable isotope dimethyl-labeling approaches for quantitative proteomics*. J Proteome Res, 2014. **13**(9): p. 4164-74.
103. Bubis, J.A., et al., *Comparative evaluation of label-free quantification methods for shotgun proteomics*. Rapid Commun Mass Spectrom, 2017. **31**(7): p. 606-612.
104. Zhu, W., J.W. Smith, and C.M. Huang, *Mass spectrometry-based label-free quantitative proteomics*. J Biomed Biotechnol, 2010. **2010**: p. 840518.
105. Ishihama, Y., et al., *Exponentially modified protein abundance index (emPAI) for estimation of absolute protein amount in proteomics by the number of sequenced peptides per protein*. Mol Cell Proteomics, 2005. **4**(9): p. 1265-72.
106. Kudlicki, A., *The optimal exponent base for emPAI is 6.5*. PLoS One, 2012. **7**(3): p. e32339.
107. Luge, T. and S. Sauer, *Generating Sample-Specific Databases for Mass Spectrometry-Based Proteomic Analysis by Using RNA Sequencing*, in *Proteomics in System Biology. Methods in Molecular Biology*, J. Reinders, Editor. 2016, Humana Press: New York. p. 219-232.
108. The Gene Ontology, C., *Expansion of the Gene Ontology knowledgebase and resources*. Nucleic Acids Res, 2017. **45**(D1): p. D331-D338.
109. Ashburner, M., et al., *Gene ontology: tool for the unification of biology. The Gene Ontology Consortium*. Nat Genet, 2000. **25**(1): p. 25-9.
110. Binns, D., et al., *QuickGO: a web-based tool for Gene Ontology searching*. Bioinformatics, 2009. **25**(22): p. 3045-6.
111. Szklarczyk, D., et al., *STRING v10: protein-protein interaction networks, integrated over the tree of life*. Nucleic Acids Res, 2015. **43**(Database issue): p. D447-52.
112. Hu, X., et al., *Analysis of protein expression profiles in the thymus of chickens infected with Marek's disease virus*. Virol J, 2012. **9**: p. 256.
113. Jie, H., et al., *Differential expression of Toll-like receptor genes in lymphoid tissues between Marek's disease virus-infected and noninfected chickens*. Poult Sci, 2013. **92**(3): p. 645-54.
114. Espina, V., et al., *Laser-capture microdissection*. Nat Protoc, 2006. **1**(2): p. 586-603.
115. Golubeva, Y., et al., *Laser capture microdissection for protein and NanoString RNA analysis*. Methods Mol Biol, 2013. **931**: p. 213-57.
116. Emmert-Buck, M.R., et al., *Laser capture microdissection*. Science, 1996. **274**(5289): p. 998-1001.
117. Laemmli, U.K., *Cleavage of structural proteins during the assembly of the head of bacteriophage T4*. Nature, 1970. **227**(259): p. 680-685.

118. Neuhoﬀ, V., et al., *Improved staining of proteins in polyacrylamide gels including isoelectric focusing gels with clear background at nanogram sensitivity using Coomassie Brilliant Blue G-250 and R-250*. Electrophoresis, 1988. **9**(6): p. 255-62.
119. Wisniewski, J.R., et al., *Universal sample preparation method for proteome analysis*. Nat Methods, 2009. **6**(5): p. 359-62.
120. Nagaraj, N., et al., *Deep proteome and transcriptome mapping of a human cancer cell line*. Mol Syst Biol, 2011. **7**: p. 548.
121. Sambrook, J., E.F. Fritsch, and T. Maniatis, *Molecular cloning: a laboratory manual*. 1989, Cold Spring Harbor, NY: Cold Spring Harbor Laboratory Press.
122. Ye, J., et al., *Primer-BLAST: a tool to design target-specific primers for polymerase chain reaction*. BMC Bioinformatics, 2012. **13**: p. 134.
123. Reimand, J., et al., *g:Profiler--a web-based toolset for functional profiling of gene lists from large-scale experiments*. Nucleic Acids Res, 2007. **35**(Web Server issue): p. W193-200.
124. R_Development_Core_Team. *R: A language and environment for statistical computing*. 2011; Available from: <http://www.R-project.org/>.
125. Szklarczyk, D., et al., *The STRING database in 2017: quality-controlled protein-protein association networks, made broadly accessible*. Nucleic Acids Res, 2017. **45**(D1): p. D362-D368.
126. Zerbino, D.R., et al., *Ensembl 2018*. Nucleic Acids Res, 2018. **46**(D1): p. D754-D761.
127. Reimand, J., et al., *g:Profiler-a web server for functional interpretation of gene lists (2016 update)*. Nucleic Acids Res, 2016. **44**(W1): p. W83-9.
128. Kothlow, S., et al., *CD40 ligand supports the long-term maintenance and differentiation of chicken B cells in culture*. Dev Comp Immunol, 2008. **32**(9): p. 1015-26.
129. Spath, P.J. and H. Koblet, *Properties of SDS-polyacrylamide gels highly cross-linked with N,N'-diallyltartardiamide and the rapid isolation of macromolecules from the gel matrix*. Anal Biochem, 1979. **93**(2): p. 275-85.
130. Lian, L., et al., *Gene expression analysis of host spleen responses to Marek's disease virus infection at late tumor transformation phase*. Poult Sci, 2012. **91**(9): p. 2130-8.
131. Abdallah, C., et al., *Optimization of iTRAQ labelling coupled to OFFGEL fractionation as a proteomic workflow to the analysis of microsomal proteins of Medicago truncatula roots*. Proteome Sci, 2012. **10**(1): p. 37.
132. The UniProt, C., *UniProt: the universal protein knowledgebase*. Nucleic Acids Res, 2017. **45**(D1): p. D158-D169.
133. Lambeth, L.S., et al., *Targeting Marek's disease virus by RNA interference delivered from a herpesvirus vaccine*. Vaccine, 2009. **27**(2): p. 298-306.
134. Lv, H., et al., *Genetic evolution of Gallid herpesvirus 2 isolated in China*. Infect Genet Evol, 2017. **51**: p. 263-274.
135. Dorange, F., et al., *Characterization of Marek's disease virus serotype 1 (MDV-1) deletion mutants that lack UL46 to UL49 genes: MDV-1 UL49, encoding VP22, is indispensable for virus growth*. J Virol, 2002. **76**(4): p. 1959-70.
136. Omar, A.R. and K.A. Schat, *Syngeneic Marek's disease virus (MDV)-specific cell-mediated immune responses against immediate early, late, and unique MDV proteins*. Virology, 1996. **222**(1): p. 87-99.
137. Patro, R., et al., *Salmon provides fast and bias-aware quantification of transcript expression*. Nat Methods, 2017. **14**(4): p. 417-419.
138. Benjamini, Y. and Y. Hochberg, *Controlling the False Discovery Rate: A Practical and Powerful Approach to Multiple Testing*. Journal of the Royal Statistical Society 1995. **57**(1): p. 289-300.
139. Azimi, A., et al., *In Silico Analysis Validates Proteomic Findings of Formalin-fixed Paraffin Embedded Cutaneous Squamous Cell Carcinoma Tissue*. Cancer Genomics Proteomics, 2016. **13**(6): p. 453-465.
140. Burgess, S.C., et al., *Marek's disease is a natural model for lymphomas overexpressing Hodgkin's disease antigen (CD30)*. Proc Natl Acad Sci U S A, 2004. **101**(38): p. 13879-84.

141. Mikulak, J., et al., *Host Immune Responses in HIV-1 Infection: The Emerging Pathogenic Role of Siglecs and Their Clinical Correlates*. Front Immunol, 2017. **8**: p. 314.
142. Shannon-Lowe, C., A.B. Rickinson, and A.I. Bell, *Epstein-Barr virus-associated lymphomas*. Philos Trans R Soc Lond B Biol Sci, 2017. **372**(1732).
143. Feist, P.E., et al., *Bottom-up proteomic analysis of single HCT 116 colon carcinoma multicellular spheroids*. Rapid Commun Mass Spectrom, 2015. **29**(7): p. 654-8.
144. Sangster, T.P., et al., *Investigation of analytical variation in metabolomic analysis using liquid chromatography/mass spectrometry*. Rapid Commun Mass Spectrom, 2007. **21**(18): p. 2965-70.
145. Frey, J.R., M. Fountoulakis, and I. Lefkovits, *Proteome analysis of activated murine B-lymphocytes*. Electrophoresis, 2000. **21**(17): p. 3730-9.
146. Zanker, D., et al., *Compartment resolved reference proteome map from highly purified naive, activated, effector, and memory CD8(+) murine immune cells*. Proteomics, 2015. **15**(11): p. 1808-12.
147. Palmer, C., et al., *Cell-type specific gene expression profiles of leukocytes in human peripheral blood*. BMC Genomics, 2006. **7**: p. 115.
148. Du, X., et al., *Genomic profiles for human peripheral blood T cells, B cells, natural killer cells, monocytes, and polymorphonuclear cells: comparisons to ischemic stroke, migraine, and Tourette syndrome*. Genomics, 2006. **87**(6): p. 693-703.
149. Ehrhardt, G.R., et al., *Discriminating gene expression profiles of memory B cell subpopulations*. J Exp Med, 2008. **205**(8): p. 1807-17.
150. Mitchell, C.J., et al., *A multi-omic analysis of human naive CD4+ T cells*. BMC Syst Biol, 2015. **9**: p. 75.
151. Painter, M.W., et al., *Transcriptomes of the B and T lineages compared by multiplatform microarray profiling*. J Immunol, 2011. **186**(5): p. 3047-57.
152. Skiba, M., T.C. Mettenleiter, and A. Karger, *Quantitative whole-cell proteome analysis of pseudorabies virus-infected cells*. J Virol, 2008. **82**(19): p. 9689-99.
153. Matis, J. and M. Kudelova, *Early shutoff of host protein synthesis in cells infected with herpes simplex viruses*. Acta Virol, 2001. **45**(5-6): p. 269-77.
154. Berard, A.R., K.M. Coombs, and A. Severini, *Quantification of the host response proteome after herpes simplex virus type 1 infection*. J Proteome Res, 2015. **14**(5): p. 2121-42.
155. Stahl, J.A., et al., *Phosphoproteomic analyses reveal signaling pathways that facilitate lytic gammaherpesvirus replication*. PLoS Pathog, 2013. **9**(9): p. e1003583.
156. Esclatine, A., B. Taddeo, and B. Roizman, *The UL41 protein of herpes simplex virus mediates selective stabilization or degradation of cellular mRNAs*. Proc Natl Acad Sci U S A, 2004. **101**(52): p. 18165-70.
157. Engel, E.A., et al., *Investigating the biology of alpha herpesviruses with MS-based proteomics*. Proteomics, 2015. **15**(12): p. 1943-56.
158. Lin, J.H., et al., *Epstein-Barr virus LMP2A suppresses MHC class II expression by regulating the B-cell transcription factors E47 and PU.1*. Blood, 2015. **125**(14): p. 2228-38.
159. Thantrige-Don, N., et al., *Analyses of the spleen proteome of chickens infected with Marek's disease virus*. Virology, 2009. **390**(2): p. 356-67.
160. Sarson, A.J., et al., *Transcriptional analysis of host responses to Marek's disease virus infection in genetically resistant and susceptible chickens*. Anim Genet, 2008. **39**(3): p. 232-40.
161. Thantrige-Don, N., et al., *Marek's disease virus influences the expression of genes associated with IFN-gamma-inducible MHC class II expression*. Viral Immunol, 2010. **23**(2): p. 227-32.
162. Dinarello, C.A., et al., *Interleukin-18 and IL-18 binding protein*. Front Immunol, 2013. **4**: p. 289.
163. Ting, J.P. and J. Trowsdale, *Genetic control of MHC class II expression*. Cell, 2002. **109** Suppl: p. S21-33.
164. Abdul-Careem, M.F., et al., *Marek's disease virus-induced expression of cytokine genes in feathers of genetically defined chickens*. Dev Comp Immunol, 2009. **33**(4): p. 618-23.

165. Parvizi, P., et al., *Cytokine gene expression in splenic CD4+ and CD8+ T cell subsets of genetically resistant and susceptible chickens infected with Marek's disease virus*. Vet Immunol Immunopathol, 2009. **132**(2-4): p. 209-17.
166. Heidari, M., et al., *Marek's disease virus-induced immunosuppression: array analysis of chicken immune response gene expression profiling*. Viral Immunol, 2010. **23**(3): p. 309-19.
167. Parnas, O., D.L. Corcoran, and B.R. Cullen, *Analysis of the mRNA targetome of microRNAs expressed by Marek's disease virus*. MBio, 2014. **5**(1): p. e01060-13.
168. Cebulla, C.M., D.M. Miller, and D.D. Sedmak, *Viral inhibition of interferon signal transduction*. Intervirology, 1999. **42**(5-6): p. 325-30.
169. Wiertz, E.J., et al., *Herpesvirus interference with major histocompatibility complex class II-restricted T-cell activation*. J Virol, 2007. **81**(9): p. 4389-96.
170. Sugiarto, H. and P.L. Yu, *Avian antimicrobial peptides: the defense role of beta-defensins*. Biochem Biophys Res Commun, 2004. **323**(3): p. 721-7.
171. Oppenheim, J.J., et al., *Roles of antimicrobial peptides such as defensins in innate and adaptive immunity*. Ann Rheum Dis, 2003. **62 Suppl 2**: p. ii17-21.
172. Cuperus, T., et al., *Avian host defense peptides*. Dev Comp Immunol, 2013. **41**(3): p. 352-69.
173. Wilson, S.S., M.E. Wiens, and J.G. Smith, *Antiviral mechanisms of human defensins*. J Mol Biol, 2013. **425**(24): p. 4965-80.
174. Heidari, M., et al., *Transcriptional profiling of Marek's disease virus genes during cytolytic and latent infection*. Virus Genes, 2008. **36**(2): p. 383-92.
175. Vogel, C. and E.M. Marcotte, *Insights into the regulation of protein abundance from proteomic and transcriptomic analyses*. Nat Rev Genet, 2012. **13**(4): p. 227-32.
176. Skiba, M., et al., *Gene expression profiling of Pseudorabies virus (PrV) infected bovine cells by combination of transcript analysis and quantitative proteomic techniques*. Vet Microbiol, 2010. **143**(1): p. 14-20.
177. Liu, Y., A. Beyer, and R. Aebersold, *On the Dependency of Cellular Protein Levels on mRNA Abundance*. Cell, 2016. **165**(3): p. 535-50.
178. van Egmond, M., et al., *IgA and the IgA Fc receptor*. Trends Immunol, 2001. **22**(4): p. 205-11.
179. Diamond, M.S., *IFIT1: A dual sensor and effector molecule that detects non-2'-O methylated viral RNA and inhibits its translation*. Cytokine Growth Factor Rev, 2014. **25**(5): p. 543-50.
180. Fensterl, V. and G.C. Sen, *Interferon-induced Ifit proteins: their role in viral pathogenesis*. J Virol, 2015. **89**(5): p. 2462-8.
181. Haq, K., et al., *Transcriptome and proteome profiling of host responses to Marek's disease virus in chickens*. Vet Immunol Immunopathol, 2010. **138**(4): p. 292-302.
182. Choi, U.Y., et al., *Oligoadenylate synthase-like (OASL) proteins: dual functions and associations with diseases*. Exp Mol Med, 2015. **47**: p. e144.
183. Buza, J.J. and S.C. Burgess, *Different signaling pathways expressed by chicken naive CD4(+) T cells, CD4(+) lymphocytes activated with staphylococcal enterotoxin B, and those malignantly transformed by Marek's disease virus*. J Proteome Res, 2008. **7**(6): p. 2380-7.
184. Smyth, M.J., et al., *Cytokines in cancer immunity and immunotherapy*. Immunol Rev, 2004. **202**: p. 275-93.
185. Kim, J.A., et al., *STING Is Involved in Antiviral Immune Response against VZV Infection via the Induction of Type I and III IFN Pathways*. J Invest Dermatol, 2017. **137**(10): p. 2101-2109.
186. Dang, L., et al., *Dynamic Changes in the Splenic Transcriptome of Chickens during the Early Infection and Progress of Marek's Disease*. Sci Rep, 2017. **7**(1): p. 11648.
187. Rauch, J.N., et al., *BAG3 Is a Modular, Scaffolding Protein that physically Links Heat Shock Protein 70 (Hsp70) to the Small Heat Shock Proteins*. J Mol Biol, 2017. **429**(1): p. 128-141.
188. Carra, S., S.J. Seguin, and J. Landry, *HspB8 and Bag3: a new chaperone complex targeting misfolded proteins to macroautophagy*. Autophagy, 2008. **4**(2): p. 237-9.
189. Kyratsous, C.A. and S.J. Silverstein, *The co-chaperone BAG3 regulates Herpes Simplex Virus replication*. Proc Natl Acad Sci U S A, 2008. **105**(52): p. 20912-7.

190. Kyratsous, C.A. and S.J. Silverstein, *BAG3, a host cochaperone, facilitates varicella-zoster virus replication*. J Virol, 2007. **81**(14): p. 7491-503.
191. Drafa K.A., McAndrew C.W., and Donoghue D.J., *Chapter 237 – Signaling from Fibroblast Growth Factor Receptors in Development and Disease*, in *Handbook of Cell Signaling (Second Edition)*, Bradshaw R.A. and Dennis E.A., Editors. 2010, Academic Press: London, UK. p. 1939-1947.
192. Presta, M., et al., *Fibroblast growth factor/fibroblast growth factor receptor system in angiogenesis*. Cytokine Growth Factor Rev, 2005. **16**(2): p. 159-78.
193. Elfenbein, A. and M. Simons, *Syndecan-4 signaling at a glance*. J Cell Sci, 2013. **126**(Pt 17): p. 3799-804.
194. Subramaniam, S., et al., *Integrated analyses of genome-wide DNA occupancy and expression profiling identify key genes and pathways involved in cellular transformation by a Marek's disease virus oncoprotein, Meq*. J Virol, 2013. **87**(16): p. 9016-29.
195. Dellis, O., et al., *Modulation of B-cell endoplasmic reticulum calcium homeostasis by Epstein-Barr virus latent membrane protein-1*. Mol Cancer, 2009. **8**: p. 59.
196. Oh-hora, M. and A. Rao, *Calcium signaling in lymphocytes*. Curr Opin Immunol, 2008. **20**(3): p. 250-8.
197. Zhou, Y., T.K. Frey, and J.J. Yang, *Viral calciomics: interplays between Ca²⁺ and virus*. Cell Calcium, 2009. **46**(1): p. 1-17.
198. Sangaletti, S., et al., *SPARC oppositely regulates inflammation and fibrosis in bleomycin-induced lung damage*. Am J Pathol, 2011. **179**(6): p. 3000-10.
199. Yiu, G.K., et al., *SPARC (secreted protein acidic and rich in cysteine) induces apoptosis in ovarian cancer cells*. Am J Pathol, 2001. **159**(2): p. 609-22.
200. Drev, D., et al., *Proteomic profiling identifies markers for inflammation-related tumor-fibroblast interaction*. Clin Proteomics, 2017. **14**: p. 33.
201. Ernst, B.P., et al., *Association of eIF4E and SPARC Expression with Lymphangiogenesis and Lymph Node Metastasis in Hypopharyngeal Cancer*. Anticancer Res, 2018. **38**(2): p. 699-706.
202. Guo, W., et al., *The clinical significance of secreted protein acidic and rich in cysteine expression in breast cancer tissue and its association with prognosis*. J Cancer Res Ther, 2017. **13**(5): p. 833-836.
203. Black, M.M. and J.T. Kurdyla, *Microtubule-associated proteins of neurons*. J Cell Biol, 1983. **97**(4): p. 1020-8.
204. Ma, Y., et al., *Autophagy and cellular immune responses*. Immunity, 2013. **39**(2): p. 211-27.
205. Ladoire, S., et al., *Biomarkers of immunogenic stress in metastases from melanoma patients: Correlations with the immune infiltrate*. Oncoimmunology, 2016. **5**(6): p. e1160193.
206. Kroemer, G., G. Marino, and B. Levine, *Autophagy and the integrated stress response*. Mol Cell, 2010. **40**(2): p. 280-93.
207. Sun, Y., et al., *Autophagy benefits the replication of Newcastle disease virus in chicken cells and tissues*. J Virol, 2014. **88**(1): p. 525-37.
208. Santana, S., et al., *Herpes simplex virus type 1 induces an incomplete autophagic response in human neuroblastoma cells*. J Alzheimers Dis, 2012. **30**(4): p. 815-31.
209. Sun, M., et al., *Pseudorabies virus infection inhibits autophagy in permissive cells in vitro*. Sci Rep, 2017. **7**: p. 39964.
210. Olesch, C., et al., *Beyond Immune Cell Migration: The Emerging Role of the Sphingosine-1-phosphate Receptor S1PR4 as a Modulator of Innate Immune Cell Activation*. Mediators Inflamm, 2017. **2017**: p. 6059203.
211. Crouch, E.E. and F. Doetsch, *FACS isolation of endothelial cells and pericytes from mouse brain microregions*. Nat Protoc, 2018. **13**(4): p. 738-751.
212. Espina, V., et al., *Laser capture microdissection technology*. Expert Rev Mol Diagn, 2007. **7**(5): p. 647-57.
213. Rausch, M.P. and K.T. Hastings, *Diverse cellular and organismal functions of the lysosomal thiol reductase GILT*. Mol Immunol, 2015. **68**(2 Pt A): p. 124-8.

214. Singh, R. and P. Cresswell, *Defective cross-presentation of viral antigens in GILT-free mice*. Science, 2010. **328**(5984): p. 1394-8.
215. Yang, L., et al., *Molecular structure, tissue distribution and functional characterization of interferon-gamma-inducible lysosomal thiol reductase (GILT) gene in chicken (Gallus gallus)*. Vet Immunol Immunopathol, 2013. **153**(1-2): p. 140-5.
216. West, L.C. and P. Cresswell, *Expanding roles for GILT in immunity*. Curr Opin Immunol, 2013. **25**(1): p. 103-8.
217. Walker, B.A., et al., *The dominantly expressed class I molecule of the chicken MHC is explained by coevolution with the polymorphic peptide transporter (TAP) genes*. Proc Natl Acad Sci U S A, 2011. **108**(20): p. 8396-401.
218. Abdul-Careem, M.F., et al., *Host responses are induced in feathers of chickens infected with Marek's disease virus*. Virology, 2008. **370**(2): p. 323-32.
219. Ramaroson, M.F., et al., *Changes in the Gallus gallus proteome induced by Marek's disease virus*. J Proteome Res, 2008. **7**(10): p. 4346-58.
220. Lee, K.W., A.M. Bode, and Z. Dong, *Molecular targets of phytochemicals for cancer prevention*. Nat Rev Cancer, 2011. **11**(3): p. 211-8.
221. Wang, S., et al., *Noncanonical TGF-beta pathways, mTORC1 and Abl, in renal interstitial fibrogenesis*. Am J Physiol Renal Physiol, 2010. **298**(1): p. F142-9.
222. Manzanares-Meza, L.D., C.I. Gutierrez-Roman, and O. Medina-Contreras, *MALDI imaging: beyond classic diagnosis*. Bol Med Hosp Infant Mex, 2017. **74**(3): p. 212-218.
223. Day, R.E. and I. Palubeckaite, *The Future in Disease Models for Mass Spectrometry Imaging, Ethical Issues, and the Way Forward*. Methods Mol Biol, 2017. **1618**: p. 191-201.

13. Attachments

13.1. Publications and contributions at Conferences

Publications

Pauker, V. I., Thoma, B. R., Grass, G., Bleichert, P., Hanczaruk, M., Zoller, L., Zange, S. (2018). *Improved discrimination of Bacillus anthracis from Closely Related Species in the Bacillus cereus sensu lato Group based on MALDI-TOF Mass Spectrometry.* J Clin Microbiol.

Pauker V. I., Thoma B.R., and G. Grass., 2015. *Hochpathogene Bakterien identifizieren.* Management & Krankenhaus-Zeitung für Entscheider im Gesundheitswesen. 34. Jahrgang (37).

Pauker V.I., Thoma B.R., Grass G. and S. Zange, 2014. *Identification and differentiation of B. anthracis From closely related members of the Bacillus cereus sensu lato group via MALDI-TOF mass Spectrometry.* Military Scientific Research Annual Report. p72-73.

Contributions at Conferences

6th FLI Junior Scientist Symposium

20.-22. September 2017, Brunswick in Germany, Talk

Proteome Analysis of Laser Capture Micro-Dissected Tumors from Chickens Infected with Marek's Disease Virus

Pauker V.I., Bertzbach L.D., Czerwinski G., Teifke J.P., Mettenleiter T.C., Kaufer B.B. and A. Karger

42nd International Herpesvirus Workshop (IHW)

29. July – 02. August 2017, Ghent in Belgium, Poster

Proteome Analysis of Laser Capture Micro-Dissected Tumors from Chickens Infected with Marek's Disease Virus

Pauker V.I., Bertzbach L.D., Czerwinski G., Teifke J.P., Mettenleiter T.C., Kaufer B.B. and A. Karger

1st Summer School 'Infectionbiology'

28. – 30. September 2016, Greifswald in Germany, Talk

Proteomic Analysis of Lymphocytes after Infection and Transformation with the oncogenic Marek's Disease Virus

Pauker V.I., Bertzbach L.D., Mettenleiter T.C., Kaufer B.B. and A. Karger

5th FLI Junior Scientist Symposium

21.-23. September 2016, Jena in Germany, Poster

Proteome Analysis of Lymphocytes after Infection and Transformation with the oncogenic Gallid Herpesvirus 2

Pauker V.I., Bertzbach L.D., Kaufer B.B. and A. Karger

4th FLI Junior Scientist Symposium

21.-23. September 2015, Züssow in Germany, Poster

Proteome Analysis of Primary Lymphocytes after Infection and Transformation with the Marek's Disease Virus

Pauker V.I., Bertzbach L.D., Kaufer B.B. and A. Karger

67th Annual Meeting of the Germany Society of Hygiene and Microbiology (DGHM)

27.-30. September 2015, Münster in Germany, Poster

Improving the differentiation of Bacillus anthracis from closely related species in the Bacillus cereus sensu lato Group via MALDI-TOF MS

Pauker V.I., Zange S., Grass G., Scherer S., Zöller L. and B. R. Thoma

Annual Conference 2015 of the Associatio of General and Applied Microbiology (VAAM)

01.-04. March 2015, Marburg in Germany, Poster

Improving the differentiation of Bacillus anthracis from closely related species in the Bacillus cereus sensu lato Group via MALDI-TOF MS

Pauker V.I., Zange S., Grass G., Scherer S., Zöller L. and B. R. Thoma

Bruker MALDI Biotyper Application meeting

12.-13. November 2014, Bremen in Germany, Poster

Improving the differentiation of Bacillus anthracis from the remaining members of the Bacillus cereus sensu lato Group via MALDI-TOF MS

Pauker V.I., Zange S., Grass G., Scherer S., Zöller L. and B. R. Thoma

23rd European Congress of Clinical Microbiology and Infectious Diseases (ECCMID)

27.-30. April 2013, Berlin in Germany, Poster

Detecting Aminoglycoside Resistance by Mass Spectrometry

Burckhardt I., Pauker V., Bode K. and S. Zimmermann

13.2. Acknowledgment

First and foremost, I would like to thank Prof. Dr. Dr. h.c. Thomas C. Mettenleiter for the opportunity to complete this dissertation at the Institute of Molecular Virology and Cell biology of the Friedrich-Loeffler-Institut and for the outstanding and valuable guidance throughout my thesis.

My gratitude goes to Dr. Axel Karger for the excellent supervision in the laboratory, the constructive discussions and the reliable helpfulness.

I also want to thank Prof. Dr. Benedikt Kaufer and Luca Bertzbach, FU Berlin, for the great collaboration during this thesis, the support and fruitful meetings.

I also want to thank Prof. Jens Teifke for the cell type analyses and the excellent support and help in all the pathological and histological aspects of this work. For the help and good discussions, especially during the laser-capture microdissection, I also want to thank Gabriele Czerwinski.

In addition, for the pleasant atmosphere, the good conversations and willingness to help during the laboratory work, I would like to thank Barbara Bettin and Catharina Keßler.

I also want to thank Stephie, Svenja, Franzi, Melina and Lars. I am forever thankful for our friendship, the good laughter, the joy, the motivation and always a friendly ear especially during lunchtime and beyond. Especially, I want to thank Lars for all the support, the constructive distractions and that he never lost faith in me, particularly in the final stage of this dissertation.

My dearest family, Mama, Papa, Vroni and Felix, I am outmost thankful for all the support. I definitely would not be, where I am today without your faith, your love, your patience and your advices.